Combining High Activity and Durability in Automotive Three-Way Catalysts

Toshitaka Tanabe

2012

Preface

Science and technology improved quality of our life through a lot of inventions. Automobile is one of the great inventions in last century. It changed our life and society very much by serving mobility. Although automobile is very useful, it caused some problems such as casualties in traffic accidents, air pollutions by its exhaust and a lot of consumption of oil. In the late 1970's, automotive three-way catalyst was invented to abate harmful emissions in automotive exhaust. It has been developed by continuous works in research and development and emissions from automobile have decreased quite a lot from untreated levels. Although the efficiency of catalytic abatement is very high, legislations become tightened more and more. Recently, automobile production and usage has been increasing all over the world, especially in emerging countries such as China and India. This situation requires more decreases of emissions from each automobile not to increase total emissions from automobiles over the world. Three-way catalyst is Pt, Pd and Rh supported catalyst. Natural resources of these metals are quite scarce and limited. To sustain our quality of life and global environment, a lot of efforts are necessary to develop more sophisticated catalytic technology for automotive emissions abatement.

This thesis presents design concepts to combine high catalytic activity and durability of automotive three-way catalyst. These studies should help to decrease automotive emissions and usage of scarce Pt, Pd and Rh in automotive three-way catalysts.

These present studies were conducted in Toyota Central R&D Labs., Inc (TCRDL) during 2001-2012. In this period the author worked on research and development of automotive catalysts. From 2001 to 2002, the author stayed in Eindhoven University of Technology (TU/e) in the Netherlands as a visiting researcher. Some part of these works was conducted in TU/e.

The author is grateful to his supervisors, Dr. Masahiro Sugiura, Mr. Hideo Sobukawa, Dr. Hirohumi Shinjoh, Mr. Kouji Yokota, the heads of catalyst laboratory at TCRDL for giving opportunity to work in the field of catalyst research. The author gives special gratitude to Dr. Naoki Takahashi, who is the present head of the catalyst laboratory, for his valuable discussions and encouragements to complete these studies.

The author gives deep appreciation to Prof. J. C. Schouten and dr.ir. Jozef Hoebink as supervisors during his stay in TU/e. The author is also grateful to Prof. H. H. Brongersma in TU/e and Prof. J. N. Kondo in Tokyo Institute of Technology for their valuable discussions.

The author thanks to his co-researchers of Dr. Shin'ichi Matsumoto, Mr. Nobuyuki Takagi, Mr. Takeshi Hirabayashi, Ms. Akemi Satoh, Mr. Oji Kuno and Mr. Hiromasa

Suzuki in Toyota Motor Corporation. The author also thanks to his co-researchers and great friends of Mr. Kazuhiko Dohmae, Dr. Yasutaka Nagai, Ms. Miho Hatanaka and Dr. Akira Morikawa in TCRDL.

The author is deeply grateful to Prof. Atsushi Satsuma for the comments and clarifications regarding his present thesis. The author is also grateful to Prof. Takahiro Seki, Prof. Tomoko Yoshida and Prof. Kyoichi Sawabe for reviewing this thesis.

Finally, the author is extremely grateful to his father and mother for very kind and great supports for his life. The author gives heartfelt thanks to his loving wife Satoko for her very warmest help and his son Yasuhiro, daughter Mayuko for their warm encouragements to complete this thesis.

2012
Aichi
Toshitaka Tanabe

Contents

Chapter 1

General Introduction

1. 1 Historical view of catalytic technology for abatement of automotive exhaust

Automobiles with internal combustion engine were invented in the late 19th century. Its production and usage have been expanding to very large volume over the century. Nowadays, automobiles are very important and necessary for our life, which serve our mobility and also logistics in a society. Although automobiles are very useful, it have caused some problems; casualties in traffic accidents, air pollutions by harmful emissions in its exhaust and huge consumptions of petroleum. In recent, CO_2 is also discussed as "Green House Effect Gas" which should be a reason of global climate change. Scope this thesis is catalytic abatement of emissions which are harmful to human being. In this thesis, "emissions" is used to mean the substances in automotive exhaust which are harmful to human being and CO_2 is not discussed as automotive emission.

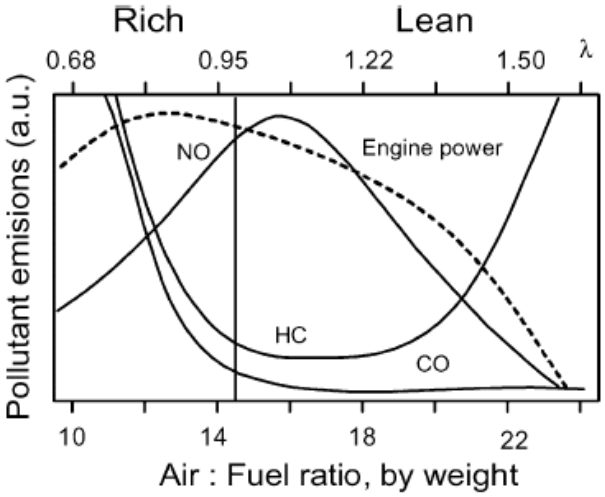

Fig. 1 Effect of A/F ratio on engine emissions and power [1].

Main emissions in automotive exhaust are hydrocarbons (HC), carbon monoxide (CO) and nitrogen oxides (NO or NO_2, which are abbreviated as NO_x). Fig 1 shows concentrations of HC, CO and NO_x in automotive exhaust as a function of air to fuel ratio (A/F) introduced into internal combustion engine. The ratio is determined in weight. Fuel is introduced with air into an internal combustion engine and oxidized to

carbon dioxide (CO_2) and water (H_2O) during combustion in cylinders. This process is an oxidation reaction of hydrocarbon;

$$C_nH_m+(2n+m)O_2 = nCO_2+(m/2)\ H_2O$$

Air to fuel ratio of 14.7 is a stoichiometric condition of this reaction. Although all fuel should be oxidized to CO_2 and H_2O at this condition, the combustion reaction in cylinders is not perfect. This imperfection produces unburned hydrocarbons and CO. Temperature in cylinders is very high during the combustion. This high temperature caused a reaction between nitrogen and oxygen in air to produce NO;

$$N_2 + O_2 \rightleftarrows 2NO$$

HC and CO emissions are high at fuel rich condition (A/F lower than 14.7) because of shortage of oxygen. At fuel lean condition (A/F higher than 14.7), HC and CO concentrations are low because of high oxygen concentration during the combustion.

Table 1 Historical overview of passenger's car emissions standards in the U.S.[2].

Year	Area	Level (g/mile)			Test method
		CO	HC	NOx	
1970	Federal & California	23	2.2	-	7 mode
1972	California	39	3.2	3.2	FTP-72
	Federal	39	3.4	-	
1975	California	9	0.9	2	FTP-75
	Federal	15	1.5	2.0	
1977	California	9	0.41	1.5	
	Federal	15	1.5	2.0	
1980	California	8	0.39	1	
	Federal	7	0.41	2	
1981	Federal & California	3.4	0.41	1	
1993	California	3.4	0.26	0.4	
	Federal	7	0.41	1	
1994	California	3.4	0.125	0.4	
1997	California 25% of the fleet 2% of the fleet	 3.4 1.7	 0.075 0.040	 0.2 0.2	

Table 2 Passenger's car Emission standards in Japan (g/km) [3].

	CO		HC		NOx	
Year	max	mean	max	mean	max	mean
1978	2.7	2.1	0.39	0.25	0.84	0.6
1991	2.7	2.1	0.39	0.25	0.48	0.25
2002	1.27	0.67	0.17	0.08	0.17	0.08

Concerning NO, the concentration is highest at just fuel lean condition of stoichiometric because the combustion temperature is highest at this point.

Air pollution became serious in late 1960's in major cities such as Los Angels in the Unites States and Tokyo in Japan. Causes of air pollution were emissions from stationary sources; electrical power plants, chemical plants, steel plants and mobile sources; automobiles, air planes and ships. Especially in Los Angels, the emissions from automobile were major causes of air pollution problem. This situation is the reason why the legislation of automotive emission control in California was/is most severe over the world. A need to control automobile emissions became strong in 1960's and the U. S. congress passed 1970 Clean Air Act. The requirement of the Act were 90% reduction of CO and HC emissions from 1970 model year levels by 1975, and a 90% reduction of NO emissions from 1971 model year levels by 1976. In Japan, legislation was introduced in 1978 and the emissions standard was similar to California standard. Emissions standards in the legislations in the U.S and Japan are shown in Table 1 and 2, respectively. In 1985, the European Community passed strict legislation for passenger's car.

These legislations define measurement methods of emissions. Because a driving condition of automobile is not constant, diving patterns were defined to measure the automotive emissions. Those driving patterns depend on the nations or regions which are shown in Fig. 2. Those patterns were determined according to typical traffic conditions in each region. The legislation in the U.S. required emissions standard to be met after 50000 miles run. This durability requirement for emission abatement system was very high standard at that age.

It was a very challenging problem to meet the emission requirements in 1970's. A lot of technologies, such as a combustion modification, exhaust gas recirculation (EGR), catalytic abatement of emissions, were tried to achieve the requirements. After struggling in research and development, first-generation converter of an oxidation catalyst for hydrocarbon (HC) and carbon monoxide (CO) abatement was implemented to automobiles in 1975. With this catalytic technique, exhaust gas recirculation was used

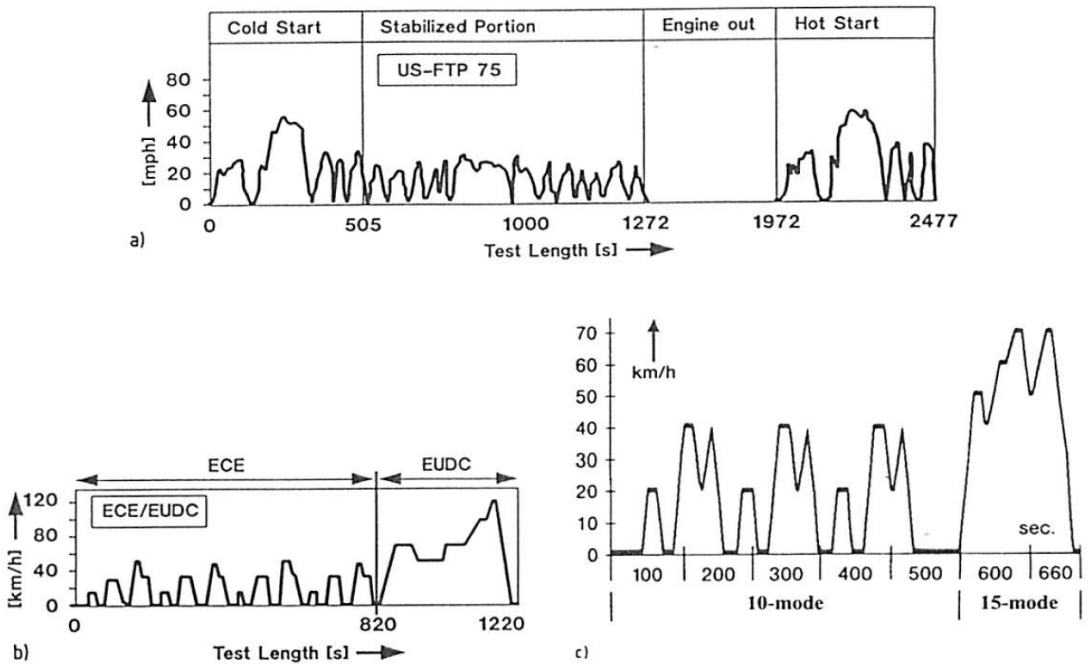

Fig. 2 Vehicle test cycles to measure the exhaust gas emissions from passenger's car (a) the U.S., (b) the European Union, (c) Japan [2].

to abate NO_x emission. An engine is operated at just fuel rich of stoichiometric condition to reduce NO_x formation in cylinders. Secondary air was pumped into the exhaust gas to supply enough amount of oxygen to oxidized HC and CO as shown in Fig. 3 [2].

At this stage, a lot of catalytic material was investigated. Noble metal of Pt and Pd showed excellent catalytic activities but those cost and supply were worried. A lot of base metal candidates were investigated, such as Cu, Co, Cr, Ni, Mn, and so on. These base metals were less active than noble metal.

In addition to the activity, durability of catalyst was also important issue for practical use. Deactivation of catalyst is classified into two categories; one is thermal

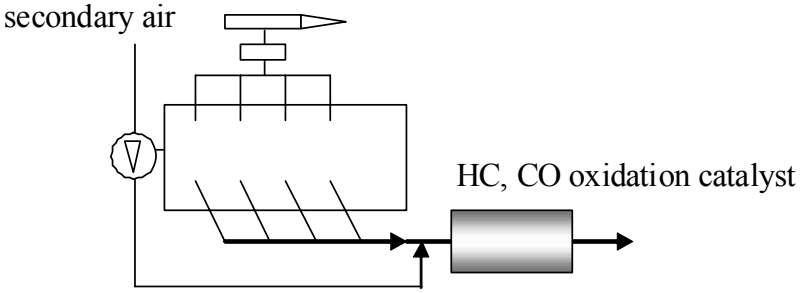

Fig. 3 The scheme of oxidation catalyst with secondary air injection [2].

deactivation in high temperature using and another is poisonings with sulfur, lead, phosphorus etc. those are included in automotive exhaust. Lead was added as tetraethyl lead to boost octane number of gasoline. The use of lead additive had harmful impact for human being and also automotive catalyst. The use of lead additive was prohibited in the late 1970'for regular gasoline. This was one of the tuning points of automotive emission abatement by catalyst technology. Sulfur is intrinsically contained in gasoline because the sulfur elimination is not perfect in crude oil refinery to produce gasoline.

Base metal catalyst looses its catalytic activity very soon with poisoning of sulfur, phosphorus, etc. And also thermal durability was not enough. This durability problem was fatal for base metal catalysts to install on automobiles. Therefore Pt and Pd were used active components in the first-generation of catalytic converter. Meanwhile support material to support Pt and Pd was investigated and alumina with high surface are was used in the catalyst.

After the installation of oxidation catalysts, dual bed catalysts were used for catalytic abatement of NO_x. NO_x reduction catalyst and HC and CO oxidation catalyst is placed in series in exhaust pipe as shown in Fig. 4. In this system, an engine was operated at fuel rich condition to reduce NO_x over NO_x reduction catalyst. Secondary air is pumped into the exhaust to oxidized HC and CO over oxidation catalyst.

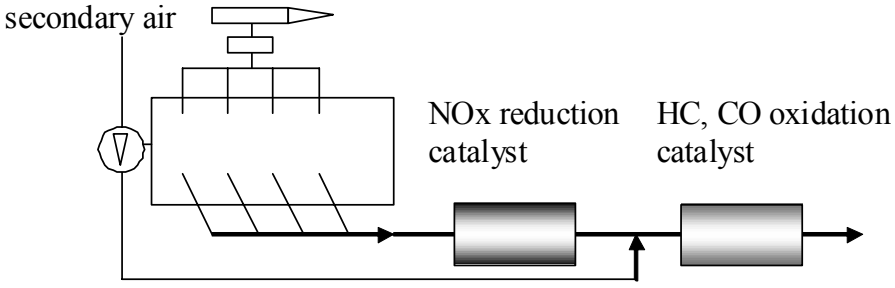

Fig. 4 The scheme of dual bed catalyst of NOx reduction catalyst and oxidation catalyst with secondary air injection [2].

1.2 Automotive three-way catalysts

In 1972, Ford researchers found that catalytic reaction rates of HC, CO and NO_x over noble metal (Pt, Pd, Rh) supported catalyst is extremely high when atmospheric condition of exhaust is very close to stoichiometric condition [4]. At that moment, there was no technical solution to control the exhaust atmospheric condition to stoichiometry. Bendix and also Bosch reported an electronic fuel injection control by using O_2 sensor [5, 6]. This system is an electronic control of automotive engine to maintain the exhaust atmosphere to stoichiometric condition. This system was a break through of catalytic

technology for abatement automotive exhaust. This catalytic system is called as "three-way catalyst" that converts HC, CO and NO_x simultaneously to CO_2, H_2O and N_2 through following reaction;

$$HC + CO + NO_x + O_2 = CO_2 + H_2O + N_2$$

Three-way catalyst is Pt, Pd, Rh supported catalyst on oxide supports. Pt and Pd are

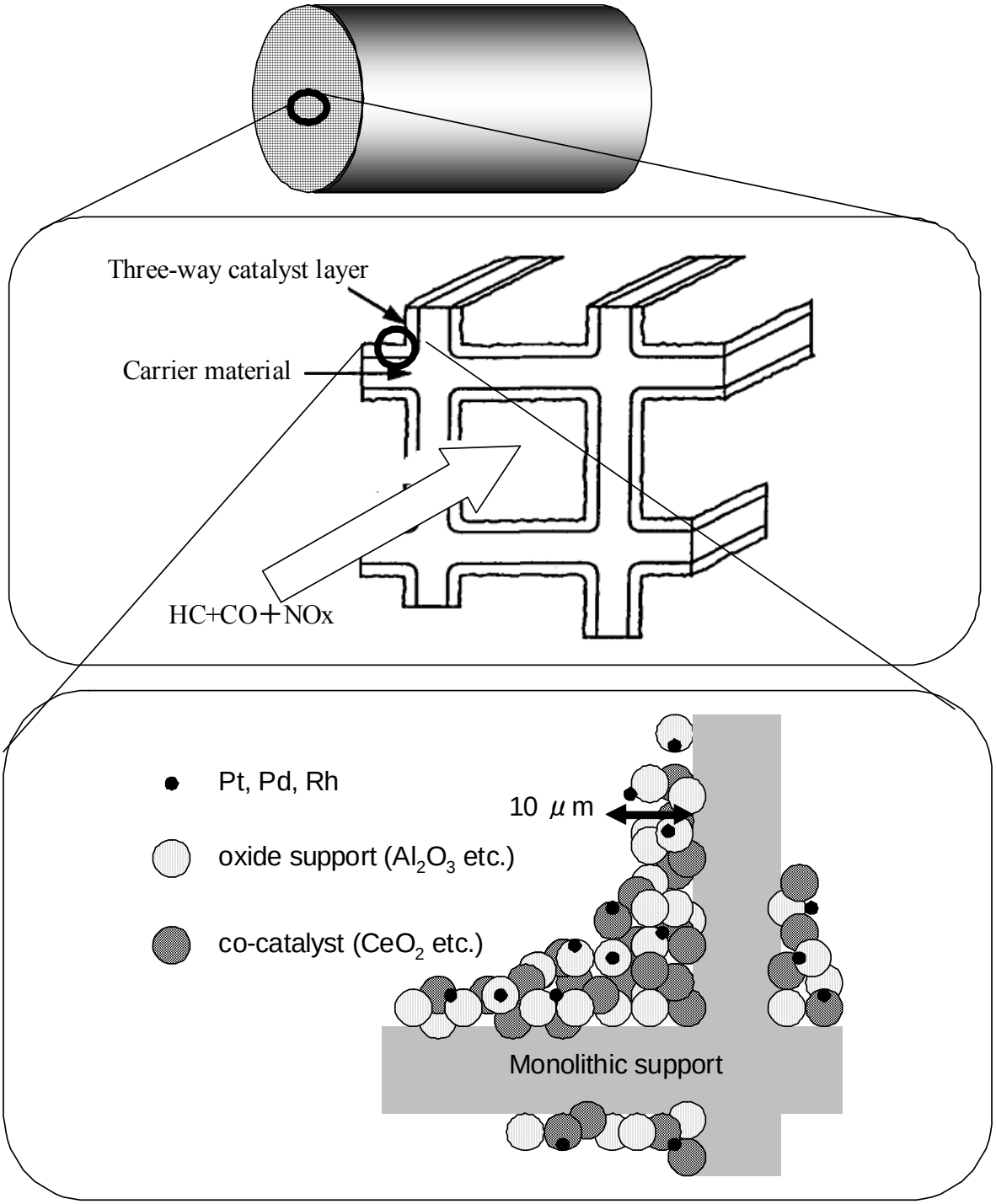

Fig. 5 Structure illustrations of monolithic automotive three-way catalyst.

active component for HC and CO oxidation. Rh is an active component for NO_x reduction. Alumina with high surface area is used as a typical support. Monolithic catalysts are commonly used although pelletized catalysts are used in the early stage of commercialization. Fig. 5 illustrates structures of monolithic three-way catalyst. Catalyst carrier that is made of ceramic or metal has honey comb structure. Noble metal supported catalyst powders are coated on the wall of the carrier. Exhaust gas go through channels of honey comb structure and converted through the catalytic reactions over the coated noble metal supported catalyst.

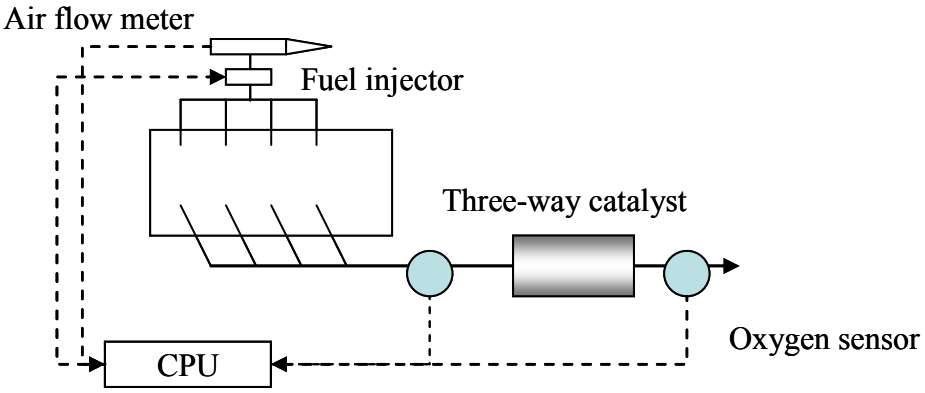

Fig. 6 The scheme of three-way catalyst system [2].

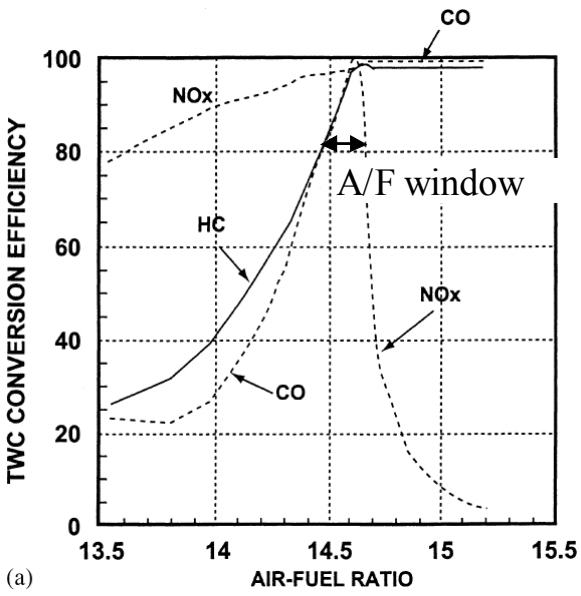

Fig. 7 HC, CO and NOx conversion efficiencies as a function of air to fuel ratio [7].

Three-way automotive catalyst system is illustrated in Fig. 6. An atmospheric condition is monitored by using O_2 sensors in the exhaust pipe. The amount of fuel injection is controlled by electromagnetic valves to maintain the exhaust atmosphere to stoichiometric condition. The control system is a feed-back technique; fuel injection is increased if O_2 sensor found higher oxygen concentration than stoichiometry or decreased if the sensor found lower oxygen concentration than stoichiometric. Because the feed-back response time is finite, the exhaust atmosphere is oscillating with time around stoichiometric condition in this system. Typical conversion behaviors are shown in Fig. 7. HC, CO conversion is high in the fuel lean atmosphere and NO_x conversion is the high in fuel rich atmosphere. At exact stoichiometric condition, all HC, CO and NO_x conversions are highest. Because the exact stoichiometric condition can not be achieved technically in actual automobile implementation, the atmosphere is controlled within so called "A/F window" to obtain enough high HC, CO and NOx conversions.

Cerium oxide is used in three-way catalysts to enlarge the A/F window by using its redox activity [8, 9]. Oxidation state of Ce changes with exhaust atmospheric condition;

$$CeO_2 \rightleftarrows CeO_{2-x} + (x/2)O_2,$$
$$[\ Ce^{4+} + e^- = Ce^{3+}\ ,\ O^{2-} = (1/2)O_2 + 2e^-\ ]$$

Cerium oxide release oxygen to the exhaust in fuel rich reducing condition and absorb oxygen from the exhaust in fuel lean oxidizing condition. This redox behavior of cerium oxide acts as oxygen buffering function to exhaust atmosphere. This function helps to keep the exhaust atmosphere around stoichiometric condition and increase HC, CO and NO_x conversions. Cerium oxide is very important material in three-way automotive catalysts and a lot of works have been conducting to improve its function and durability. Nowadays, cerium-zirconium mixed oxides with some additives are used every three-way automotive catalyst [10].

The basis of three-way catalyst system was constructed by the early 1980's and it has been using nowadays. This system looks nearly complete if the atmospheric control of exhaust works well at stoichiometric condition and exhaust temperature is high enough to activate catalytic reaction on three-way catalysts. In the real world, the atmospheric control is not perfect because the automobile driving condition is not steady and the exhaust temperature is ambient at the start-up of the engine. Improvements are necessary for more sophisticated atmospheric control technique and more active catalyst at low temperature.

Table 3 Emissions standards in California (U.S) since 1993 [11]

Year	Category	Emissions (g/mile, FTP test)			
		HC	CO	NOx	PM
1993		0.25[a]	3.40	0.40	
1994	Tier 1	0.25[b]	3.40	0.40	
2003	Tier 1	0.25[c]	3.40	0.40	
2004	$TLEV_1$[d]	0.125	3.40	0.40	0.08
	LEV_2[e,f]	0.075	3.40	0.05	0.01
2005	LEV_1[d]	0.075	3.40	0.40	0.08
	$ULEV_2$[e,f]	0.040	1.70	0.05	0.01
2006	$ULEV_1$[d]	0.040	1.70	0.20	0.04
	$SULEV_2$[e,f,g]	0.010	1.0	0.02	0.01
2007	ZEV_1	0	0	0	0
	ZEV_2	0	0	0	0

Note. LEV: low emission vehicles, SULEV: super low emission vehicles, ZEV: zero emission vehicles.

[a] NMHC: non-methane hydrocarbons, i.e., all hydrocarbons excluding methane.

[b] NMOG: non-methane organic gases, i.e., all hydrocarbons and reactive oxygenated hydrocarbon species such as aldehydes, but excluding methane. Formaldehyde limits (not shown) are legislated separately.

[c] FAN MOG: fleet average NMOG reduced progressively from 1994 to 2003.

[d] LEV_1 type emissions categories phasing out 2004–2007.

[e] LEV_2 type emissions limits phasing in 2004 onwards.

[f] LEV_2 standards have same emission limits for passenger cars and trucks <8500 lb gross weight.

[g] $SULEV_2$ onwards 120,000 miles durability mandated.

1.3 Challenges of automotive three-way catalysts

After the great success of emission abatement with three-way automotive catalysts, tightening of legislations has been continuing over the world. For example, legislation trend in California (U.S.) is shown in Table 3. Emissions standards are decreasing and durability requirement goes high. The legislation requires that emissions standards must be achieved even after 150000 miles running (200000 km). This means that life of automotive three-way catalysts must be very long.

Fig.8 shows temporal changes of HC and NOx concentrations in exhaust after reactions over three-way catalyst in the U.S. driving mode test. Because this test mode is “cold start”, temperature is ambient at beginning of the test and increase to 600 ºC in 100 sec. During this period, HC and NOx concentrations are high because catalytic reactions are not activated enough to achieve high conversion efficiencies. To meet more tight legislations, catalytic reactions over three-way catalysts should be activated at lower temperature to decrease emissions in the exhaust.

Concerning durability of three-way automotive catalyst, as mentioned before, deactivation of the catalyst is caused by thermal degradation of catalytic material and poisoning with sulfur and other substances (P, Ca, Mg, etc.) originating from fuel and

lubricants. Among these causes, sintering of supported noble metals at high temperature is a central issue of catalyst deactivation. The exhaust temperature exceeds more than 1000 ˚C in some automobile driving conditions. At this high temperature, highly dispersed supported noble metals migrate on the support oxide and aggregate to larger particles. This sintering of supported noble metals decreases number of active site for catalytic reaction.

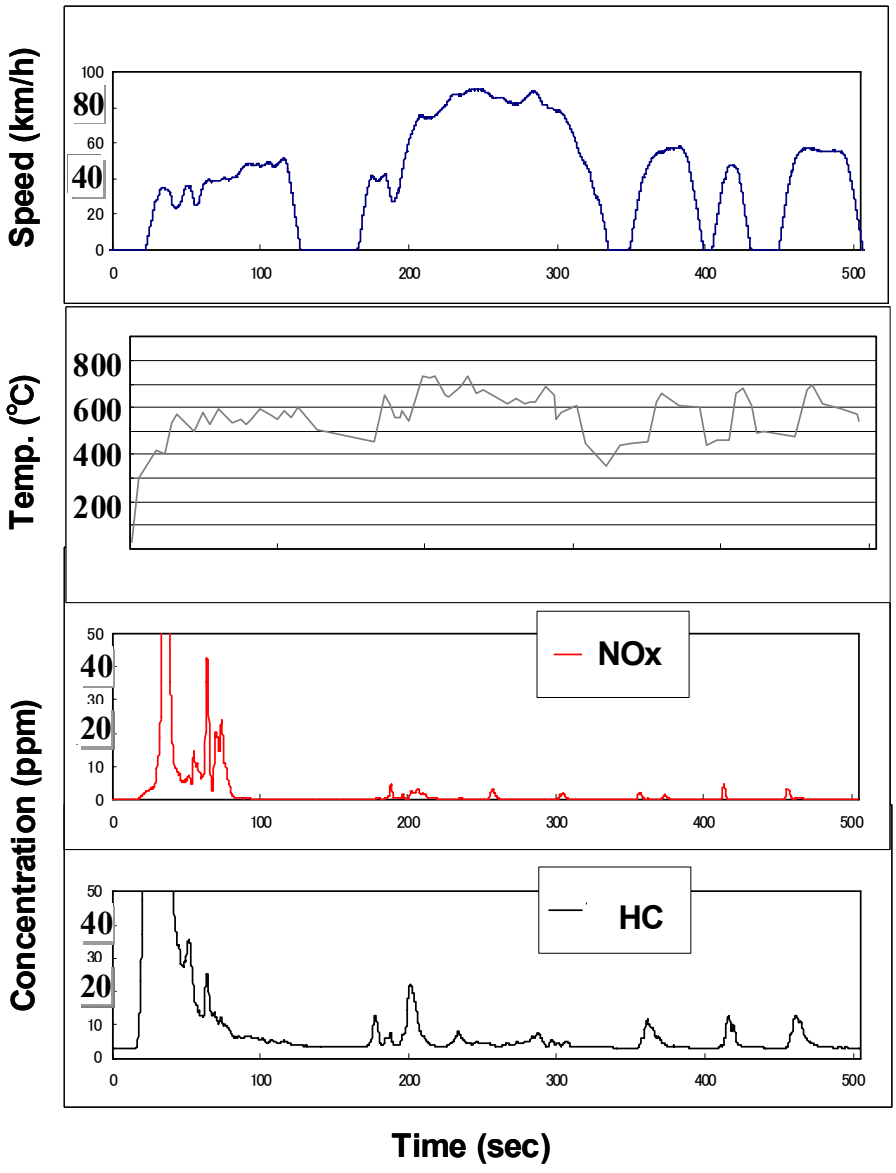

Fig. 8 Temporal changes of vehicle speed, inlet gas temperature, NOx, HC concentrations in ehaust after reactions over three-way catalyst in a U.S driving mode test.

An increase of loading amount of noble metals improves the durability of the catalyst and also helps to increase the catalytic activity at low temperature. This approach is not practical because natural resources of noble metals are very scarce. Fig. 9 shows trends of Pt, Pd and Rh demands for automotive catalysts in the last 10 years. The demands of Pt, Pd and Rh for automotive catalyst were increasing steadily from 2002 to 2007. This was caused by the increase of automobile productions all over the world and strengthening of legislations of automotive exhaust emissions. After the sharp decrease in 2008, which was caused by economical crisis, the demands have been increasing slowly. Fig. 10 shows the trend of total demands of Pt, Pd and Rh in the last 10 years. The demand of Pt and Pd for automotive catalyst is almost half of total demands and the demand of Rh for automotive catalyst was above 80% of total demand. Concerning prices of Pt, Pd and Rh, those prices have been increasing in last 20 years as shown in

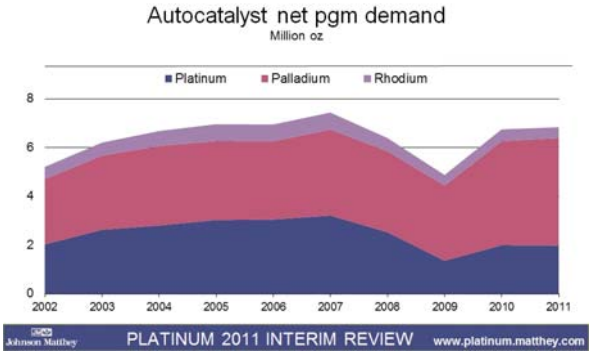

Fig. 9 A trend of Pt, Pd and Rh demands for automotive catalyst in last 10 years [12].

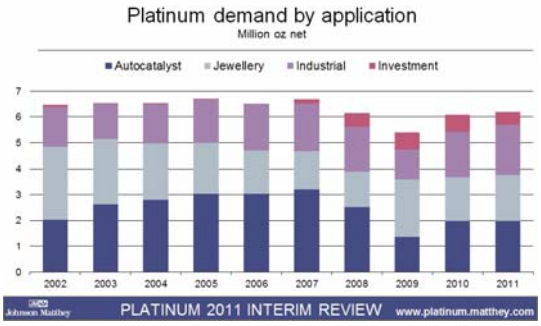

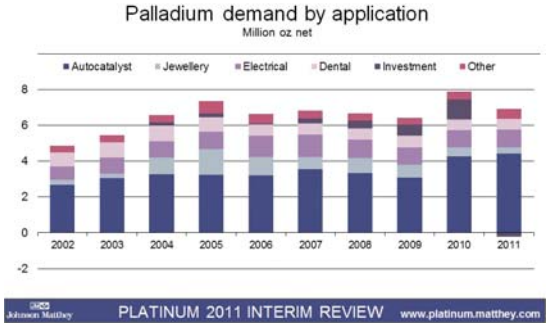

Fig. 10 Trends of total demands of Pt, Pd and Rh in last 10 years [12].

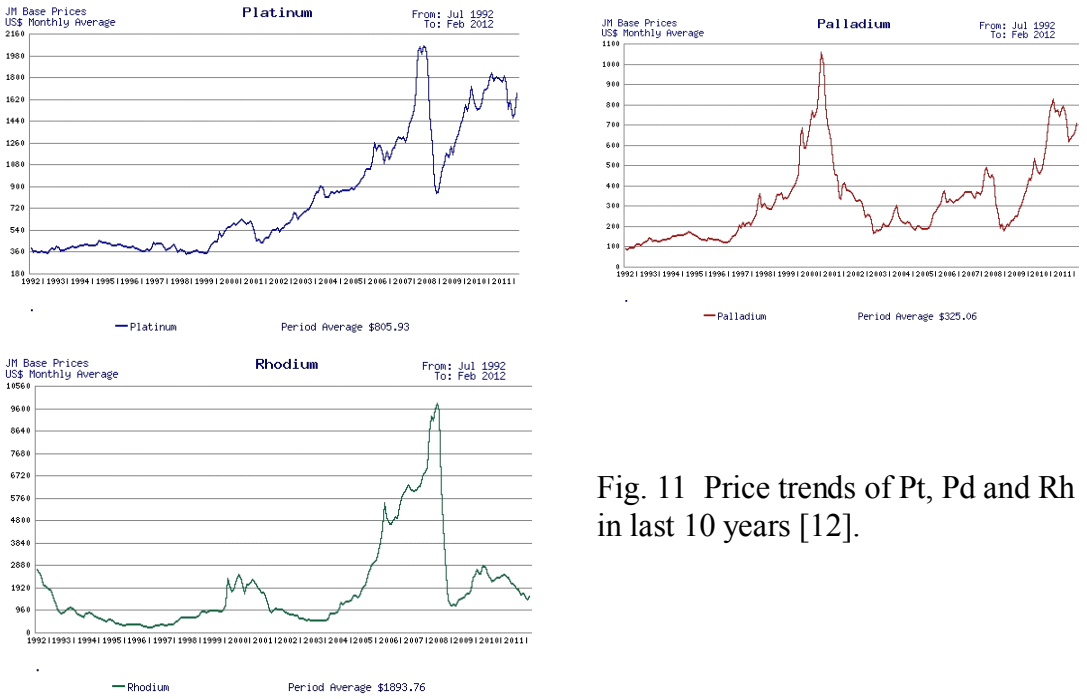

Fig. 11 Price trends of Pt, Pd and Rh in last 10 years [12].

Fig. 11. Although the trends of those prices are not only determined by the real demand but speculation, the noble metal demands for automotive catalysts are dominant and have large impact on the price of noble metals.

All over the world, especially in emerging countries such as China, the number of automotive productions and use will increase. Legislations of automotive emissions will not be relaxed in future. This situation should cause the increase of Pt, Pd and Rh demands for automotive catalysts. From a view point of sustainability, the usage of noble metals in automotive catalyst must be decreased by advances of technology. This is a task in the research and development of automotive catalyst. Combining high catalytic activity and durability in automotive three-way catalysts is a key issue to achieve this task.

1.4 Objectives and outline of this research

Objective of this study is combining high catalytic activity and durability in automotive three-way catalysts. The study was conducted on noble metal supported catalysts. This thesis consists of seven chapters. General introduction to automotive three-way catalyst is discussed in Chapter 1. Design concepts of highly active three-way catalysts were discussed in chapter 2, 3 and 4. In chapter 5 and 6, sintering suppressions of supported Pt and Rh were investigated, respectively. Combing high catalytic activity and durability of Rh supported catalyst was discussed in Chapter 6. Chapter 7

summarizes this thesis and gives the general conclusion.

Following is outline of this thesis. In chapter 2, activation of Pt supported catalyst was investigated with operando X-ray absorption fine structure spectroscopy (XAFS) during C_3H_6 oxidation. This study revealed that reduction of supported Pt to metallic state is an important step for activations of Pt supported catalyst in both reducing and oxidizing atmosphere. Chapter 3 shows comparative studies on NO reduction over Pt, Pd, and Rh supported catalysts in automotive simulated exhaust gas reaction. C_3H_6-O_2 reaction was found as a key reaction for NO reduction activity over Pt, Pd, and Rh supported catalysts. Kinetic studies revealed that C_3H_6 self poisoning effect in C_3H_6-O_2 reaction was a key factor to control the NO reduction rate over Pt or Pd supported catalysts. Over Rh supported catalyst, oxygen poisoning effect was a key factor to control NO reduction. This self poisoning effect can be controlled by an addition of Ba to Pt or Rh supported catalyst. Ba addition to Pt supported catalyst enhance NO reduction activity by weakening C_3H_6 poisoning effect while its addition to Rh supported catalyst suppressed NO reduction activity by strengthening oxygen poisoning effect. In Chapter 4, operando XAFS investigation was conducted on Pt catalysts supported on four kinds of oxide during NO reduction by hydrocarbons. This investigation suggested that the activation of catalytic NO reduction should be determined by both the reduction of supported Pt to metallic state and self poisoning effect of hydrocarbon. The appropriate design of support material should be important to achieve high activity from the both perspectives of the reduction of supported Pt to metallic state and the suppression of hydrocarbon poising.

The sintering behaviors of supported Pt and Rh were studied in Chapter 5 and 6, respectively. MgO was used as support oxide for Pt in Chapter 5. Strong Pt-MgO interaction in oxidizing atmosphere helped not only to suppress Pt sintering but enable re-dispersion of agglomerated Pt. On the other hand, this strong interaction decrease the catalytic activity of supported Pt because the interaction inhibited the reduction of supported Pt to metallic state. This result showed the appropriate control of noble metal-support interaction should be important to combine high catalytic activity and durability of noble metal supported catalysts. In Chapter 6 the development of Rh catalyst combining high activity and durability was discussed. The Nd_2O_3 enriched surface layer was introduced on ZrO_2 oxide to control the Rh-support interaction. The appropriate control of Rh-Nd_2O_3 interaction suppressed the sintering of supported Rh without any degradation of Rh reducibility to metallic state which is important to achieve high catalytic activity.

References

[1] J. Kašpar, P. Fornasiero, N. Hickey, Catal. Today 77 (2003) 419–449.

[2] T. Kreuzer, E.S. Lox, D. Lindner, J. Leyrer, Catal. Today 29 (1996) 17-27.

[3] Barry J.Cooper, Honda Zaidan Report, No.102.

[4] M. Shelef, J. H. Jones, J. T. Kummer, K. Otto, E. E. Weaver, Environ. Sci. Tech. 5 (1971) 790.

[5] J. G. Rivard, SAE, Paper No.730005 (1973).

[6] I. Gorille, N. Rittnannsberger , P Werner, SAE Paper No.750368 (1975).

[7] M. Shelef_, R.W. McCabe, Catal. Today 62 (2000) 35–50.

[8] H. S. Gandhi, A. G. Piken, M. Shelef, R. G. Delosh, SAE paper 760201 (1976).

[9] H.C. Yao, Y.F.Yu Yao, J. Catal., 86 (1984) 254.

[10] M. Sugiura, M. Ozawa, A. Suda, T. Suzuki, T. Kanazawa, Bull. Chem. Soc. Jpn., 78 (2005) 752-767.

[11] M.V. Twigg, Catal. Today, 163 (2011) 33–41.

[12] Platinum interim review 2011, http://www.platinum.matthey.com

Chapter 2

Activation of Pt supported catalyst～operando observation of Pt metallization during catalytic reaction～

Abstract

Operando X-ray absorption fine structure (XAFS) investigations were performed on Pt/γ-Al_2O_3 during the total oxidation of C_3H_6 in reducing and oxidizing atmospheres. Study of the Pt valance state and catalytic conversion behavior as a function of temperature revealed that both the creation of metallic Pt sites and the activation of adsorbed species on Pt are important for the functioning of the catalytic reaction at low temperature.

Keywords; Pt, γ-Al_2O_3, X-ray absorption fine structure, C_3H_6 oxidation, Valence state, Operando

1. Introduction

The operando spectroscopic methodology was recently introduced in catalysis research [1-3]. This methodology is the spectroscopic investigation of the catalyst during the reaction with simultaneous measurements of the reaction; i.e., activity, selectivity and stability by using gas chromatograph or mass spectrometer [2, 3]. Since the state of the catalyst; e.g. surface structure, surface composition and valence state of the supported metal, is easily affected by temperature, atmosphere and adsorbed species, this operando approach should be a very powerful technique for uncovering the real state of the catalyst under working conditions [2]. The insights obtained from this approach will help to understand the catalytic function at the molecular level and assist rational developments and improvements of the catalyst and catalytic processes. Operando spectroscopy is used also for the control of a catalyst material. In this approach, the catalytic reaction condition and regeneration procedure are controlled by the aide of operando spectroscopic technique to achieve the high catalytic performance [4, 5]. Many spectroscopic techniques such as Raman [4-6], Infrared (IR) [7-10, 19, 20], Ultraviolet-Visible (UV-VIS) [11,12], X-ray absorption fine structure (XAFS) [13-15, 19-21], X-ray diffraction (XRD) [21], Electron spin resonance (ESR) [16] and Nuclear magnetic resonance (NMR) [17, 18] have been applied in operando studies. Recently, two or more spectroscopic techniques were combined into one experimental setup in operando investigations [19, 22-25]. These approaches provide more detailed

information on the state of the catalyst and also the species involved in the catalytic reaction. In this methodology, the operando cell design is important so that the catalytic activity and spectroscopy can be measured simultaneously. Some designs are proposed and their feasibilities were revealed [26].

This operando methodology has also been applied to the field of environmental catalysts. Baiker et al. investigated the Pd oxidation state in the total oxidation of methane [21]. They combined operando X-ray absorption near edge structure (XANES) and XRD techniques to observe the state of supported Pd in the methane oxidation reaction up to 800 °C. Sintering of Pd and a change of valence state were observed in the methane oxidation reaction above 700 °C; these changes should be the cause of the characteristic hysteresis of the conversion as a function of temperature in a heating and cooling cycle. As shown in their work, the XAFS technique is useful for investigating the local structure and valence state of the supported noble metal in the operando experiment. Since noble metal supported catalysts are commonly used in automotive catalysts, the XAFS technique should be suitable for monitoring these during reaction. Highly intensive X-ray available in the synchrotron radiation facilities [27] help us to do XAFS experiments on catalysts loaded with low amounts of noble metal (~ 1 wt%) and with short measurement times. In this way, time-resolved XAFS experiments have been performed to observe the dynamic changes of the catalyst during reactions [15, 28]. These techniques help us to study automotive catalysts because the amounts of noble metal are typically low and the reaction conditions are always transient during driving.

This paper reports the results of operando experiments with the XAFS technique on Pt supported catalysts in the total oxidation of C_3H_6, an important reaction for automotive catalysts. The aims of this work are the following: 1) to build up the operando XAFS technique and demonstrate its feasibility, 2) to probe the catalyst activation process during the reaction. Many properties are needed for an automotive catalyst for it to achieve highly efficient exhaust purification; the catalyst activation behavior should be one of the most important for the functioning of exhaust purification system from lower temperature. Because the catalyst is at ambient temperature at the start up of an automotive engine, the catalyst has to be activated from as low a temperature as possible. In this work, the activation behavior of a supported Pt catalyst was investigated with the operando XAFS technique. The Pt valence state and catalytic reaction were monitored simultaneously as the temperature increased. The operando approach was essential in this work because the state of the catalyst has to be monitored at the start of the catalytic reaction in order to investigate the activation behavior. Using separate experiments to study the catalytic reaction in a conventional reactor then using

an in situ spectroscopic investigation under similar conditions in another cell is not useful since there would be no guarantee that both experiments were conducted under exactly the same conditions. Minor atmosphere and temperature differences can affect the results and complicate discussions. Our results suggest that the operando study of automotive catalysts will provide a detailed understand of the functioning of automotive catalyst and allow the development of advanced catalysts in a more rational way.

2. Experimental

2.1 Catalyst

Pt/γ-Al_2O_3 was prepared by the usual impregnation method. γ-Al_2O_3 (Nikki Universal) was impregnated with $Pt(NH_3)_2(NO_2)_2$ (Tanaka Kikinzoku Kogyo K.K). The impregnated catalyst was dried in an oven at 110 °C for 24 h and calcined in flowing air at 500 °C for 5 h. The Pt loading was controlled at 1 wt%. 35 mg samples of catalyst powder were pressed into disks of 10 mm diameter for the operando XAFS experiment.

The Pt dispersion was determined by CO pulse chemisorption at 50 °C using an Ohkura Riken R6015-S instrument. The sample was heated to 400 °C in flowing O_2 and held at this temperature for 15 min. After purging with He, the sample was reduced in H_2 for 15 min and then cooled to 50 °C in flowing He. A CO pulse was injected into the sample at 50 °C until the adsorption reached saturation. The amount of CO adsorbed was calculated as the difference between total amount of CO injected and the outlet from the sample. Metal dispersion was calculated by assuming a CO/surface Pt atom ratio of 1:1

2.2 Operando XAFS experiment

The XAFS investigation was carried out at the BL01B1 and BL16B2 beamlines of Spring-8 (Hyogo, Japan). The storage ring energy was 8 GeV with a typical current of 100 mA. Pt L_3-edge (11.5 keV) X-ray absorption near edge structure (XANES) spectra was measured using a Si (111) double crystal monochromator in transmission mode. Ionization chambers were used to measure the intensity of the incident and transmitted X-rays. The Quick scan technique was used in this measurement. In this technique, the monocromator was continuously moved and the energy was scanned between 11445 and 11705 eV in 40 sec [29]. Standard samples of Pt foil and PtO_2 were also measured as references for the valence state of metallic Pt^0 and oxidized Pt^{+4}. The XANES spectrum of Pt foil was also used for the energy calibration.

The operando XAFS measurements were performed with an operando spectroscopic cell. The schematic diagram for the operando XAFS experiment and side view of operando spectroscopic cell are shown Fig. 1. The cell body was made of quartz and a

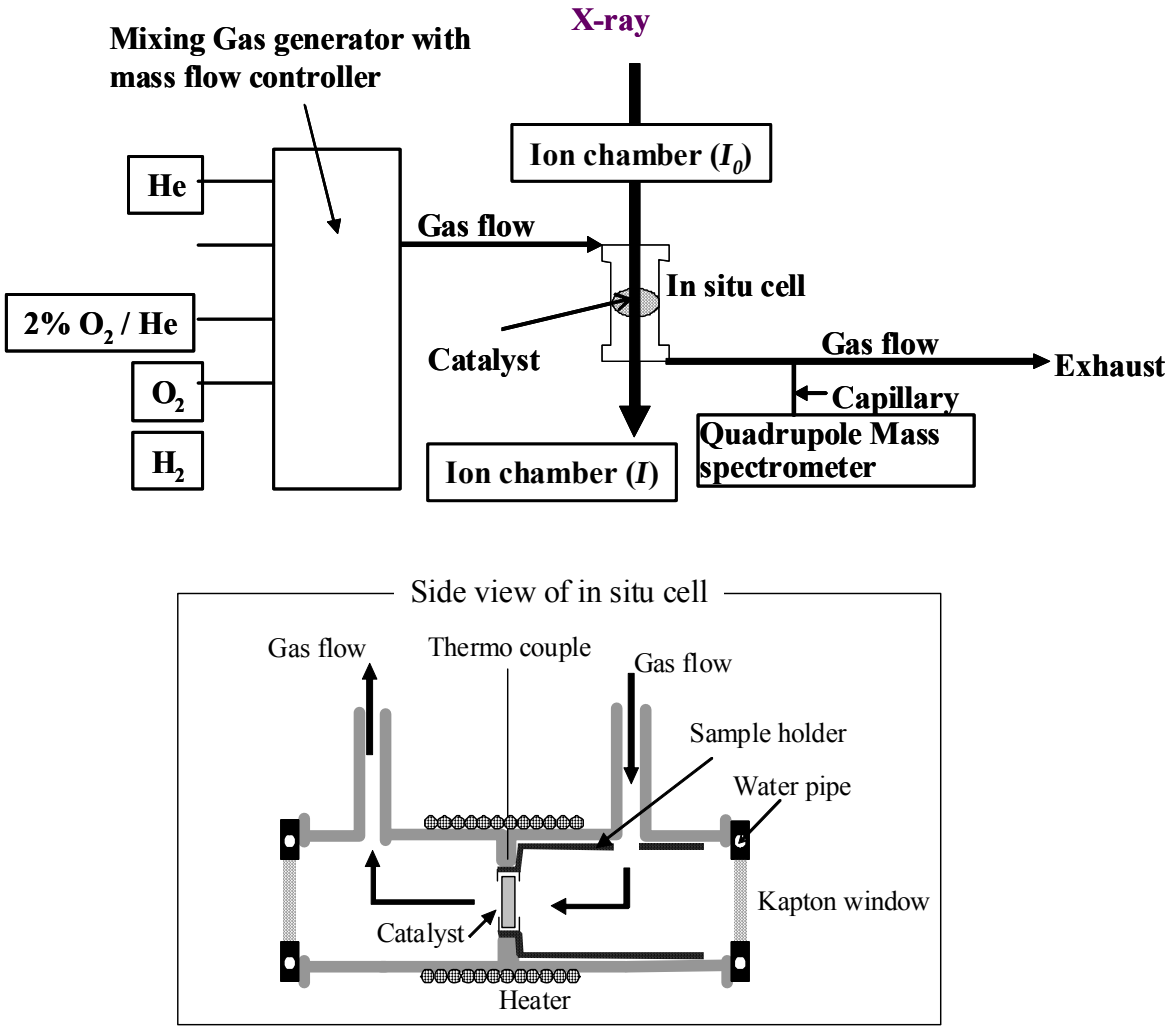

Fig.1 Diagram of the experimental set up for the operando XAFS investigation and side view of operando cell.

polyimide film (Kapton®, Du pont) window is attached to the cell for X-ray penetration. The cell body was equipped with a heater and the Kapton window was cooled with circulating water to prevent thermal breakdown of the film. This cell can be used up to 800 °C with the reaction mixture gas flow at atmospheric pressure. The self-supported catalyst disk was placed in the sample holder and the gas was introduced into this holder to make the gas flow through the catalyst disk. Gas cylinders of 1% C_3H_6/He, 2% O_2/He and He were used as sources to make the reaction mixture; O_2, H_2 and He were used for the pretreatment. The flow rate of each gas was controlled using mass flow controllers to get the correct reaction mixture. The reaction mixture was introduced into the operando spectroscopic cell and a portion of the outlet gas from the cell was introduced to the mass spectrometer (ANELVA type-M-100QA) using the capillary to measure the

concentration of H_2O, O_2, C_3H_6 and CO_2.

A self-supported catalyst disk (35 mg, 10 mm diameter) was placed in the operando spectroscopic cell and the reaction was conducted at atmospheric pressure. In the operando experiment the catalyst was pre treated as follows. At first, the catalyst was heated to 500 °C in a flow of 20% O_2 /He to burn out any adsorbed contaminations on the catalyst. The catalyst was reduced for 10 min in the flow of 3% H_2/He and oxidized for 10 min in the flow of 20% O_2 /He at 500 °C then cooled to 50 °C in the flow of 20% O_2 /He. This reduction pretreatment was performed to decompose any remaining Pt salt in the catalyst and to make dispersed metallic Pt particle. The final oxidation in pretreatment was used to simulate a situation in which automotive catalyst is oxidized by ambient atmosphere before the start up of automotive engine. After the pretreatment, the gas was switched to the reaction mixture. In this operando experiments, the total oxidation of C_3H_6 was investigated in reducing and oxidizing reaction conditions because automotive exhaust is in both atmospheres, depending on the driving conditions. Reducing (0.3% O_2 and 0.1% C_3H_6 in He) or oxidizing (0.6% O_2 and 0.1% C_3H_6 in He) reaction mixture was used in this investigation. The total flow rate was 100 ml/min for pretreatment and reaction. The heating of the cell was begun 5 min after switching to the reaction mixture to make sure that the atmosphere in the cell was completely replaced by the reaction mixture. The temperature ramping rate was controlled at 10 °C /min. During the temperature ramping, the XANES spectra were recorded every 1 min and the catalytic reaction was monitored every 1 sec by measuring the concentrations of gases in the outlet gas from the operando cell. The experimental XANES raw data were energy calibrated and normalized using homemade software.

3. Results and discussions

3.1 Reaction in reducing conditions

Fig. 2 (A) shows the change of the Pt L_3-edge XANES spectra during the ramping up of the temperature for the total oxidation of C_3H_6 in reducing conditions. Since the pretreatment consisted of oxidation in 20% O_2 /He at 500 °C, the strong peak corresponding to the oxidized Pt was observed below 100 °C, at the beginning of the reaction. During the reaction, the XANES peak height decreased as the temperature increased. This decrease of the XANES peak height corresponds to a reduction of oxidized Pt with increasing temperature because the XANES peak height corresponds to the Pt valence state [30]. While the XANES spectra were being recorded, the catalytic reaction in operando cell was monitored by measuring the outlet concentrations of H_2O, O_2, C_3H_6 and CO_2 using the mass spectrometer. The concentration changes of each

species and the fraction of oxidized Pt are plotted versus reaction temperature in Fig. 2 (B). The fraction of oxidized Pt was estimated from the peak height of the XANES

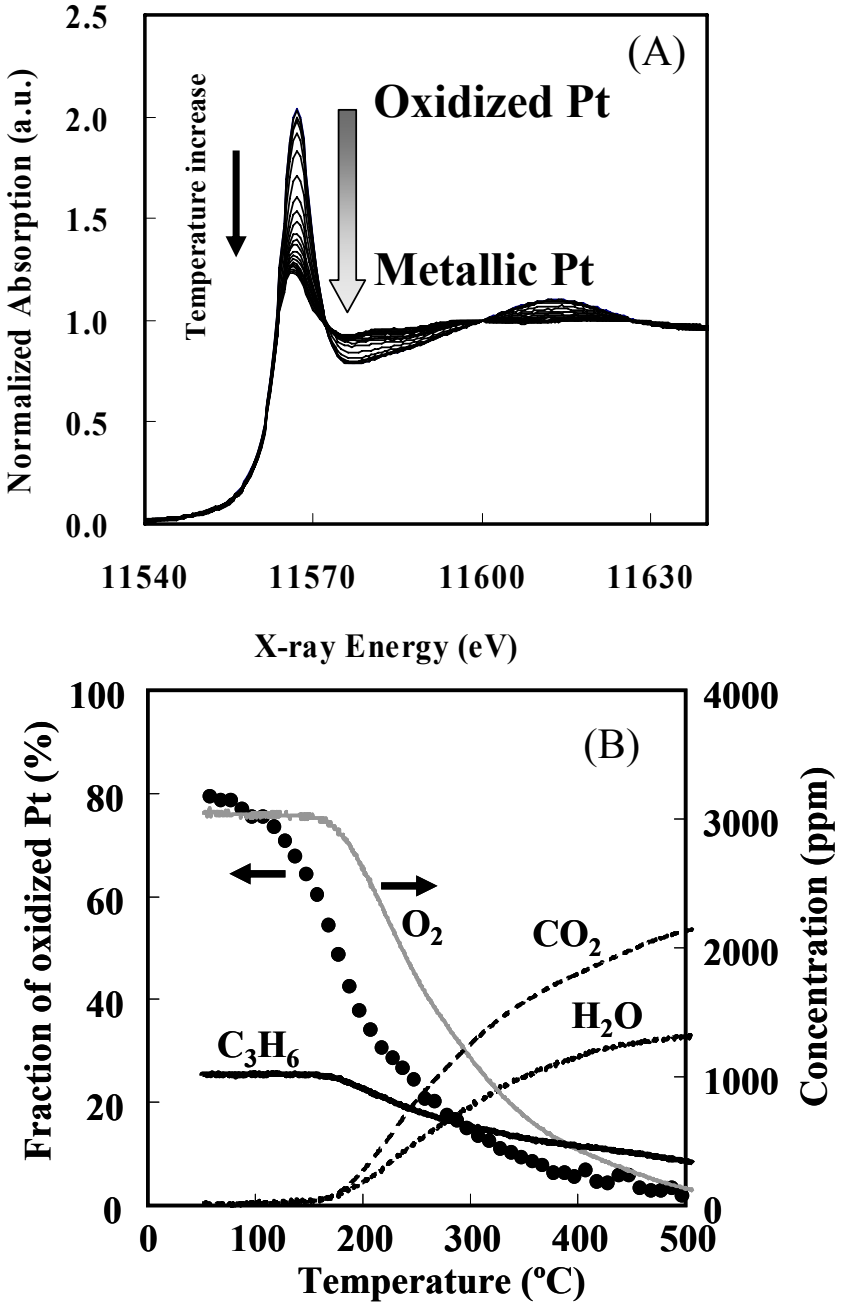

Fig. 2 (A) The Pt L_3-edge XANES spectrum during C_3H_6 oxidation reaction in reducing mixture (0.3% O_2 and 0.1% C_3H_6 in He, total flow of 100 ml/min) over Pt/ γ -Al_2O_3 (35mg). (B) Changes of the fraction of oxidized Pt and the concentrations of C_3H_6, O_2, CO_2 and H_2O during the reaction of the reducing mixture over Pt/ γ -Al_2O_3 as a function of temperature. The oxidized Pt fraction was estimated from the XANES peak height based on the linear correlation between Pt valence state and XANES peak height.

spectra, based on the assumption of linear correlation between the valence state of Pt and the XANES peak height [31]. In this assumption, the XANES peak heights of PtO_2 and Pt foil were assigned to 100% oxidized Pt and 0% oxidized Pt (100% metallic Pt). Since the measured XANES peak height of Pt /γ-Al_2O_3 during reaction located between these two peak heights, oxidized Pt fraction was estimated by linear correlation between the peak height and oxidized Pt fraction. The fraction of oxidized Pt was found as 80% at 50° C. At this temperature, no change of XAENS spectrum was observed in gas switching from 20% O_2/He to reducing reaction mixture. This means there was no reaction between oxidized Pt and reducing reaction mixture at 50° C. The reason is not clear why 80% oxidized Pt fraction was found after oxidizing pretreatment. A possible interpretation would be following; 20% of metallic Pt could be located in inner part of some large Pt particles formed during pretreatment procedure. Such large Pt particles could exist in particle size distribution and inner part Pt in such a large Pt particle might be difficult to be oxidized at 500 ° C. In comparing the catalytic reaction and the Pt valence change, the valence state change began at about 100 °C, fairly lower than the temperature at which the catalytic reaction started. The catalytic reaction started at about 160 °C and about 40% of Pt was reduced at this temperature. After the start of the catalytic reaction, the reduction of Pt proceeded with the catalytic conversion increasing with increasing temperature. This result showed that some of the oxidized Pt was reduced without net catalytic reaction at low temperature. The reaction between the adsorbed species relating to hydrocarbon and oxidized Pt is likely to be responsible for this Pt reduction.

3.2 Reaction in oxidizing conditions

Fig. 3 (A) shows XANES spectra measured during the reaction in oxidizing conditions. Even in this oxidizing condition, spectra changed with reaction temperature although the change was not monotonous and as large as in reducing condition. This means some of the oxidized Pt was reduced during reaction even in oxidizing condition. As the same in reducing condition, fraction of oxidized Pt was estimated and plotted versus temperature in Fig. 3 (B) with the concentration of C_3H_6, O_2, CO_2 and H_2O. As the same as in reducing conditions, some of the oxidized Pt was reduced at low temperature without net catalytic reaction. The catalytic reaction began at about 160 °C and about 40% of Pt was reduced at this temperature. This result was almost the same as in reducing conditions. After the start of the catalytic reaction, Pt reduction proceeded and the conversion increased as the temperature was ramped up. In contrast to reducing conditions, the fraction of oxidized Pt turned to increase above 200 °C. It is worth noting that some of the oxidized Pt was reduced at low reaction temperatures even in

oxidizing conditions, although re-oxidation at higher temperature is reasonable.

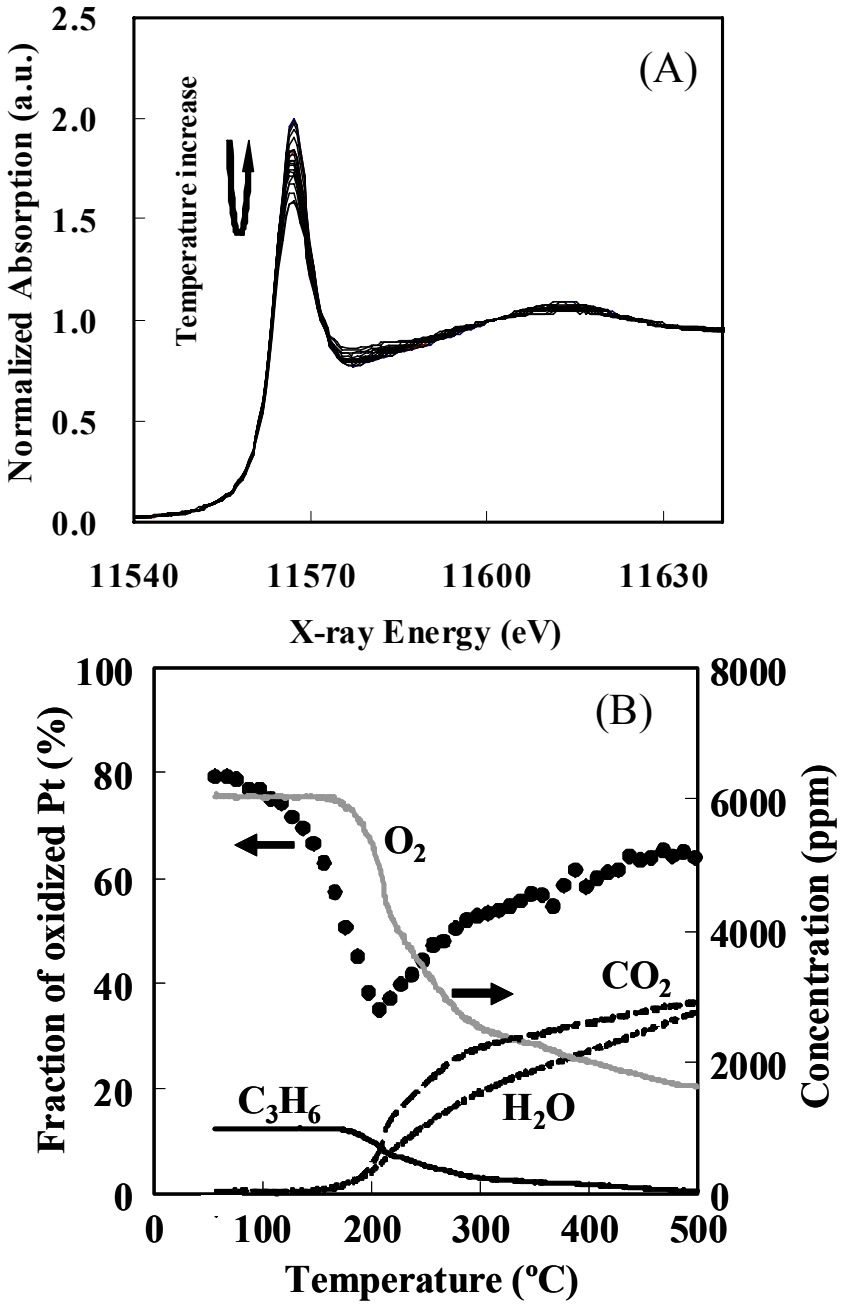

Fig.3 (A) The Pt L_3-edge XANES spectrum during C_3H_6 oxidation reaction in oxidizing mixture (0.6% O_2 and 0.1% C_3H_6 in He, total flow of 100 ml/min) over Pt/ γ -Al_2O_3 (35mg). (B) Changes of the fraction of oxidized Pt and the concentrations of C_3H_6, O_2, CO_2 and H_2O during the reaction of the reducing mixture over Pt/ γ -Al_2O_3 as a function of temperature. The oxidized Pt fraction was estimated from the XANES peak height based on the linear correlation between Pt valence state and XANES peak height.

3.3 Reaction scheme based on the operando investigations

Fig. 4 was illustrated to discuss the catalyst activation behavior in the two atmospheric conditions in unified fashion, where the fraction of metallic Pt and conversions are plotted together. The metallic Pt fraction was chosen since metallic Pt sites are considered as the active sites for the catalytic reactions [32]. In Fig.4 the conversions were calculated from the concentration changes during ramping up temperature as shown Fig. 2(B) and 3(B). So, Fig.4 shows the truly operando results; i.e., valence state of noble metal and catalytic activity were measured simultaneously in operando cell. The C_3H_6 conversion in oxidizing and the O_2 conversion in reducing conditions were chosen as the reaction progress indicator, because those conversions

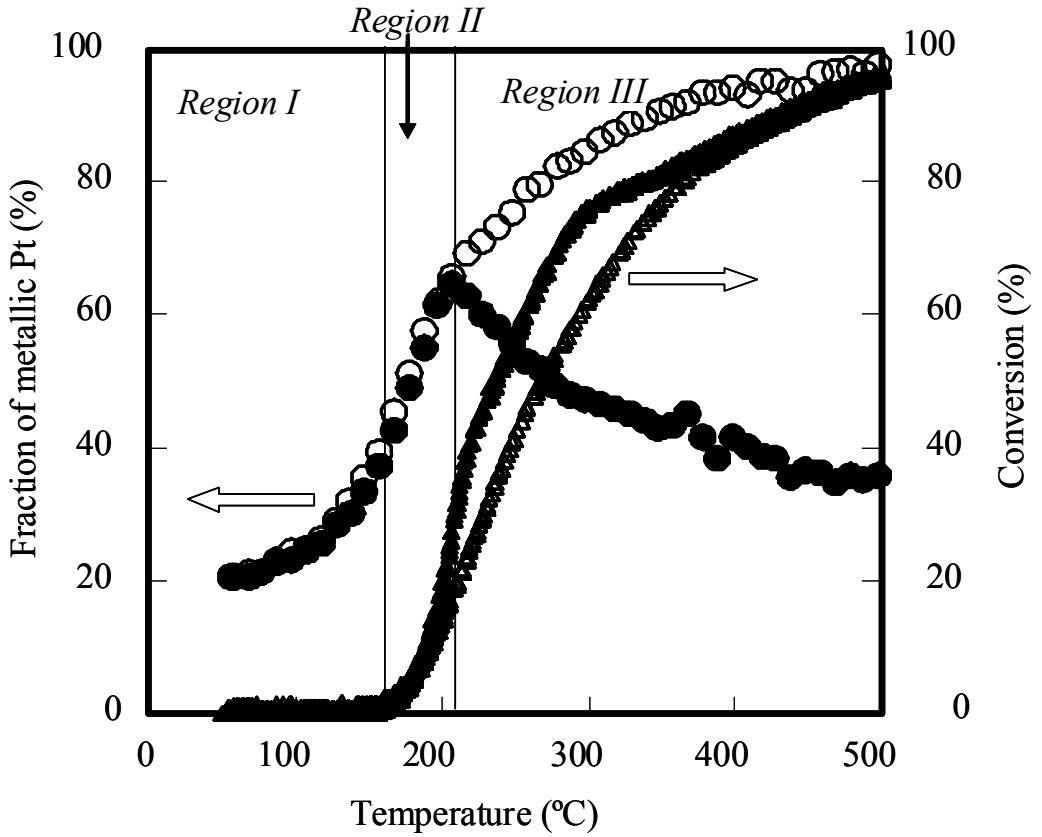

Fig.4 The temperature dependences of the fraction of metallic Pt and the conversions in the catalytic reaction over Pt/ γ -Al_2O_3 in reducing and oxidizing conditions: the fraction of metallic Pt in reducing conditions (○), in oxidizing conditions (●), O_2 conversion in reducing conditions (Δ), C_3H_6 conversion in oxidizing conditions (▲). Region I; metallic Pt fraction increases without any increase of conversion for both conditions. Region II; the conversions increased with increasing fraction of metallic Pt for both conditions. Region III; the correlations between the conversion and metallic Pt fraction were different for both conditions.

start from 0% at the beginning of the reaction at low temperature and reach 100% at a sufficiently high temperature. In this figure, the temperature can be divided into three regions as indicated in Fig. 4. In region I, the Pt valence changed without any catalytic conversion in both oxidizing and reducing conditions. In region II, the Pt valence changed along with the catalytic conversions but the temperature dependences of metallic Pt fraction were the same in both cases. In region III, the temperature dependences of metallic Pt fractions under the two atmospheric conditions were different. Fig. 5 shows the proposed schemes that correspond to the situation on the catalyst in each temperature region and each atmospheric condition.

In region I, the oxidized Pt was reduced without any increase of C_3H_6 or O_2 conversion under both conditions. Also, the temperature dependences of the metallic Pt fractions were almost the same. The catalytic reaction start temperatures were also the same in both cases and 40% of Pt was reduced at the start temperature. The kinetic study on the C_3H_6 - O_2 reaction over the Pt catalyst showed that the reaction order was negative for C_3H_6 and positive for O_2 [32]. This C_3H_6 self-poisoning effect means that C_3H_6 should be preferentially adsorbed on Pt compared with O_2 and the adsorption of C_3H_6 is likely to predominate regardless of whether the atmosphere is reducing or oxidizing, as shown in Fig. 5. The reaction between the adsorbed C_3H_6 and the oxidized Pt should cause the reduction of the oxidized Pt. In this region, the temperature might not be high enough for the reaction between the adsorbed C_3H_6 and oxygen to produce gaseous CO_2 that mean the net catalytic reaction cycle of the total oxidation of C_3H_6. The C_3H_6 oxidation mechanism on Pt(111) has been investigated with in situ soft X-ray fluorescence methods in the presence of O_2 [33, 34]. That study showed that the oxidation of pre-adsorbed C_3H_6 proceeded in two steps, the oxydehydrogenation of adsorbed C_3H_6 occurring around ambient temperature prior to skeletal oxidation. The oxydehydrogenation creates the 1-methylvinyl species as the intermediate on the Pt surface. They reported that this intermediate was sufficiently stable in some temperature regions and that the skeletal oxidation occurred above 100 °C to produce gaseous CO_2. Our results for region I agree well with this proposed mechanism. The oxydehydrogenation process for adsorbed C_3H_6 is likely to be responsible for Pt reduction. Because the skeletal oxidation of the intermediate 1-methylvinyl did not occur in this region of temperature, it would cover the Pt surface and the catalytic reaction should stop since no vacant site is available. During this oxydehydrogenation, H_2O should be produced corresponding to oxidized Pt reduction. The amount of H_2O produced in this process should correspond to the amount of reduced Pt that was estimated as about 10 μmol (20% of total Pt). Because this value should be too small to

detect H_2O concentration change in the flow reactor system, no catalytic reaction was observed in the gas phase.

In region II, the net catalytic reactions began and the conversions increased with increasing temperature. The temperature dependences of the metallic Pt fractions were the same for both atmospheric conditions. Because the conversion was below 30% in this region, the overall reaction may be determined by the reaction on active sites. In other words, the number of active sites and their turnover frequency determines the overall reaction with all active sites contributing equally to the reaction. The observed Pt valence state should therefore be linked to the observed catalytic reaction. The dispersion of Pt in Pt/γ-Al_2O_3 was 55% as determined by the CO pulse adsorption method. If the reduction of oxidized Pt proceeds from the surface of Pt particle, some metallic Pt fraction value corresponds to monolayer Pt reduction of Pt particle. Taking into account that 20% metallic fraction was found before the reaction and 55% dispersion was determined by CO adsorption, about 75% metallic fraction would correspond to monolayer reduction of Pt particle. Based on this consideration, the metallic Pt fraction was less than the monolayer of Pt Particle in Region II. This means

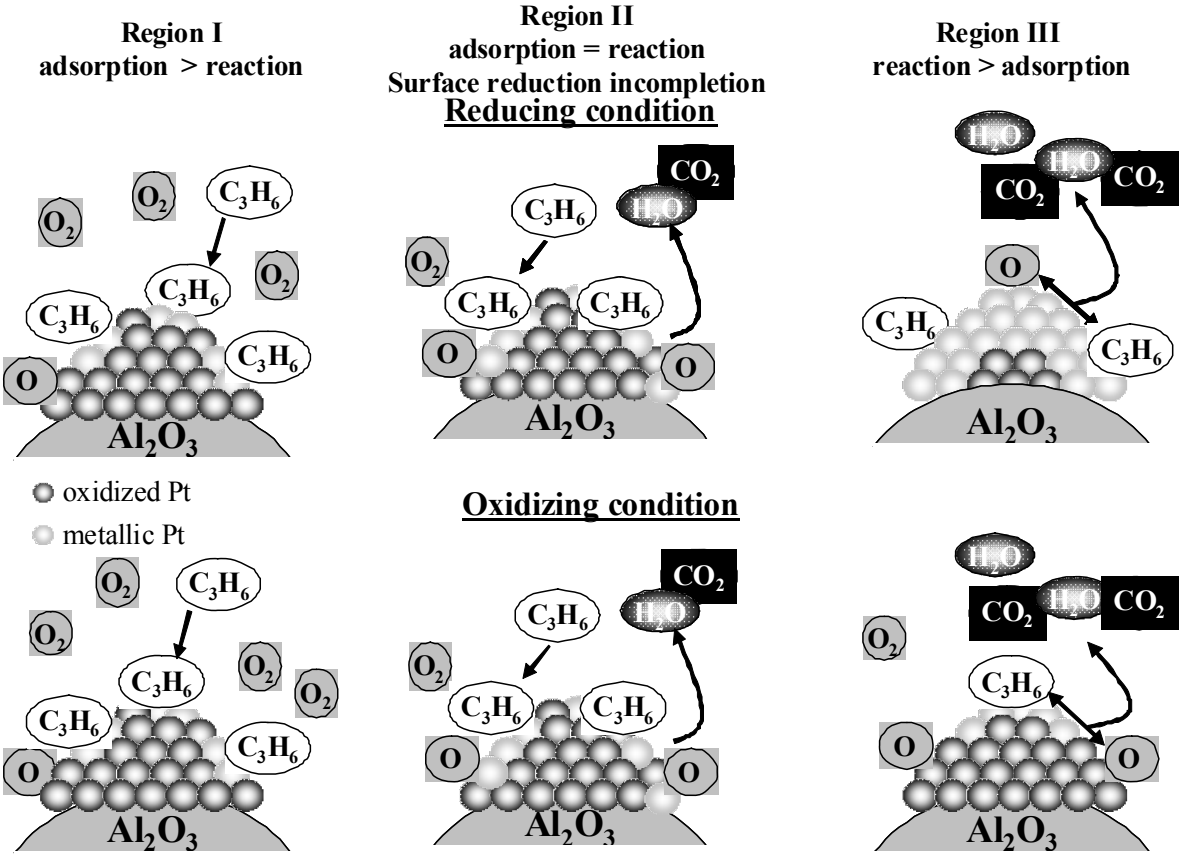

Fig.5 The proposed schemes of the situation on the catalyst in regions I, II and III in reducing and oxidizing reaction conditions.

that oxidized and metallic Pt would coexist at the surface of the Pt particles, as shown Fig. 5. The fraction of metallic Pt at the surface of Pt particles increases with increasing temperature in region II. Accordingly, the creation of active sites on the surface of Pt particles and the net catalytic reaction on them occurred simultaneously in this region. This result means that the early stage of the catalyst activation process was the coupled phenomenon combining the creation of the active sites and the catalytic reaction on them. In relatively higher temperature part of region II, the conversion in oxidizing conditions was slightly higher for the same fraction of metallic Pt. Because the number of active sites was considered to be the same for both conditions, the oxygen kinetic promotional effect on the C_3H_6 oxidation should be responsible for the slightly higher conversion in oxidizing conditions [32].

In region III the Pt valence behavior for the two conditions were totally different. The metallic Pt fraction increased with increasing temperature in reducing conditions but decreased in oxidizing conditions. Because the conversions were greater than 30% in region III, behavior on the active sites does not determine the overall reaction nor do these contribute equally. This means that the observed Pt valence states should not be directly correlated with the catalytic reaction. The residual C_3H_6 and oxygen after the reaction should affect the observed Pt valence in both reducing and oxidizing conditions as shown in Fig. 5. This situation would be the reason for the behavior in region III in which the same conversion was obtained over catalysts with different fractions of metallic Pt. The result obtained here might be spectroscopic evidence for a kinetically controlled regime restricted to below 30% in the fixed bed reactor.

4. Conclusion

The operando XAFS experiments were performed with the Quick-XAFS technique and catalytic conversions measurements using a mass spectrometer in ramping temperature mode. These experiments have enabled us to simultaneously monitor the Pt valence state and the catalytic conversion in the total oxidation of C_3H_6 over Pt/γ-Al_2O_3 catalysts. The observation of the Pt valence state in the catalyst activation process revealed that early stage of catalyst activation was the combination of creating active sites and the catalytic reaction on them. This activation process was the same in reducing and oxidizing conditions. These results indicate that both the creation of metallic Pt sites and the activation of adsorbed species on Pt are important for the functioning of the catalytic reaction at low temperature. These results provide an important basis for improvement of the catalytic purification system both by developing the catalyst material and controlling the exhaust atmosphere that promotes Pt reduction

and suppresses the poisoning. As shown here, the operando methodology was found to be a very useful technique for the automotive catalyst research field.

Acknowledgements

We gratefully thank Dr. Uruga, Dr. Tanida and Dr. Kato (Japan Synchrotron Research Institute) for their assistance in the XAFS experiments at Spring-8.

References

[1] H. Topsøe, J. Catal. 216 (2003) 155.

[2] B.M. Weckhuysen, Phys. Chem. Chem. Phys. 5 (2003) 4351.

[3] M.A. Banares, Catal. Today 100 (2005) 71.

[4] S.M. Bennici, B.M. Vogelaar, T.A. Nijhuis and B.M. Weckhuysen, Angew. Chemie. Int. Edt. 46 (2007) 5412.

[5] T. A. Nijhuis, S. J. Tinnemans, T.Visser and B .Weckhuysen, Chem. Eng. Sci. 59 (2004) 5487.

[6] O. Demoulin, M. Navez, E.M. Gaigneaux, P. Ruiz, A. Mamede, P. Granger and E. Payen, Phys. Chem. Chem. Phys. 5 (2003) 4394.

[7] T. Lesage, C. Verrier, P. Bazin, J. Saussey and M. Daturi, Phys. Chem. Chem. Phys. 5 (2003) 4435.

[8] T. Lesage, J. Saussey, S. Malo, M. Hervieu, C. Hedouin, G. Blanchard and M. Daturi, Appl. Catal. B Environ. 72 (2007) 166.

[9] F.C. Meunier, A. Goguet, C. Hardacre, R. Burch and D. Thompsett, J. Catal. 252 (2007) 18.

[10] D. Tibiletti, F.C Meunier, A. Goguet, D. Reid, R. Burch, M. Boaro, M. Vicario and A. Trovarelli, J. Catal. 244 (2006) 183.

[11] R.L. Puurunen, B.G. Beheydt and B.M. Weckhuysen, J. Catal. 204 (2001) 253.

[12] R.L. Puurunen and B.M. Weckhuysen, J. Catal. 210 (2002) 418.

[13] C. Lamberti, S. Bordiga, F. Bonino, C. Prestipino, G. Berlier, L. Capello, F. D'Acapito, F.X.L.I. Xamena, A. Zecchina, Phys. Chem. Chem. Phys., 5 (2003) 4502.

[14] M. Caravati, J.D. Grunwaldt and A. Baiker, Catal.Today 126 (2007) 27.

[15] M. Tada, S. Murata, T. Asakoka, K. Hiroshima, K. Okumura, H. Tanida, T. Uruga, H. Nakanishi, S. Matsumoto, Y. Inada, M. Nomura and Y. Iwasawa, Angew. Chem. Int. Edit. 46 (2007) 4310.

[16] A. Bruckner, Phys. Chem. Chem. Phys. 5 (2003) 4461.

[17] M. Hunger, W. Wang, Chem. Commun. (2004) 584.

[18] M. Hunger and T. Horvath, J. Chem. Soc., Chem. Commun. (1995) 1423.

[19] M.A. Newton, A.J. Dent, S.G. Fiddy, B. Jyoti and J. Evans, Catal. Today 126 (2007) 64.

[20] C. Mondelli, D. Ferri, J.D.Grunwaldt, F. Krumeich, S. Mangold, R. Psaro and A. Baiker, J. Catal. 252 (2007) 77.

[21] J.D. Grunwaldt, N. van Vegten and A. Baiker, Chem. Commun. (2007) 4635.

[22] A. Brückner, Chem. Commun (2005) 1761.

[23] A.M.Beale, A.M.J. van der Eerden, K. Kervinen, M.A.Newton, and B.M. Weckhuysen, Chem. Commun (2005) 3015.

[24] S.J. Tinnemans, J.G. Mesu, K. Kervinen, T. Visser, T.A. Nijhuis, A.M. Beale, D.E. Keller, A.M.J. van der Eerden and B.M. Weckhuysen, Catal. Today 113 (2006) 3.

[25] A. Brückner and E. Kondratenko, Catal. Today 113 (2006) 16.

[26] S. R. Bare, N. Yang, S.D. Kelly, G.E. Mickelson and F.S. Modica, Catal. Today 126 (2007) 18.

[27] S. Ferrer and Y. Petroff, Surf. Sci. 500 (2002) 605.

[28] T. Yamamoto, A. Suzuki, Y. Nagai, T. Tanabe, F. Dong, Y. Inada, M. Nomura, M. Tada and Y. Iwasawa, Angew. Chem. Int. Ed. 46 (2007) 9253.

[29] K. Okumura, K. Kato, T. Sanada and M. Niwa, J. Phys. Chem. C 111 (2007) 14426.

[30] A.N. Mansour, J.W. Cook, D.E. Sayers, J. Phys. Chem. A 88 (1984) 2330.

[31] H. Yoshida, S. Nonoyama, Y. Yazawa, T. Hattori, Phys. Scr. T 115 (2005) 813.

[32] Yung-Fang and Yu Yao, J. Catal. 87 (1984) 152.

[33] D.J. Burnett, A.M. Gabelnick, A.L. Marsh, D.A. Fischer, J.L. Gland, Surf. Sci. 553 (2004) 1.

[34] A.M. Gabelnick, A.T. Capitano, S.M. Kane, J.L. Gland and D.A. Fischer, J. Am. Chem. Soc. 122 (2000) 143.

Chapter 3

Controlling factors in catalytic activities of noble metal supported catalysts ～control of self poisoning by reactants～

3.1 Comparative NO_x reduction behavior of Pt, Pd, and Rh supported catalysts in simulated exhaust gases as a function of oxygen concentration

Abstract

NO_x reduction activity on Pt and Pd catalysts had a maximum for S value as stoichiometry number at a fixed temperature, and the S value at the maximum NO_x conversion increased with decreasing temperature. NO_x conversion on Rh catalyst increased with decreasing S value, but independent of temperature. As for the effect of HC on NO_x reduction behavior, it was concluded that, for Pt and Pd catalysts, HC adsorbs strongly on the catalysts surface to cause the self-inhibition. Increasing O_2 concentration lead to oxidation of HC, but decreased the value of NO/O_2 ratio. The balance point of the two factors generated a maximum NO_x conversion. For Rh catalyst, the strongly adsorbed oxygen is more reactive with decreasing S value, and thus NO_x conversion is increased.

1. Introduction

Automotive exhaust catalysts containing noble metals have been extensively used as three-way catalyst. It is well known that NO_x is reduced almost perfectly into nitrogen on the three-way catalysts under the stoichiometric condition. But, the efficiency of NO_x reduction on the three-way catalysts is very poor under oxidizing condition because of competitive reduction between a large excess oxygen and NO_x with reducing gases. Many researchers have investigated the selective NO_x reduction by hydrocarbons (HC) on supported noble metal catalysts under oxidizing condition [1–4]. Pt supported catalysts reveal the NO_x reduction activity under relatively low temperature, around 200 ˚C, and the activity decreases to negligible small level with increasing temperature. That is, there is a maximum of NO_x reduction activity for temperature on Pt catalyst under oxidizing condition. On the other hand, the NO_x conversion is nearly 100% at stoichiometric point, but nearly 0% level under large excess oxidizing condition in high temperature region around 500 ˚C. Though temperature and atmosphere are key functions for NO_x reduction activity on the catalysts, the relationship has not yet been clarified.

This study is to reveal the influence of both functions of temperature and atmosphere on the NO_x reduction activity on Pt, Pd and Rh catalysts, which are used in current commercial three-way catalysts, loaded on alumina. This report mainly concentrated on the NO_x reduction activities on the catalysts using simulated automotive exhaust gases at 200 to 500 ˚C, and O_2 concentration at 0.1% to 10%, respectively.

2. Experimental

2.1 Catalysts

All catalysts were prepared by a conventional impregnation method using 210–420 μm diameter α-alumina pellets (a BET area of 10 m^2/g; bulk density of 0.79 g/cm^3). α-Alumina was used to know the intrinsic character of noble metals on the catalysts. The details of the catalyst preparation have been reported elsewhere [5]. The amounts of Pt, Pd and Rh loaded were 0.25 wt% as the noble metal. The noble metal dispersion of the Pt, Pd and Rh catalysts were 0.08, 0.13 and 0.11, respectively, by CO pulse method, assuming one molecule adsorbs to a noble metal atom [6].

2.2 Catalytic activity measurements

Catalytic activity data were obtained using a conventional fixed-bed flow reactor at atmospheric pressure as described elsewhere [7]. A quartz tube with an inner diameter of 18 mm was chosen as the reactor tube. A catalyst was placed on a quartz filter at the middle part of the reactor. The upper part of the catalyst bed was packed with inactive SiC spheres of 3 mm o.d. for preheating the feed gas. Furnace temperature was controlled within a maximum variation of 1.5 ˚C by an automatic temperature controller. The gas leaving the reactor was led to a condenser to remove the water vapor. The remaining components were continuously analyzed by non dispersive infrared (CO and CO_2), flame ionization (HC), flame photometry (SO_2), magnetic susceptibility (O_2), and chemiluminescence (NO_x), respectively.

In this study, catalytic activity using simulated exhaust gases were mainly measured as both a function of temperature and O_2 concentration for the catalysts. A feed composition of simulated exhaust gas was 0.015 vol% CO, 1200 ppm C as C_3H_6, 230 ppm NO, 25 ppm SO_2, 5 vol% H_2O, 6.7 vol% CO_2, and the balance N_2. O_2 concentration was changed 23 times between 0.1 and 10 vol%. The temperature was changed from 200 to 500 ˚C every 50 ˚C. Space velocity was kept at 30,000 h^{-1}. Catalytic activity was expressed as the percent conversions of HC, CO, SO_2 and NO_x. The conversion of N_2O is defined as 2[N_2O formation] / [inlet NO]. The stoichiometry number, S, used to identify the redox characteristic of the model gas mixtures is defined as in the following formula (1).

$$S = (2[O_2] + [NO]) / ([CO] + 9[C_3H_6]) \quad (1)$$

When S < 1, S=1, and S > 1, the composition of the feed stream is net reducing, stoichiometric, and net oxidizing, respectively.

The other catalytic activity test, which replaced 1200 ppmC C_3H_6 by 0.36 vol% CO, was done for the catalysts in the same way for clarifying the effect of HC. Another test with changing C_3H_6 concentration from 430 to 4650 ppmC at a fixed O_2 concentration of 0.4 vol% was also done for Pt catalyst in the same way.

3. Results and discussion

3.1 Pt catalyst

The conversions of HC, CO, SO_2, NO_x, and N_2O on a Pt catalyst were measured from 200 to 500 ˚C every 50 ˚C. As an example, the results at 250 ˚C were plotted as a function of S, as shown in figure 1. From these data, the conversions of CO, HC and SO_2 as a function of S at several temperatures on the Pt catalyst were summarized in figures 2–4, respectively. These conversions were higher as increasing with temperature and O_2 concentration. Among of the three gases, the order of oxidation on the Pt catalyst was: CO > HC > SO_2. The NO_x conversion on the Pt catalyst plotted as both a function of temperature and S in the simulated exhaust gases are summarized in Figure 5. Above 400 ˚C, NO_x conversion reached the highest value at stoichiometric conditions. However, below 400 ˚C, NOx conversion curve had a maximum for S values at every temperature. The S value at the NO_x maximum conversion increased with decreasing temperature. Figure 6 shows the NOx maximum conversion points for the Pt catalyst as both a function of temperature and S value. Considering Pt catalysts in practical use, if O_2 concentration in exhaust gas could be systematically controlled, a great improvement of NO_x reduction activity could be attained by fitting S value to a NO_x maximum at every temperature.

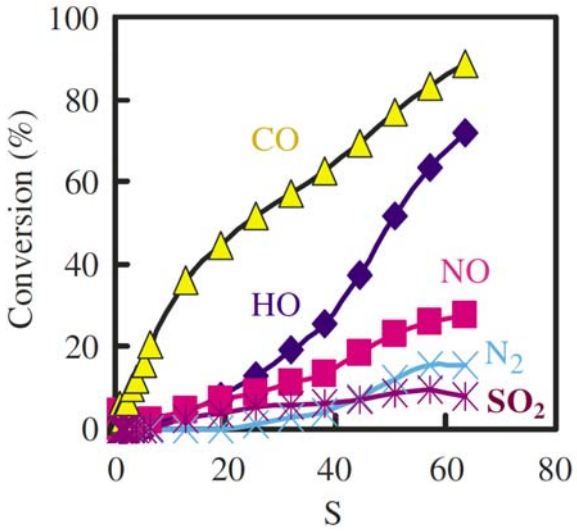

Fig. 1 Conversions of HC, CO, SO_2, NO_x, and formation of N_2O as a function of S on Pt catalyst at 250 °C in the simulated exhaust gases.

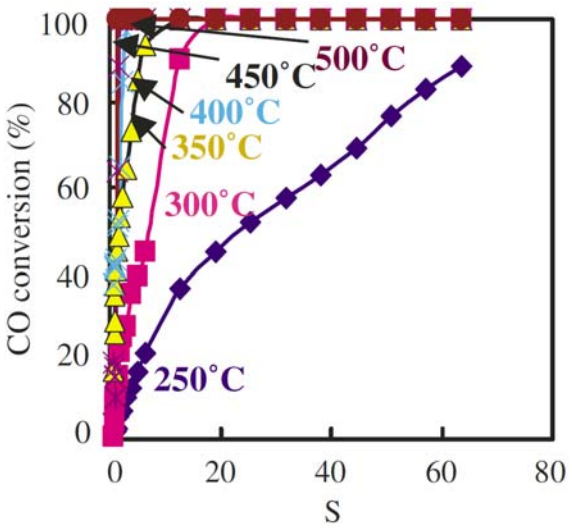

Fig. 2 CO conversions as a function of S on Pt catalyst at several temperatures in the simulated exhaust gases.

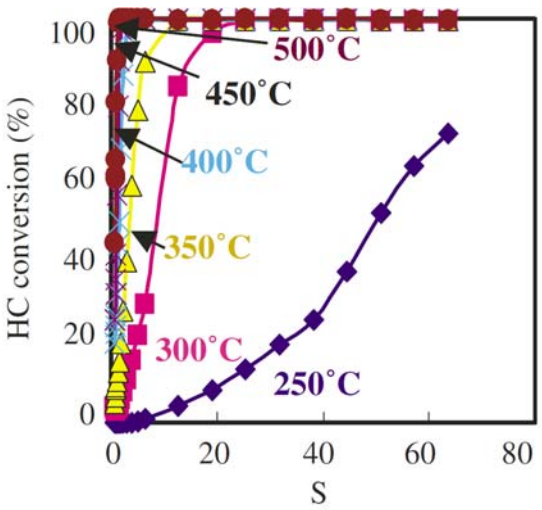

Fig. 3 HC conversions as a function of S on Pt catalyst at several temperatures in the simulated exhaust gases.

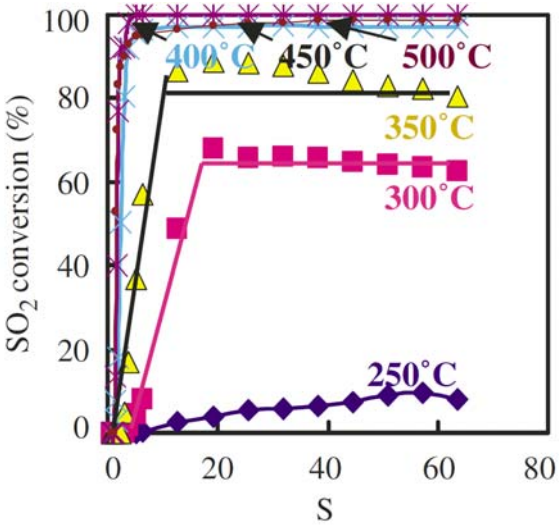

Fig.4 SO_2 conversions as a function of S on Pt catalyst at several temperatures in the simulated exhaust gases.

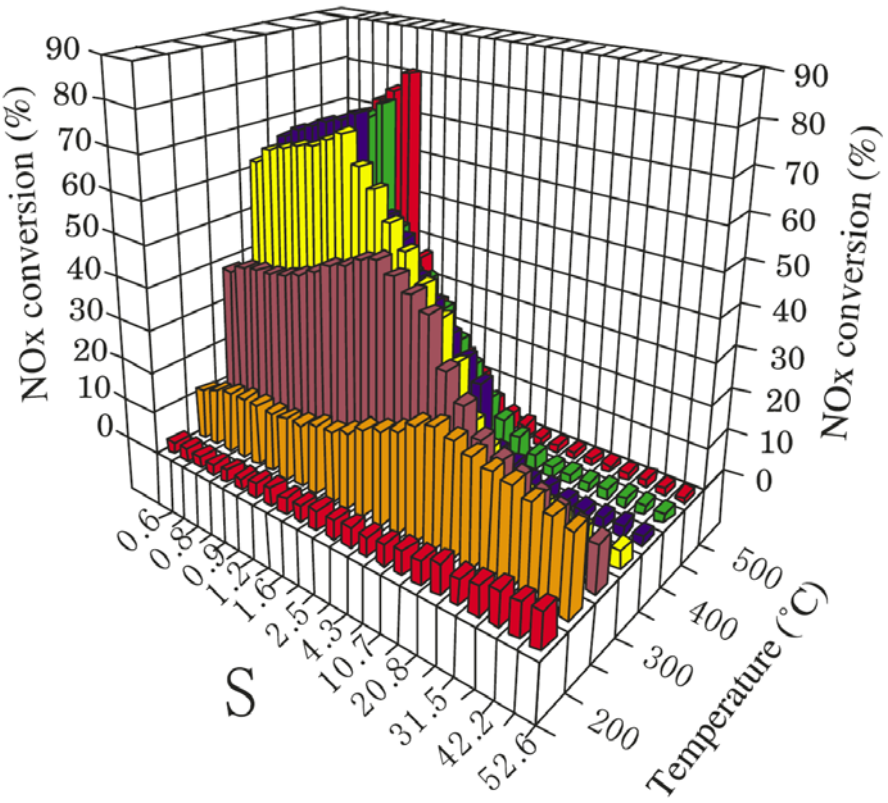

Fig.5 NO_x conversion on Pt catalyst in the simulated exhaust gases as both a function of temperature and S.

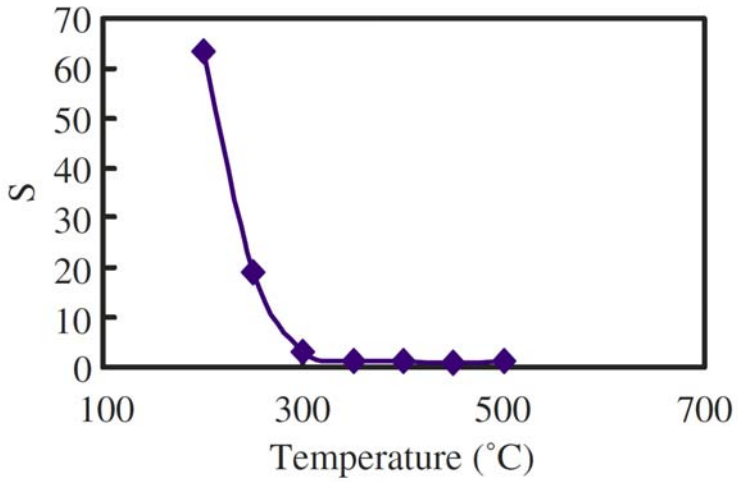

Fig. 6 S value for the maximum NO_x conversion at each temperature on Pt catalyst.

3.2 Pd catalyst

Figure 7 shows the NO_x conversion as both a function of temperature and S for a Pd catalyst. NO_x reduction activity on the Pd catalyst was not superior to that on the Pt catalyst. NO_x reduction behavior was similar to the Pt catalyst, that is, a maximum of NO_x conversion for S values existed at every temperature, and the S value at the NO_x maximum conversion was increased with decreasing temperature.

3.3 Rh catalyst

Figure 8 shows the NO_x conversion as both a function of temperature and S on a Rh catalyst. NO_x reduction behavior on the Rh catalyst was different from that on the Pt and Pd catalysts. That is, NO_x conversion was increased with decreasing S value, but independent of temperature.

3.4 NO_x reduction on Pt and Rh catalysts without HC

NO_x conversions on the Pt and Rh catalysts using the simulated exhaust gas in which C_3H_6 was replaced by CO, are shown in figures 9 and 10. In these cases, NO_x conversion was the highest at stoichiometric condition on the both catalysts at every temperature. Comparing figures 5 and 9 for the Pt catalyst, NO_x reduction behavior changed drastically with the existence of HC. These results indicated that HC oxidation was a rate-determining step for the reaction. On the other hand, NO_x reduction behavior was similar to that on the Rh catalyst independent of the existence of HC.

3.5. Effect of HC concentration on the Pt catalyst

Figure 11 shows both NO_x and O_2 conversions, plotted as a function of S with the variable of C_3H_6 concentration at 300 ˚C. Not only the NOx conversion, but O_2 conversion has a maximum as a function of S value, and the behavior of both conversions was similar under this condition. This result supported our suggestion, that HC oxidation is a rate-determining step in the whole reaction process.

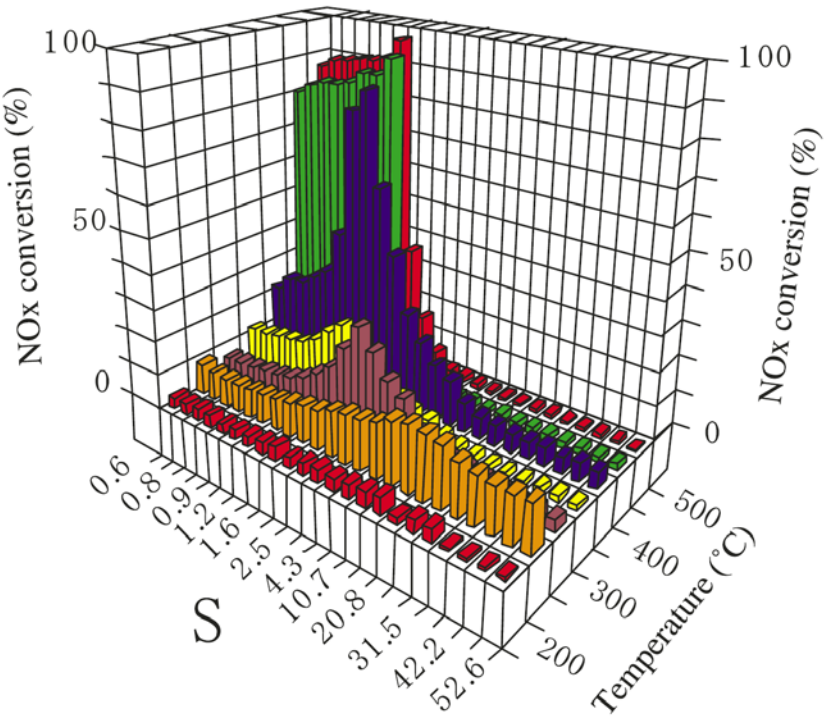

Fig. 7 NO_x conversion on Pd catalyst in the simulated exhaust gases as both a function of temperature and S.

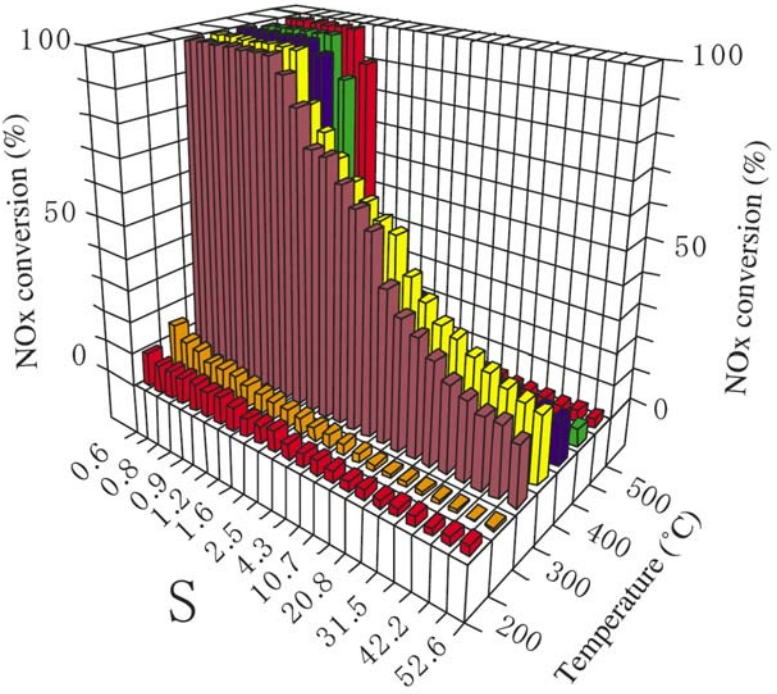

Fig. 8 NO_x conversion on Rh catalyst in the simulated exhaust gases as both a function of temperature and S.

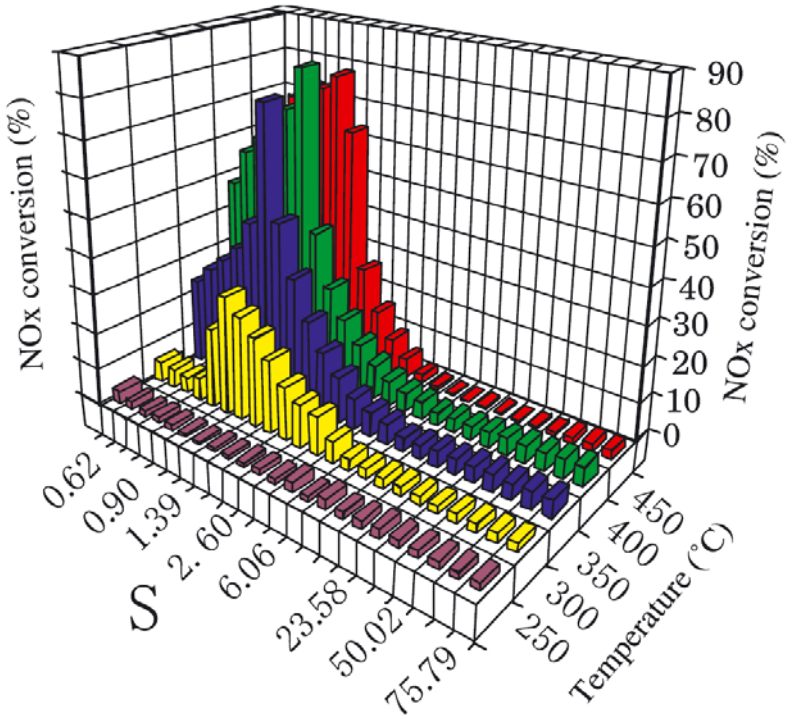

Fig. 9 NO_x conversion on Pt catalyst in the simulated exhaust gases, in which C_3H_6 replaced by CO, as both a function of temperature and S.

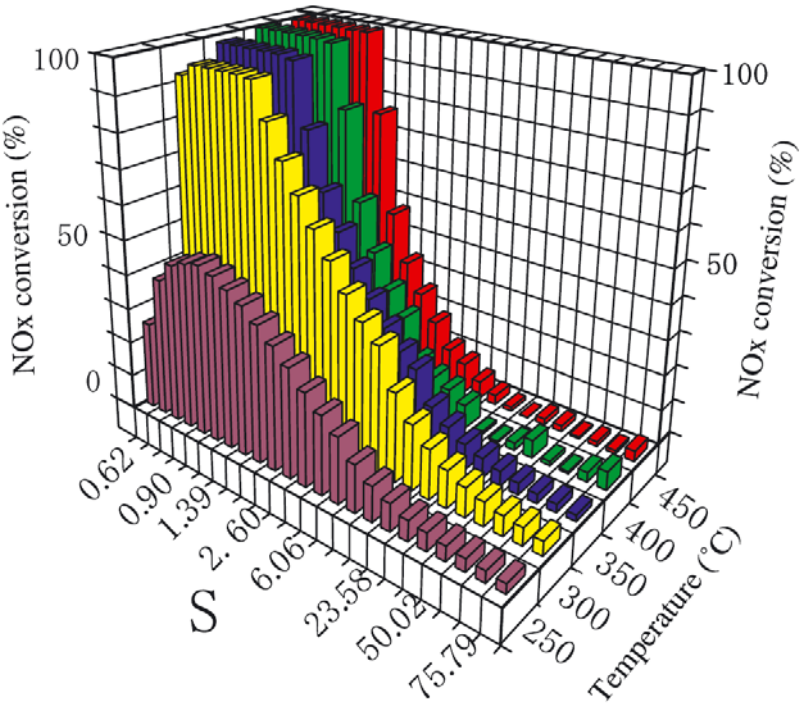

Fig. 10 NO_x conversion on Rh catalyst in the simulated exhaust gases, in which C_3H_6 replaced by CO, as both a function of temperature and S.

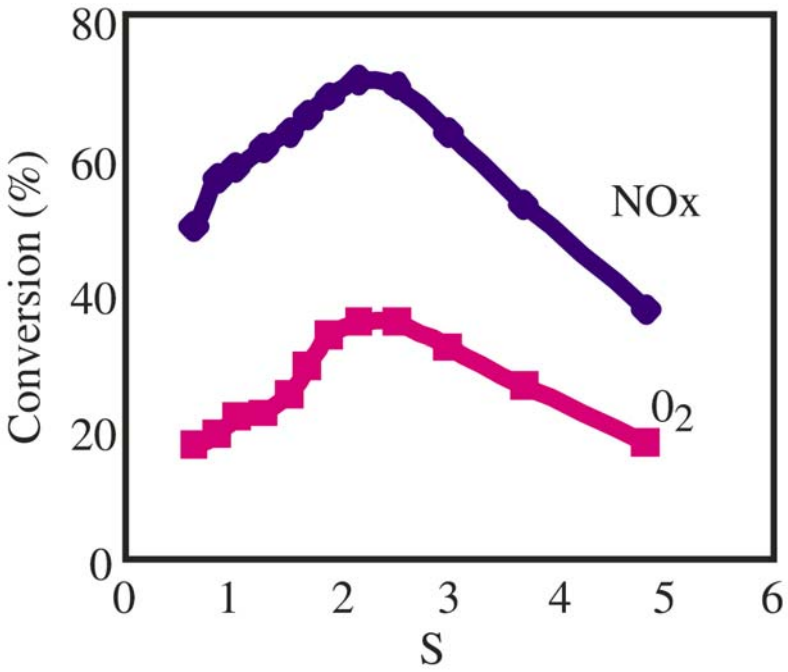

Fig. 11 NO_x and O_2 conversion on Pt catalyst in the simulated exhaust gases as a function of S with the variable of C_3H_6 concentration at 300 ºC.

3.6. Comparison of NO_x conversion on the noble metal catalysts

Under these experimental conditions, NO_x reduction behaviors on the Pt and Pd catalysts were different from that on the Rh catalyst, and the rate-determining step of the reaction in the low temperature region was a HC oxidation process as shown above. In C_3H_6–O_2 reaction system, partial reaction order was determined on the same catalysts, and it indicated that HC, or intermediates such as partial oxidation products, were adsorbed strongly on the Pt and Pd catalysts surface, and caused self-inhibition [8].

From these results, reaction scheme in low temperature region on Pt and Pd catalyst is considered as follows, at stoichiometric and reducing conditions, HC adsorbed strongly on the catalyst surface to cause self inhibition. With increasing O_2 concentration, HC poisoning is suppressed and allows adsorption of oxidative gases, and leads to HC oxidation. However, the reaction ratio of NO/O_2 with HC decreases with an increase of O_2 concentration. Therefore, the balance point of the two factors produces a maximum NO_x conversion. On the other hand, oxygen strongly adsorbed on to the surface of the Rh catalyst. Strongly adsorbed oxygen is easy to react, and thus NO_x conversion is increased with decreasing S value.

3.7. Reaction selectivity between NO_x and O_2

Figure 12 shows the ratio of NO_x and O_2 conversion as a function of S on the Pt catalyst from the data as shown in figure 5. The value of [NO_x conversion/O_2

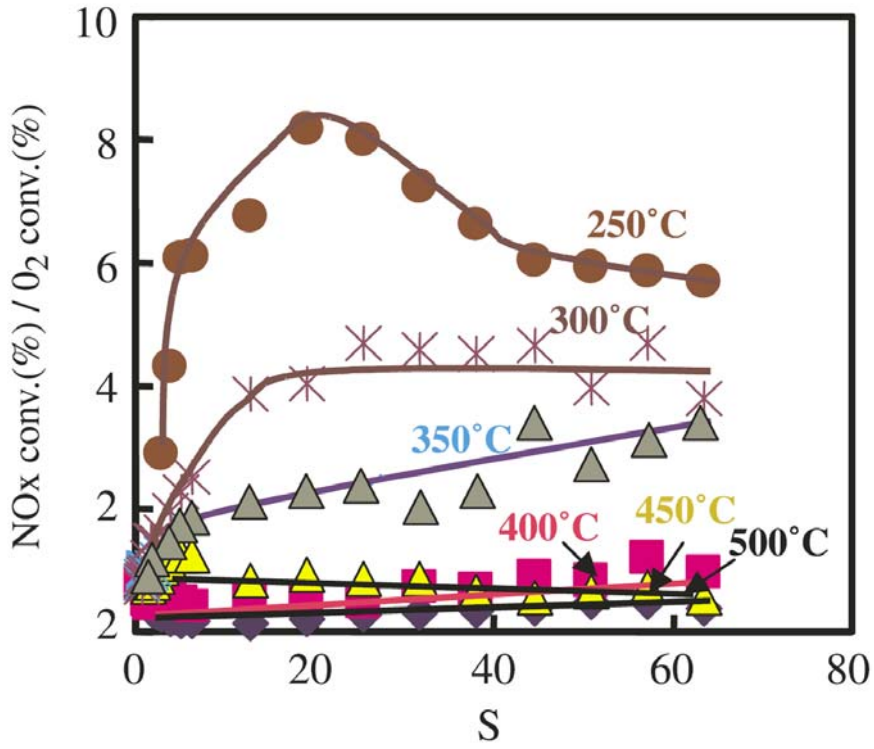

Fig. 12 Reaction selectivity between NO_x and O_2 as a function of S on Pt catalyst at several temperatures in simulated exhaust gases.

conversion] increased with decreasing temperature with a value of 6 at 250 ˚C. This means NO_x is much easier to react than O_2 with reducing gases on the Pt catalyst under the low temperature region. As described above, the rate-determining step of the reaction is considered as an oxidation process of strongly adsorbed HC. So, NO_x (NO_2) could be easier to react with pre-adsorbed HC compared to O_2 on the catalyst. However, the reason for high NO_x reaction selectivity under low temperature region on the Pt catalyst is not clear. On the Pd and Rh catalysts, the tendency of reaction selectivity between NO_x and O_2 was also not so clear. We would investigate further in this interesting phenomenon.

4. Conclusion

NOx reduction activity of Pt, Pd and Rh catalysts loaded on an α-alumina was investigated as both a function of temperature and oxygen concentration in simulated automotive exhaust gases. In the case of both Pt and Pd catalysts, a maximum of NO_x conversion for S values ($S = (2[O_2] + [NO]) / ([CO] + 9[C_3H_6])$) as a stoichiometry number existed at each temperature, and the S value at the maximum NO_x conversion was increased with decreasing temperature. In the case of Rh catalyst, NO_x reduction behavior was different from that on the Pt and Pd catalyst. NO_x conversion increased

with decreasing S value, but independent of temperature. From the partial reaction orders in C_3H_6- O_2 reaction on the catalysts, it was concluded that, in the cases of Pt and Pd catalyst, HC were adsorbed strongly on the catalysts surface, and caused self inhibition. Increasing O_2 concentration lead to HC oxidation, particularly in the low temperature region, but that decreased the value of NO_x/O_2 ratio. Therefore, the balance point of the two factors produced a maximum. For the Rh catalyst, oxygen strongly adsorbed on the surface. So, NO_x conversion increased with decreasing S value.

References

[1] G. Zhang, T. Yamaguchi, H. Kawakami and T. Suzuki, Appl. Catal. B 1 (1992), L15.

[2] A. Obuchi, A. Ohi, N. Nakamura, A. Ogata, K. Mizuno and H. Obuchi, Appl. Catal. B 2 (1993), 71.

[3] M. Iwamoto, M. Ahiro, H.-K. Shin, M. Watanabe, J. Guo, M. Konno, T. Chikahisa and T. Murayama, Appl. Catal. B 4 (1994), 65.

[4] R. Burch, P.I. Milligton and A.P. Walker, Appl. Catal. B 4 (1994), 65.

[5] H. Muraki, H. Shinjoh, H. Sobukawa, K. Yokota and Y. Fujitani, Ind. Eng. Chem. Prod. Res. Dev. 24 (1985) 43.

[6] T. Hattori, H. Matsumoto and Y. Murakami, in: Preparation of Catalyst a, B. Delmon, P. Grange, P.A. Jacobs and G. Poncelet (eds.), (Elsevier, Amsterdam, 1987) p. 815.

[7] N. Muraki, K. Yokota and Y. Fujitani, Appl. Catal. 48 (1986) 93.

[8] H. Shinjoh, H. Muraki and Y. Fujitani, Appl. Catal. 49 (1989) 195.

3.2 Effect of Ba addition on catalytic activity of Pt and Rh catalysts loaded on γ -alumina

Abstract

The catalytic activity of Pt catalyst loaded on γ-alumina was improved by Ba addition in simulated automotive exhaust gases. On the other hand, the result of Rh catalyst was the opposite. From the results of the partial reaction orders in C_3H_6–O_2 reaction and TPR, it was concluded that the Ba addition to Pt catalyst suppressed the hydrocarbon chemisorption on the Pt catalyst and therefore allowed the catalytic reaction to proceed smoothly. On the other hand, Ba addition to Rh catalyst caused such a strong oxygen adsorption on Rh that rejected the hydrocarbon adsorption and suppressed the reaction.

1. Introduction

Automotive three-way catalysts consist of noble metals, supports with a large specific surface and some additives. CeO_2 is generally added to automotive three-way catalysts to promote the water-gas shift reaction and to store oxygen under lean conditions for use under rich conditions [1.8]. Nickel is often added for scavenger of hydrogen sulfide and nickel addition reported to improve catalytic activity [9.12]. Lantana and molybdenum addition have been reported to improve NOx reduction activity [13.16].

Recently, barium (Ba) compound is often added to some kind of catalysts, for example, palladium (Pd) only three-way catalyst and NO_x storage reduction three-way catalyst. The role of Ba is an improvement for NO_x reduction activity for the former and a NO_x storage material for the latter, respectively [17.21]. Ba addition to Pd catalyst improved catalytic activity under reducing conditions, and it was concluded that the suppression of chemisorbed hydrocarbons on Pd by the addition of Ba allowed the reaction to proceed smoothly. In spite of the fact that automotive three-way catalysts containing Ba are already in practical use, the effect of Ba addition on the catalytic activities of the catalysts, especially Pt and Rh ones, are not yet clear.

This study is to reveal the effect of Ba addition on catalytic activity of Pt and Rh catalysts, which are used in current commercial three-way catalyst, loaded on γ -alumina. In this report, at first, the effect of Ba loading amount on catalytic activity of Pt and Rh catalysts were investigated using simulated automotive exhaust gases. And second, it was investigated whether the composition of the simulated exhaust gas influenced the effect of Ba addition on the catalytic activity of these catalysts. And third, hydrocarbon oxidation activity and temperature-programmed reduction (TPR) by hydrogen were measured to clarify the effect of Ba addition on these catalysts.

2. Experimental

2.1. Catalysts

The Pt catalyst was prepared by impregnating γ –alumina powder (a BET area of 200 m^2/g) with aqueous solution of dinitrodiammine platinum. The powder was dried overnight at 110 ˚C in air, followed by calcination at 600 ˚C for 5 h in air, pressed at 150 kg/cm^2, crushed, and then sieved into 0.5-1.0 mm particles. The concentration of the solution was adjusted to give 8.7 × 10.3 mol Pt metal loading to one molar γ -alumina on the finite catalyst. The Pt/Ba catalysts were prepared by impregnation of the Pt catalyst powder with aqueous solutions of barium acetate. The powder was dried and calcined, followed by pressing, crushing, and then sieved into 0.5-1.0 mm particles in the same procedure as mentioned above. Ba loading amounts were 0.042, 0.085, 0.170, and 0.340 moles to one molar γ -alumina. The Rh and Rh/Ba catalysts were prepared by impregnating the γ-alumina with aqueous solution of rhodium nitrate and barium acetate, the powders were dried and calcined, followed by pressing, crushed and sieved to 0.5-1.0 mm particles in the same manner. The loading amounts of Rh and Ba were the same as Pt and Pt/Ba catalysts. Pt/Ba(x) and Rh/Ba(x) are the name of Pt and Rh catalysts with Ba, respectively, and the x is the Ba loading amount described above, in this paper. Ba/γ -alumina was also prepared in the same manner and Ba loading amount was 0.085 mole to one molar γ-alumina. The noble metal dispersions of the Pt and Rh catalysts were 0.11 and 0.13, respectively, by CO-pulse method, assuming one molecule adsorbs to a noble metal atom [22]. The noble metal dispersions of the Pt/Ba and Rh/Ba catalysts were believed almost the same as the Pt and Rh catalysts.

2.2. Catalytic activity measurements

Catalytic activity data were obtained using a conventional fixed-bed flow reactor at atmospheric pressure, as described elsewhere [23]. A quartz tube with an inner diameter of 18 mm was chosen as the reactor tube. Catalyst was placed on a quartz filter at the middle part of the reactor. The upper part of the catalyst bed was packed with inactive SiC spheres of 3 mm o.d. for preheating the feed gas. Furnace temperature was controlled with a maximum variation of 1.5 ˚C by an automatic temperature controller. The gas leaving the reactor was led to a condenser to remove the water vapor. The remaining components were continuously analyzed by non dispersive infrared (CO and CO_2), flame ionization (HC), magnetic susceptibility (O_2), and chemiluminescence (NO_x).

In this study, catalytic activity using a simulated stoichiometric exhaust gas was measured as a function of temperature for the catalysts. The feed composition of

simulated exhaust gas was 1.0 vol% CO, 0.3 vol% H_2, 1000 ppmC as C_3H_6, 1000 ppm NO, 0.75 vol% O_2, 3 vol%H_2O, 12 vol% CO_2, and the balance N_2. The cooling rate of the reactor was kept at 6.7 ˚C /min from 400 to 100 ˚C and space velocity was kept at 200,000/h. Catalytic activity was expressed s the percent conversions of HC, CO, and NO*x*. Another test, which replaced 1000 ppmC C_3H_6 by both 0.225 vol% O plus 0.075 vol% H_2 was done for the catalysts in the same way.

C_3H_6 oxidation activity was also measured to decide the kinetic parameters, on the catalysts using the same laboratory reaction system. The compositions of C_3H_6 and O_2 were changed from 500 to 4000 ppm C and from 0.1 to 1.3 vol%, respectively, and space velocity was the same as that mentioned above.

2.3. TPR measurement

The TPR measurement was performed using a flow system with a fixed-bed tubular reactor as described elsewhere [24]. The 5 vol% H_2/Ar was used in this measurement. Space velocity was kept at 7,000/h and heating rate was a linear rate of 50 ˚C /min from −30 up to 300 ˚C. Both a thermal conductivity detector and a quadruple mass spectrometer monitored the amount of H_2 consumed or produced by the catalyst in the reactor. Before the TPR measurement, the catalyst was pretreated at 500 ˚C for 30 min in 0.3 vol% O_2/Ar and then cooled in −30 ˚C methanol bath.

3. Results and discussion

3.1. Effect of Ba loading amount for catalytic activity

The conversions of HC, CO, and NO_x on the Pt and Pt/Ba(0.34) catalysts plotted as a function of temperature in the simulated exhaust gas are shown in figures 1 and 2, respectively. The catalytic activity on the Pt/Ba(0.34) catalyst was superior to that on the Pt catalyst. Figure 3 shows the effect of Ba loading amount for the catalytic activity as temperature at 50% conversion of NO_x. It is found that the catalytic activity on Pt catalyst was improved with increasing of Ba loading amount. Similar phenomena have been observed on Pd/Ba catalysts [18, 19].

The conversions of HC, CO, and NO_x on the Rh and Rh/Ba(0.34) catalysts plotted as a function of temperature in simulated exhaust gases are shown in figures 4 and 5, respectively. And, figure 6 shows also the effect of Ba loading amount for the catalytic activity as temperature of 50% conversion of NO_x. The results of Rh catalysts were quite different from that of Pt ones. That is, the catalytic activity on Rh catalyst was deteriorated with increasing of Ba loading amount.

The conversions of CO and NO_x on the Pt, Pt/Ba(0.34) catalysts and those of the Rh, Rh/Ba(0.34) ones plotted as a function of temperature in a simulated exhaust gas that

replaced C_3H_6 by both CO and H_2 are shown in from figures 7–10, respectively. The catalytic activity on the Pt catalyst was almost the same as that of the Pt/Ba(0.34) one.

And, that on the Rh catalyst was also the same as that on the Rh/Ba(0.34) one. These results indicated that HC oxidation was a rate-determining step in the simulated exhaust gas purification reaction. And, it was found that Ba addition, on the one hand, improved the HC oxidation activity for Pt catalyst, on the other hand, deteriorated that for Rh catalyst.

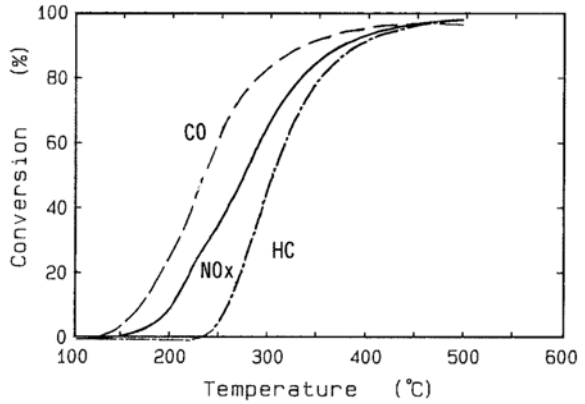

Fig. 1 Conversions of HC, CO, and NO*x* on Pt catalyst in the simulated exhaust gas.

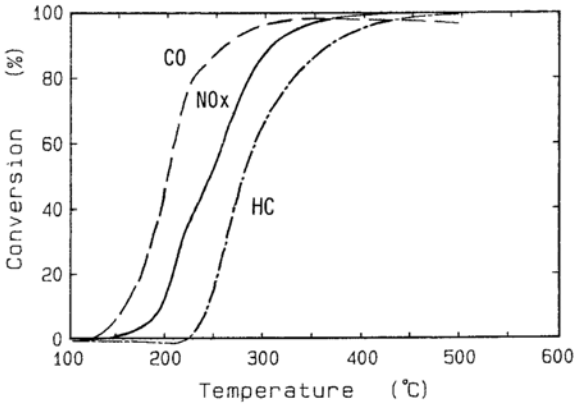

Fig. 2 Conversions of HC, CO, and NO*x* on Pt/Ba(0.34) catalyst in the simulated exhaust gas.

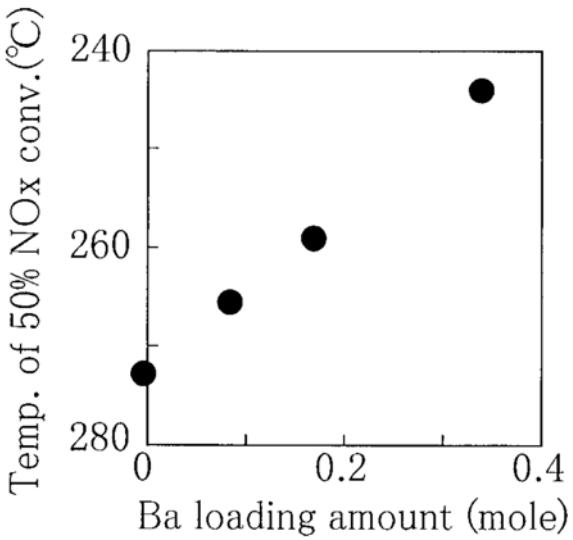

Fig. 3 The effect of Ba loading amount on Pt catalyst for the catalytic activity as temperature at 50% conversion of NO*x* .

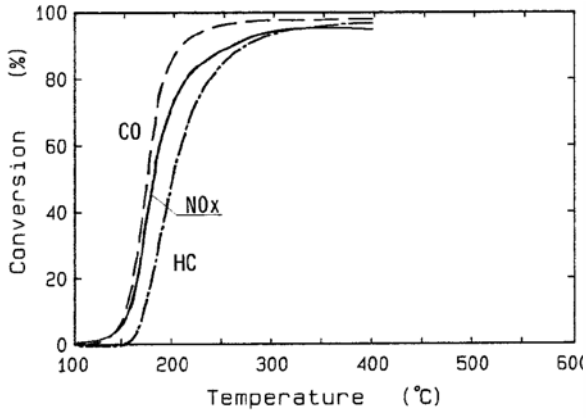

Fig. 4 Conversions of HC, CO, and NO*x* on Rh catalyst in the simulated exhaust gas.

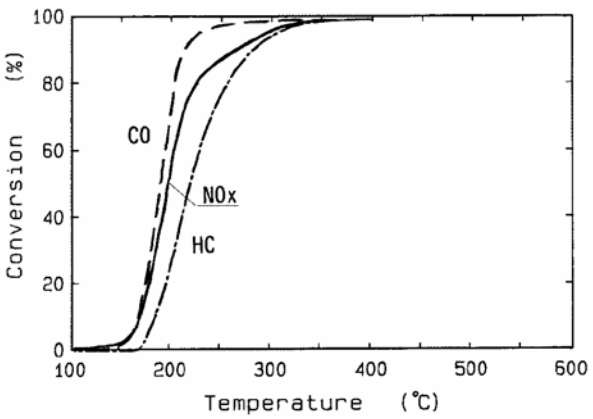

Fig. 5 Conversions of HC, CO, and NO*x* on Rh/Ba(0.34) catalyst in the simulated exhaust gas.

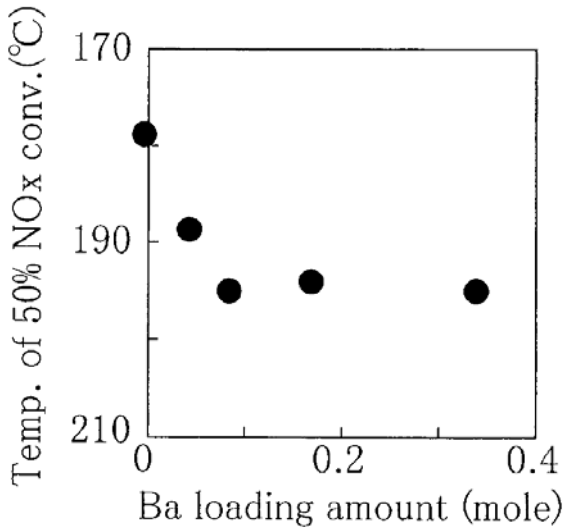

Fig. 6 The effect of Ba loading amount on Rh catalyst for the catalytic activity as temperature at 50% conversion of NO*x*.

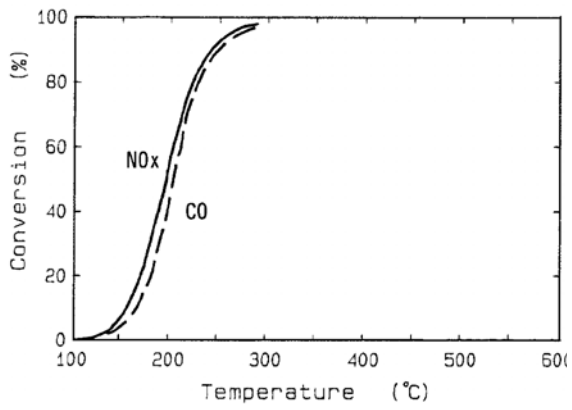

Fig. 7 Conversions of CO and NO*x* on Pt catalyst in the simulated exhaust gas without HC.

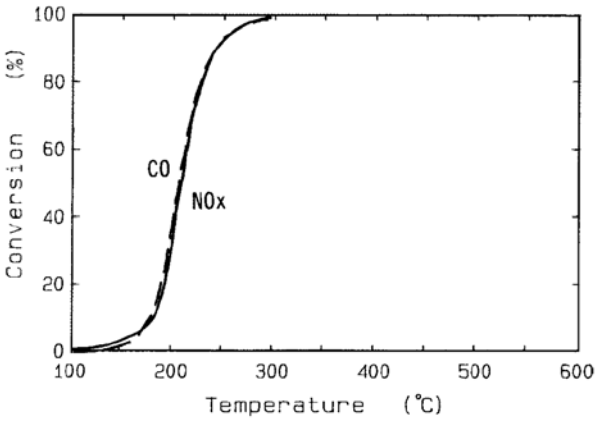

Fig. 8 Conversions of CO and NO*x* on Pt/Ba(0.34) catalyst in the simulated exhaust gas without HC.

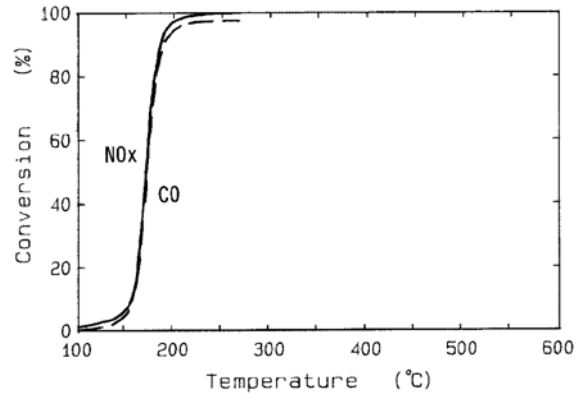

Fig. 9 Conversions of CO and NO*x* conversion on Rh catalyst in the simulated exhaust gas without HC.

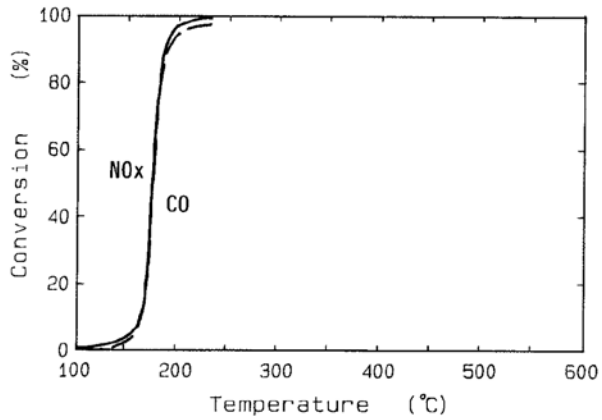

Fig. 10 Conversions of CO and NO*x* on Rh/Ba(0.34) catalyst in the simulated exhaust gas without HC.

3.2. Kinetic parameters for the HC oxidation process

In C_3H_6–O_2 reaction system, the hydrocarbon oxidation activity on the Pt, Pt/Ba(0.34), Rh and Rh/Ba(0.34) catalysts was measured to get further information. The rate of carbon dioxide formation $V(CO_2)$ in the reaction of C_3H_6 with O_2 is given by the following

$$V(CO_2) = kP_{(C_3H_6)}^{m}P_{(O_2)}^{n}exp(-E_a/RT) \qquad (1)$$

where $P(C_3H_6)$ and $P(O_2)$ are the partial pressures of C_3H_6 and O_2, *m* and *n* are the partial reaction orders of C_3H_6 and O_2, respectively. The values of *m* and *n* were determined from a conventional log–log relationship between $V(CO_2)$, obtained under conditions of low conversion of usually less than 30%, and partial pressures of respective species. The partial reaction orders in the C_3H_6–O_2 reaction system determined on the catalysts are summarized in table 1. The partial reaction order *m*, in the equation (1), was negative order and the partial reaction order *n* was positive order on the Pt and Pt/Ba(0.34) catalysts. The *m* value on the Pt/Ba(0.34) catalyst was larger than that on the Pt catalyst. A similar result on the partial reaction orders on the Pd and Pd/Ba catalysts has been reported [12]. On the other hand, *m* value was positive and *n* value was negative on the Rh and Rh/Ba(0.34) catalysts. This result was the opposite of that with the Pt catalysts, and show close agreement with the previous results [25]. The *n* value on Rh/Ba(0.34) catalyst was smaller than that on the Rh catalyst.

Table 1 Partial reaction orders in C_3H_6 oxidation on the catalysts (equation (1)).

catalyst	m	n
Pt/Al_2O_3	-0.75	1.32
$Pt/Ba/Al_2O_3$	-0.62	1.13
Rh/Al_2O_3	0.54	-0.97
$Rh/Ba/Al_2O_3$	0.72	-1.78

$$V(CO_2) = kP(C_3H_6)^m \times P(O_2)^n$$

3.3. H_2-TPR for the catalysts

The H_2-uptake on the γ-alumina, Ba/γ-alumina, Rh, Rh/Ba(0.085) and Rh/Ba(0.34) catalysts plotted as a function of temperature obtained by TPR are shown in figure 11.

H_2 was consumed only above 350˚C on the Ba/γ-alumina, and was not consumed on the γ-alumina at all. On the other hand, the oxygen adsorbed on Rh of the Rh catalyst was reduced below 300 ˚C, and the H_2-uptake peak was 110 ˚C. The H_2-uptake pattern of Rh/Ba catalysts had two peaks The first peak of H_2-uptake on the Rh/Ba catalysts was regarded as reduction of the oxidized Rh and the second peak on those as reduction of Ba compound, perhaps barium carbonate, because the amounts of the first H_2-uptake on the Rh/Ba catalysts were almost the same as that on the Rh catalyst, and the amount of the second H_2-peak was proportional to the Ba loading amount. The temperature of the first H_2-uptake peak on the Rh/Ba catalysts increased with Ba loading amount. This result suggests that Rh oxide on the Rh/Ba catalysts was harder to reduce than that on the Rh catalyst.

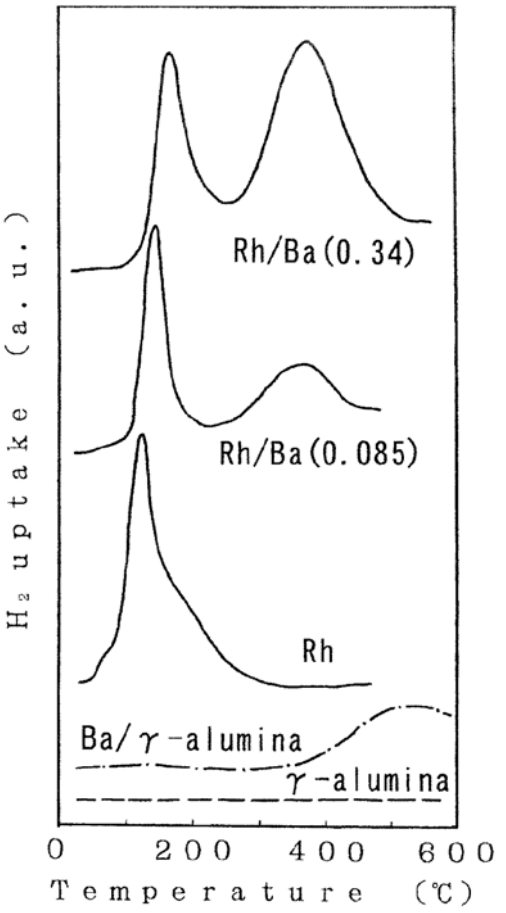

Fig. 11 H_2-uptake on the γ-alumina, Ba/γ-alumina, Rh/Ba(0.085), and Rh/Ba(0.34) catalysts obtained by TPR measurement.

4. Conclusion

The effect of Ba addition on the catalytic activity of Pt and Rh catalysts loaded on γ-alumina was investigated using simulated exhaust gases. The catalytic activity of Pt catalyst with Ba was higher than that of Pt catalyst. On the other hand, the catalytic activity of Rh catalyst with Ba was lower than that of Rh catalyst. The effect of Ba addition on the catalytic activity was not recognized using a simulated exhaust gas without HC.

From the partial reaction orders in C_3H_6–O_2 reaction system and H_2-TPR measurement on the catalysts, it was concluded that the Ba addition to the Pt catalyst weakened the adsorption strength of hydrocarbons and therefore allowed the catalytic reaction to proceed smoothly. On the other hand, the Ba addition to the Rh catalyst

caused such a strong oxygen adsorption on Rh that rejected the hydrocarbon adsorption and therefore suppressed the reaction.

It was suggested through above results that Ba should be located with Pt and be separated from Rh in the three-way catalyst for high catalytic activity.

References

[1] H.S. Gandhi, A.G. Piken, M. Shelef and R.G. Delosh, SAE paper 760201 (1976).
[2] H.C. Yao and Y.F. Yu Yao, J. Catal. 86 (1984) 254.
[3] E.D. Su, C.N. Montreuil and W.G. Rothchild, Appl. Catal. 17 (1985) 75.
[4] Y.F. Yu Yao and J.T. Kummer, J. Catal. 106 (1987) 307.
[5] J.Z. Shyu, K. Otto, L.H.Watkins, G.W. Graham, R.K. Belits and H.S. Gandhi, J. Catal. 114 (1988) 23.
[6] J.C. Schlatters and P.J. Mitchell, Ind. Eng. Chem. Prod. Res. Dev. 19 (1980) 288.
[7] J.C. Summers and S.A. Ausen, J. Catal. 58 (1979) 131.
[8] L.C. Hegedus, J.C. Summers, J.C. Schlatter and K. Baron, J. Catal. 56 (1979) 321.
[9] L.C. Klimisch and K.C. Taylor, Environ. Sci. Technol. 7 (1973) 127.
[10] B.J. Cooper and L. Keck, SAE paper 800461 (1980).
[11] M.G. Henk, J.J.White and G.W. Denison, SAE paper 872134 (1987).
[12] J.S. Rieck, W. Suares and J.E. Kubsh, SAE paper 892095 (1989).
[13] H.S. Gandhi and K.M. Adams, US Patent 284762, 284763 (1981).
[14] K.M. Adams and H.S. Gandhi, US Patent 284759 (1981).
[15] H. Muraki, H. Shinjoh, H. Sobukawa, K. Yokota and Y. Fujitani, Ind. Eng. Chem. Prod. Res. Dev. 25 (1986) 202.
[16] N. Muraki, H. Shinjoh and Y. Fujitani, Appl. Catal. 325 (1986) 22.
[17] S. Matsuura, A. Hirai, K. Arimura and H. Shinjoh, SAE paper 950257 (1995).
[18] H. Shinjoh, K. Yokota, H. Doi,M. Sugiura and S. Matsumoto, Nippon Kagaku Kaishi 10 (1995) 63.
[19] H. Shinjoh, T. Suzuki, N. Takahashi, K. Yokota, M. Sugiura and S. Matsumoto, Nippon Kagaku Kaishi 5 (1996) 433.
[20] N. Takahashi, H. Shinjoh, T. Iijima, T. Suzuki, K. Yamazaki, K. Yokota, H. Suzuki, N. Miyoshi, S. Matsumoto, T. Tanizawa, T. Tanaka, S. Tateishi and K. Kasahara, Catal. Today 27 (1996) 63.
[21] H. Shinjoh, N. Takahashi, K. Yokota and M. Sugiura, Appl. Catal. B 15 (1998) 189.
[22] T. Hattori, H. Matsumoto and Y. Murakami, in: *Preparation of Catalyst A*, eds. B. Delmon, P. Grange, P.A. Jacobs and G. Poncelet (Elsevier, Amsterdam, 1987) p. 815.

[23] N. Muraki, K. Yokota and Y. Fujitani, Appl. Catal. 48 (1986) 93.
[24] H. Muraki, H. Shinjoh, H. Sobukawa, K. Yokota and Y. Fujitani, Ind. Eng. Chem. Prod. Res. Dev. 25 (1986) 202.
[25] H. Shinjoh, H. Muraki and Y. Fujitani, Appl. Catal. 49 (1989) 195.

Chapter 4

Design of highly active Pt supported catalyst ～from the view point of Pt-support interaction～

Abstract

To investigate the support effect on the hydrocarbon-NO-O_2 reaction in automotive three-way catalytic reactions, operando X-ray absorption near edge structure (XANES) experiments were performed for reactions of C_3H_6 (or C_3H_8)-NO-O_2 over Pt supported catalysts under reducing conditions. γ-Al_2O_3, ZrO_2, CeO_2-ZrO_2 and La_2O_3 were used as the support oxides in this study. After oxidation pre-treatment, the oxidation state of the supported Pt was monitored by in situ Pt L_3-edge XANES spectra whilst the temperature in the reaction mixture was ramped up and the catalytic reaction was followed by measuring the concentrations of C_3H_6 or C_3H_8, NO and O_2. The operando experimental results were analyzed in terms of the catalytic reaction start-up temperature (20% HC conversion temperature) and the 50% Pt reduction temperature. A V-shape correlation was found between these two temperatures showing that an appropriate Pt reduction temperature should exist to lower the catalytic reaction start-up temperature. This result suggests that the creation of active metallic Pt sites together with the self-poisoning effect of adsorbed carbonaceous species on metallic Pt should determine the catalytic reaction start-up behavior of supported Pt catalysts. Besides the suitable Pt reduction temperature, the oxygen reactivity in the support oxide is also important for lowering the catalytic start-up temperature. The control of the Pt-support interactions to provide suitable Pt reducibility and also oxygen reactivity in oxide support are both important to achieve a lower catalytic reaction start-up temperature.

Keywords: operando spectroscopy, automotive catalyst, Pt, NO reduction, support effect

1. Introduction

Noble metal catalysts supported on oxide are widely used in industrial catalytic processes and also for pollution control in stationary and mobile sources. Automotive catalysts are used for the abatement of pollutants, such as hydrocarbons, NO_x and carbon monoxide, in the exhaust from automotive engines. Pt, Pd and Rh (PGM; platinum group metals) are important active components in automotive catalysts and a considerable number of studies have been performed on PGM supported catalysts to

achieve high efficiency and also high durability [1-3 and references therein]. The local structure and oxidation state of the supported PGM are important for the catalysis and can change with the atmospheric reaction conditions and also temperature [4]. Particularly for automotive catalysts, the reaction temperature and atmospheric conditions always vary with time during driving. To understand the real state of the automotive catalyst at work and develop more efficient and durable catalysts, the *operando* spectroscopic approach is attractive. This methodology is the spectroscopic investigation of the catalyst during the reaction with simultaneous measurements of the reaction, activity, selectivity and stability, by using a gas chromatograph or mass spectrometer [5-7]. Although many spectroscopic techniques have been applied in operando studies [8-19], X-ray absorption fine structure (XAFS) is the most powerful probe of the local structure and oxidation state of the supported PGM under reaction conditions and time-resolved measurements can be performed [20-26].

Recently, Newton et al. reported the results of concentration modulation spectroscopy on Rh/Al_2O_3 and Pd/Al_2O_3 catalysts during the CO / NO redox cycling reaction with combining operando dispersive Extended X-ray absorption fine structure (EXAFS) and DRIFTS [27]. This technique is a differential spectroscopy approach and increases the sensitivity to structural changes of the supported Rh and Pd during the periodic CO / NO reaction that should be dominated by surface effects. They claimed that this methodology can be used to induce a *de facto* surface sensitivity to EXAFS that normally acts as a bulk probe. Their experimental results clearly demonstrated that only a simple oxidation / reduction behavior was seen in the Rh/Al_2O_3 catalyst, although other reactive pathways were detected for the Pd/Al_2O_3 catalyst. This technique may prove to be one of the most advanced operando methodologies to probe the dynamic changes of supported PGM during catalytic reactions. Another differential XAFS approach was reported by Miller et al [28]. They determined the coverage of adsorbed species on Pt and Au supported catalysts during the water gas shift (WGS) reaction by the linear combination fitting of the difference X-ray absorption near edge structure (XANES) spectra. The Pt and Au L_3-edge XANES spectra are affected not only by those oxidation states but also the surface coverage of adsorbates on the metal particles. They identified adsorbates and quantified their individual coverage under steady-state WGS reaction conditions ($CO + H_2O + H_2$) by using the difference XANES method. Miller's work provides a significant challenge to the determination of the coverage of adsorbates on supported metals during catalytic reaction by the operando XAFS technique. These very advanced techniques have been mainly focused on the development of methodology or on the investigation of detailed catalytic mechanisms

on the atomic scale.

On the other hand, there are few operando studies which are oriented to material development in order to improve the catalytic activity of PGM supported catalysts. Yazawa et al. reported the support effects on C_3H_8 oxidation of supported Pt catalysts and discussed the correlation between the oxidation state of Pt and the catalytic activity in an oxidizing atmosphere [29-33]. They showed that Pt on an acidic oxide was found to be in a more metallic state than that on a basic oxide by combining an ex situ Pt XANES investigation and also by the titration of adsorbed oxygen in the catalyst. This more metallic Pt was responsible for the high C_3H_8 oxidation activity in an oxidizing atmosphere because metallic Pt is considered more active than oxidized Pt.

They also stated that the support effect in an oxidizing atmosphere was contrary to that in a reducing atmosphere. In reducing conditions, Pt showed electron deficient features when on an acidic oxide support [31]. The support effect in reducing conditions has also been discussed by other research groups. These studies have been mainly concerned with Pt on a zeolite support and discussions have dealt with the relationships with Pt-H adducts or Pt- Brønsted / Lewis acid site interactions [34-36]. These studies have also shown that the Pt was in an electron deficient state on an acidic oxide support. Therefore, the effect of the support on the oxidation state of the supported metal and its catalytic activity is not a static phenomenon but depends on the reaction conditions. This discussion suggests that an operando study will be necessary to provide more realistic insights into the effect of the support on the catalytic reactions.

In this work we explore the effect of the support on the hydrocarbon (C_3H_6 or C_3H_8)-NO-O_2 reaction in a reducing atmosphere using the operando XANES technique. The details of the experimental technique have already been reported [37]. This simultaneously monitors the catalytic reaction and the oxidation state of Pt using a mass spectrometer and XANES spectroscopy, respectively. The aim of this work is to obtain insights into those material properties of the support that will achieve high catalytic activity for the hydrocarbon-NO-O_2 reaction in automotive three-way catalytic reaction by probing the catalytic reaction start-up behavior and the oxidation state of the supported Pt on various support oxides whilst ramping up the temperature. In this study, four oxides, namely γ-Al_2O_3, ZrO_2, CeO_2-ZrO_2 and La_2O_3, were used as the supports for Pt. These oxides were chosen for the viewpoint of the acid-base property of the oxide; they range from the basic oxide La_2O_3 to the relatively acidic oxide Al_2O_3. C_3H_6 and C_3H_8 were used as hydrocarbons in the catalytic reaction to represent typical saturated and unsaturated hydrocarbons in automotive exhaust. We believe that this operando study will provide a more realistic understanding of the effects of the support on

automotive catalysts and allow the development of advanced catalysts in a more rational way.

2. Experimental

2.1 Catalyst

The four oxides γ-Al_2O_3, ZrO_2, CeO_2-ZrO_2 (Ce:Zr = 50:50 molar ratio) and La_2O_3 were used as supports. γ-Al_2O_3 was supplied by Nikki Universal and used as received. ZrO_2, CeO_2-ZrO_2 and La_2O_3 were prepared by conventional precipitation from aqueous solutions of $ZrO(NO_3)_2{\cdot}2H_2O$ for ZrO_2, $Ce(NO_3)_3{\cdot}6H_2O$ and $ZrO(NO_3)_2{\cdot}2H_2O$ for CeO_2-ZrO_2 and $La(NO_3)_3{\cdot}6H_2O$ for La_2O_3, respectively. Aqueous NH_3 was used for the precipitation reagent in each preparation. The filtered precipitates were dried at 383 K and then calcined at 773 K in air. Each oxide was impregnated with $Pt(NH_3)_2(NO_2)_2$ (Tanaka Kikinzoku Kogyo K.K) by the usual impregnation method to obtain Pt/γ-Al_2O_3, Pt/ZrO_2, Pt/CeO_2-ZrO_2 and Pt/La_2O_3. The impregnated catalysts were dried in an oven at 473 K for 24 h and calcined in flowing air at 773 K for 5 h. The Pt loading was controlled at 1 wt% for all samples. 35 mg samples of catalyst powder were pressed into disks 10 mm diameter for the operando XAFS experiment.

2.2 CO pulse adsorption

CO pulse adsorption measurements were performed using an Ohkura Riken R6015-S instrument modified for CO adsorption at low temperature. The sample was heated to 673 K in an oxygen flow and held at this temperature for 15 min. After purging with He, the sample was reduced in H_2 for 15 min and then cooled to CO pulse adsorption temperature in a helium flow. CO pulses were injected at 323 K for Pt/γ-Al_2O_3, Pt/ZrO_2 and Pt/La_2O_3 until the adsorption reached saturation. For Pt/CeO_2-ZrO_2, CO pulses were injected at 195 K to estimate the accurate Pt dispersion [38]. The amount of CO adsorption was calculated as the difference between the total amount of CO injected and the amount measured at the outlet from the sample. The metal dispersion was calculated by assuming a CO to surface metal atom ratio of 1:1 [39].

2.3 Operando XAFS experiment

The XAFS investigation was carried out at the BL01B1 and BL16B2 beamlines of SPring-8 (Hyogo, Japan). The storage ring energy was 8 GeV with a typical current of 100 mA. Pt L_3-edge (11.5 keV) XANES spectra was measured using a Si (111) double crystal monochromator in transmission mode. Ionization chambers were used to measure the intensity of the incident and transmitted X-rays. The Quick scan technique was used in this measurement. In this technique, the monochromator was continuously moved and the energy was scanned between 11445 and 11705 eV in 40 sec [40].

Standard samples of Pt foil and PtO_2 were also measured as references for the oxidation state of metallic Pt^0 and oxidized Pt^{+4}. The XANES spectrum of Pt foil was also used for the energy calibration.

The operando XAFS measurements were performed with an operando spectroscopic cell. The schematic diagram for the operando XAFS experiment and spectroscopic cell have been described in detail in reference [37]. In this experiment, gas cylinders of 1% C_3H_6/He, 1% C_3H_8/He, 1% NO/He, 2% O_2/He and He were used as sources to make the reaction mixture; O_2, H_2 and He were used for the pretreatment. The flow rate of each gas was controlled using mass flow controllers to get the correct reaction mixture. The reaction mixture was introduced into the operando spectroscopic cell and a portion of the outlet gas from the cell was introduced to the mass spectrometer (ANELVA type-M-100QA) using the capillary to measure the concentration of H_2O, NO, O_2, C_3H_6, C_3H_8 and CO_2.

A self-supported catalyst disk (35 mg, 10 mm diameter) was placed in the operando spectroscopic cell and the reaction was conducted at atmospheric pressure. In the operando experiment the catalyst was pre-treated as follows. At first, the catalyst was heated to 773 K in a flow of 20% O_2 /He to burn off any adsorbed contaminants on the catalyst. The catalyst was reduced for 10 min in a flow of 3% H_2/He and oxidized for 10 min in a flow of 20% O_2 /He at 773 K, then cooled to 323 K in a flow of 20% O_2 /He. This reduction pre-treatment was performed to decompose any remaining Pt salt in the catalyst and to produce the dispersed metallic Pt particles. The final oxidation in the pre-treatment was used to simulate a situation in which automotive catalyst is oxidized by ambient atmosphere before the start-up of the automotive engine. After the pre-treatment, the gas was switched to the reaction mixture. In this operando study, the NO reduction by hydrocarbon was investigated in a reducing atmosphere. C_3H_6 or C_3H_8 was used as hydrocarbon. The reaction conditions are summarized in Table 1. Four

Table 1 Reaction conditions with hydrocarbon (C_3H_6, C_3H_8) – NO – O_2

	Atmospheric condition	Total flow rate	Catalyst weight
(a)	0.11% C_3H_6 – 0.30% NO – 0.30% O_2	100 ml/min	35 mg
(b)	0.11% C_3H_6 – 0.30% NO		
(c)	0.10% C_3H_8 – 0.30% NO – 0.30% O_2		
(d)	0.10% C_3H_8 – 0.30% NO		

atmospheric conditions were employed in the experiments. The total flow rate was 100 ml/min for pre-treatment and reaction. The heating of the cell was begun 5 min after switching to the reaction mixture to make sure that the atmosphere in the cell was completely replaced by the reaction mixture. The temperature ramping rate was controlled at 10 K /minute. The XANES spectra were recorded every 1 minute and the catalytic reaction was monitored every 1 second by measuring the concentrations of gases in the outlet gas from the operando cell. The experimental XANES raw data were energy calibrated and normalized using homemade software.

3. Results

3.1 C_3H_6 –NO – O_2 reactions

Fig. 1(a) shows the Pt L_3-edge XANES spectra of Pt/γ-Al_2O_3 and Fig. 1(b) shows the temperature dependence of the white line intensity of the XANES spectra during the ramping up of the temperature for the C_3H_6 - NO - O_2 reaction. Because the pre-treatment consisted of oxidation in 20% O_2 /He at 773 K, a strong white line peak was observed below 373 K, corresponding to the oxidized Pt, at the beginning of the reaction experiment. The white line intensity decreased as the temperature increased in the reaction mixture. This decrease of the white line intensity corresponds to a reduction of oxidized Pt with increasing temperature because the white line intensity corresponds to the Pt oxidation state [41]. While the XANES spectra were being recorded, the catalytic reaction in the operando cell was monitored by measuring the outlet concentrations of NO, O_2, and C_3H_6 using the mass spectrometer. The concentration changes of each species during the ramping up of temperature are shown in Fig. 2. The reaction began at around 500 K and the concentration of each species decreased with increasing temperature. From these experimental data, the temperature dependencies of each conversion and the metal fraction of Pt can be calculated and are shown in Fig. 3. The fraction of metallic Pt was determined from the white line intensities using linear correlation with the oxidation state of Pt. The white line intensity determined on Pt foil (1.27) and PtO_2 (2.21) were used as references for Pt metal and Pt oxide. Figure 3 shows that the operando results accurately show that the catalytic conversions and the Pt oxidation state were determined simultaneously during the reaction in the operando cell. From this result, the reduction of oxidized Pt and the catalytic reaction began at almost the same temperature (around 450 K) and proceeded with increasing catalytic conversion. At 773 K, almost all the Pt in Pt/γ-Al_2O_3 had been reduced in the metallic state and the catalytic conversion reached about 90% for the reaction of C_3H_6 - NO - O_2.

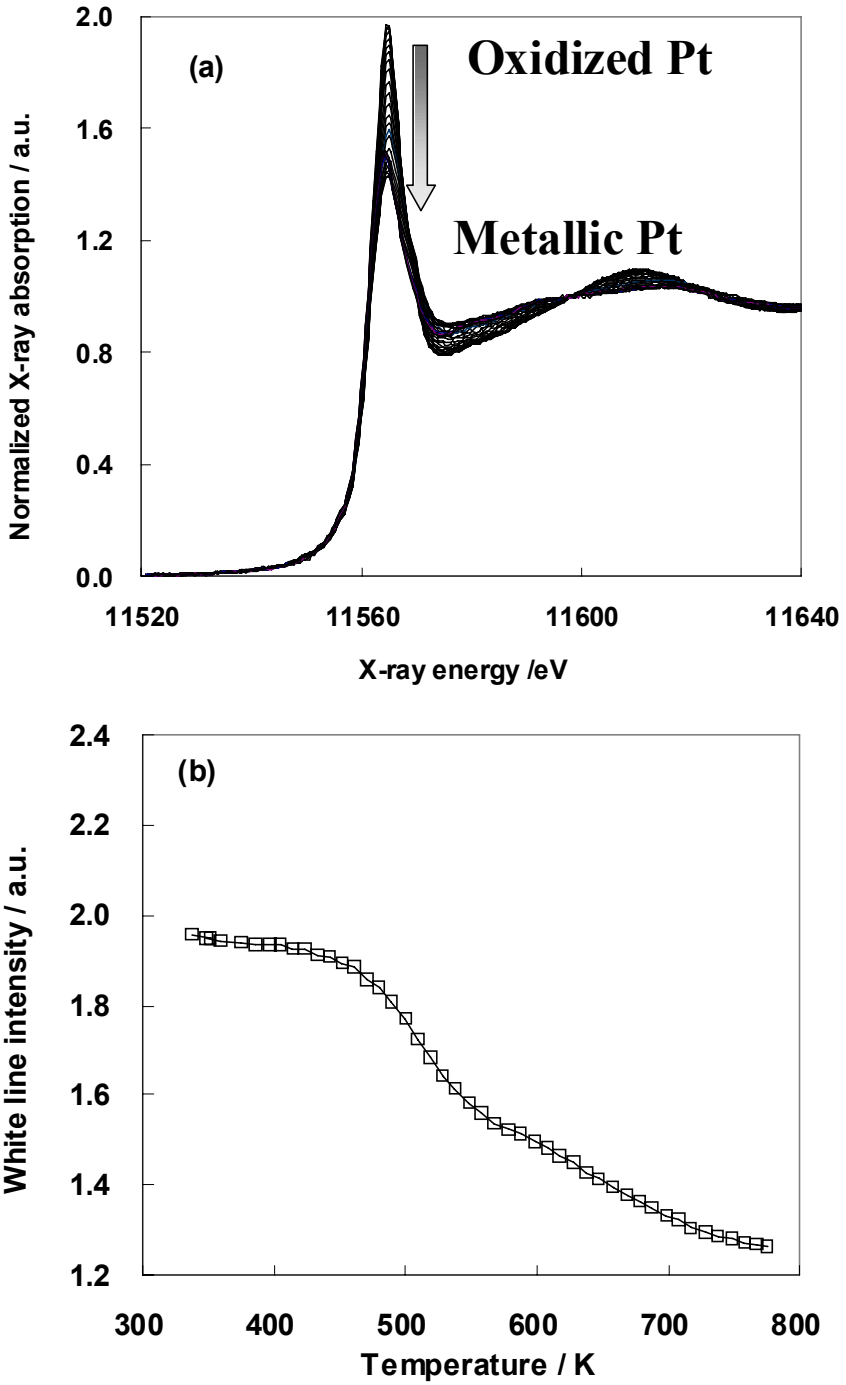

Fig. 1 (a) Normalized Pt L_3-edge XANES spectra and (b) its white line intensity change as a function of temperature increase in the C_3H_6-NO-O_2 reaction over Pt/γ-Al_2O_3.

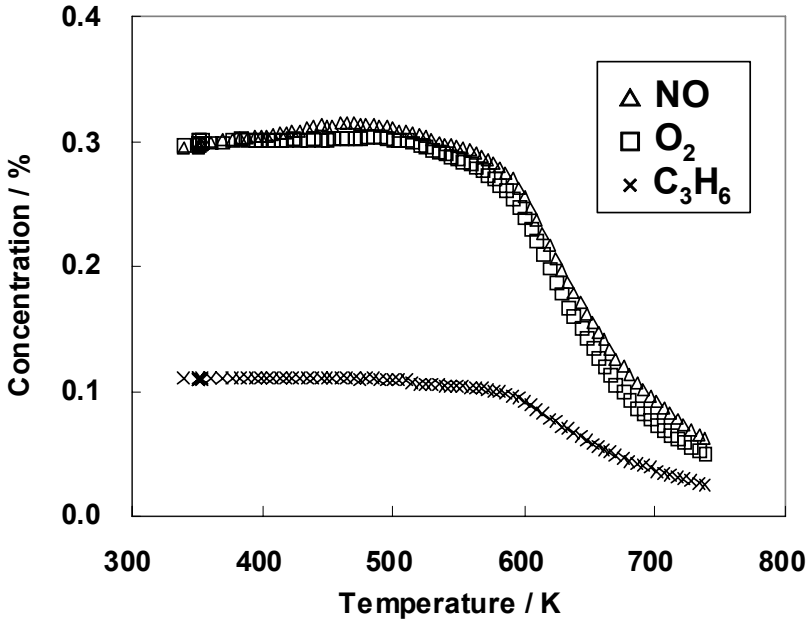

Fig. 2 C_3H_6, NO, O_2 concentration changes as a function of temperature for the C_3H_6-NO-O_2 reaction over Pt/γ-Al_2O_3.

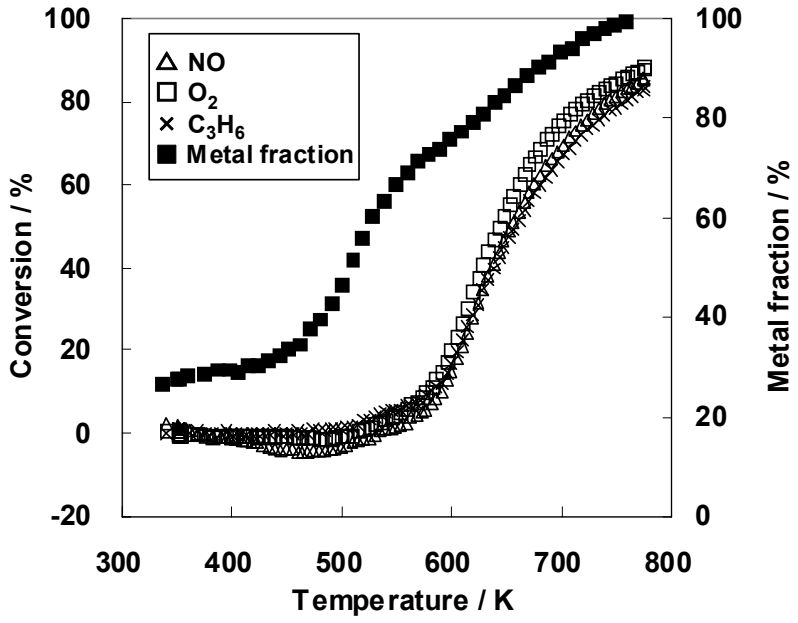

Fig. 3 Temperature dependences of the fraction of metallic Pt and C_3H_6, NO, O_2 conversions in the C_3H_6-NO-O_2 reaction over Pt/γ-Al_2O_3.

The same reaction was conducted on the four catalysts of Pt/γ-Al_2O_3, Pt/ZrO_2, Pt/CeO_2-ZrO_2 and Pt/La_2O_3. Fig. 4 shows the temperature dependences of C_3H_6 (A) and NO (B) conversions over the four catalysts and fraction of metallic Pt (C) during the catalytic reaction. In Figure 4, the conversions and metal fraction of Pt were drawn in each plot to clarify the results. The catalytic activity for NO reduction and C_3H_6 oxidation depended on the support material. The order of activity was Pt/ZrO_2 > Pt/γ-Al_2O_3 > Pt/CeO_2-ZrO_2 > Pt/La_2O_3. This order was similar to the Pt reduction behavior. The Pt in the catalyst with higher activity was reduced at a lower temperature than that in the catalyst with lower activity. Because the metallic Pt site is considered as the active site for the catalytic reaction, this correlation is very reasonable. Yazawa et al. reported that basic oxide support stabilized the oxidized state of Pt and this stabilization of oxidized Pt decreased the catalytic activity for C_3H_8 oxidation [29-33]. Fernandez et al. also reported high temperature reduction of oxidized Pt in barium oxide containing catalyst [42, 43]. They showed that this retard of Pt reduction should be responsible for NOx release without reduction by C_3H_6 in NOx storage reduction catalyst. In our result, Pt supported on La_2O_3 was reduced at the highest temperature and showed the lowest catalytic activity among the four catalysts. Pt/CeO_2-ZrO_2 showed the second lowest activity and the second highest Pt reduction temperature. The results in Fig.4 are explained well by the oxidized Pt stabilization effect of the basic oxide support although the reaction conditions for C_3H_6-NO-O_2 in a reducing atmosphere was different from the C_3H_8-O_2 reaction as reported by Yazawa et al..

3.2 C_3H_6 –NO reactions

The results for the reaction of C_3H_6-NO are shown in Fig. 5. The absence of oxygen in the reaction mixture had an impact on the catalytic reaction. The order of the catalytic activity was Pt/ZrO_2, Pt/CeO_2-ZrO_2 > >Pt/La_2O_3, Pt/γ-Al_2O_3. This order was very different from that for the reaction of C_3H_6-NO-O_2. Because the oxidizing agent in this reaction condition was less than that in the C_3H_6-NO-O_2 reaction, C_3H_6 conversions were much lower than those in the C_3H_6-NO-O_2 reaction. Concerning the Pt oxidation state, the reduction behaviors were similar among the three catalysts except for Pt/La_2O_3. Pt in the catalysts of Pt/ZrO_2, Pt/CeO_2-ZrO_2 and Pt/γ-Al_2O_3 was reduced at around 500 K while Pt in Pt/La_2O_3 was reduced at around 700 K. In this reaction, the catalytic reaction behavior seems not to be correlated with the Pt reduction behavior. This feature was different from the result in the C_3H_6-NO-O_2 reaction. More details of this behavior will be given in the discussion in section 4.

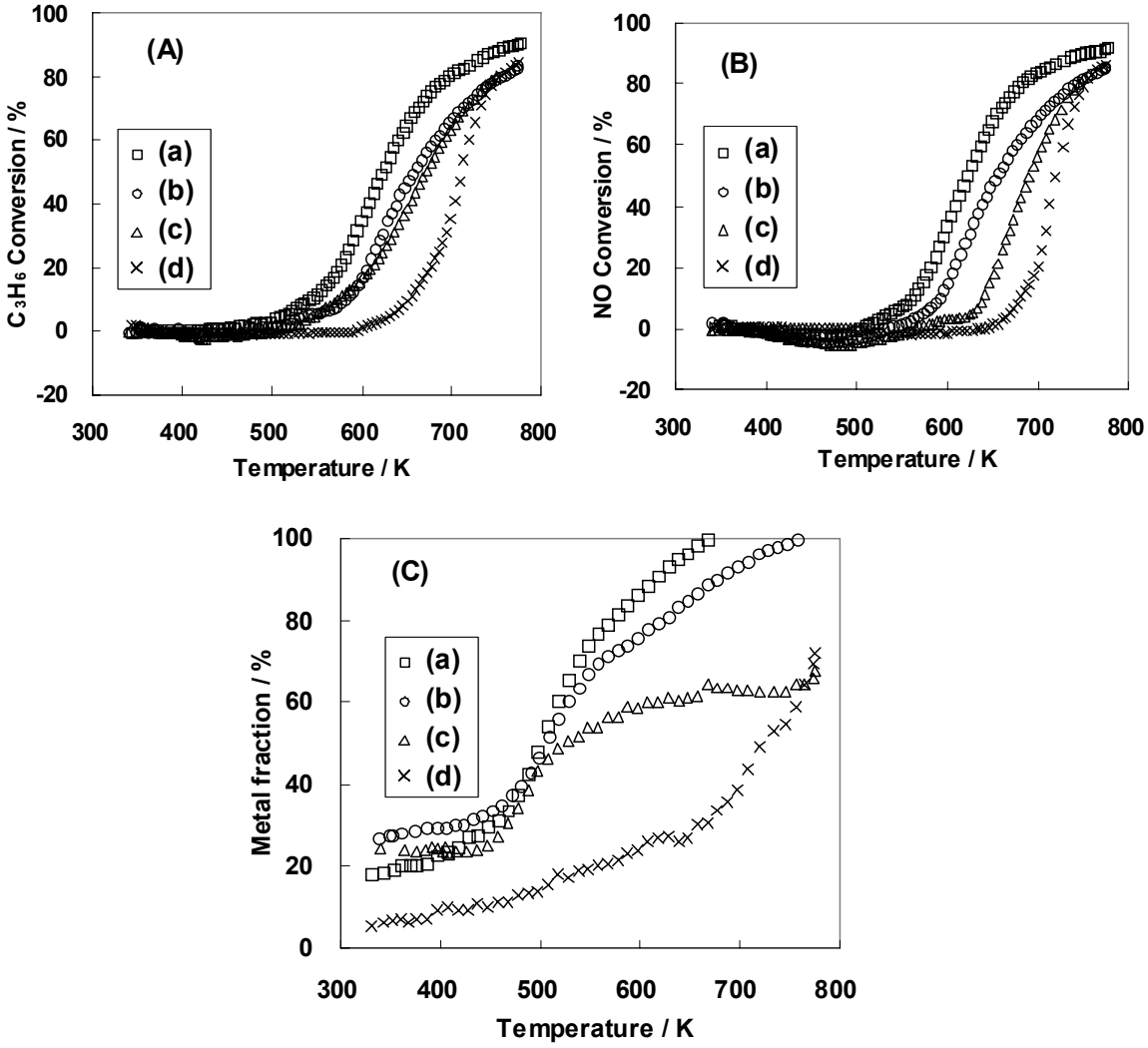

Fig. 4 Temperature dependences of C_3H_6 (A) and NO (B) conversion in the C_3H_6-NO-O_2 reaction over (a) Pt/ZrO_2, (b) Pt/γ-Al_2O_3, (c) Pt/CeO_2-ZrO_2 and (d) Pt/La_2O_3. Temperature dependences of the fraction of metallic Pt (C) determined on (a) Pt/ZrO_2, (b) Pt/γ-Al_2O_3, (c) Pt/CeO_2-ZrO_2 and (d) Pt/La_2O_3 in the C_3H_6-NO-O_2 reaction.

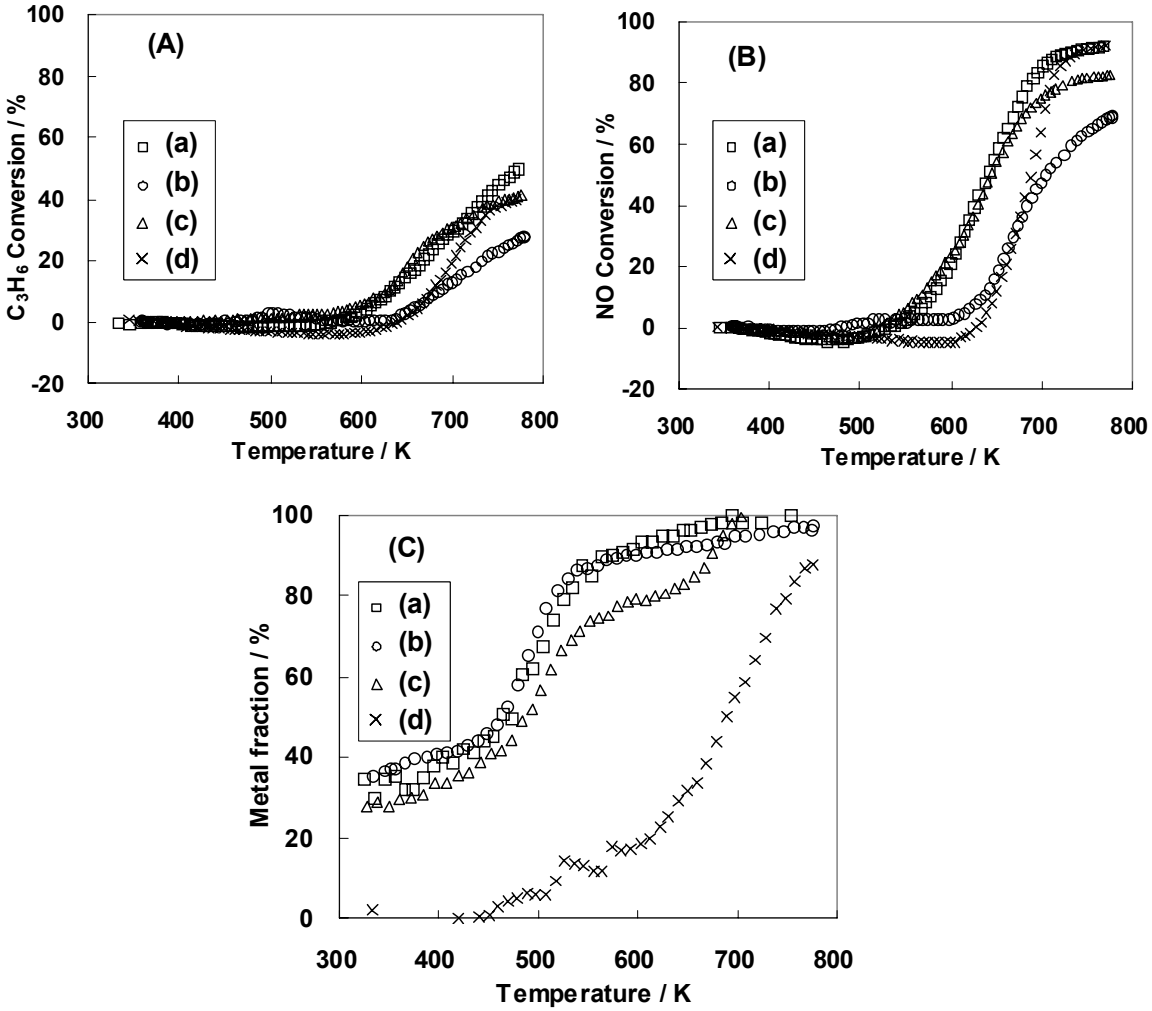

Fig. 5 Temperature dependences of C_3H_6 (A) and NO (B) conversions in the C_3H_6-NO reaction over (a) Pt/ZrO_2, (b) Pt/γ-Al_2O_3, (c) Pt/CeO_2-ZrO_2 and (d) Pt/La_2O_3. Temperature dependences of the fraction of metallic Pt (C) determined on (a) Pt/ZrO_2, (b) Pt/γ-Al_2O_3, (c) Pt/CeO_2-ZrO_2 and (d) Pt/La_2O_3 in the C_3H_6-NO reaction.

3.3 C_3H_8 -NO-O_2 reactions

Fig. 6 shows the temperature dependences of the C_3H_8 and NO conversions and also the fraction of metallic Pt during the C_3H_8-NO-O_2 reaction. The C_3H_8 oxidation began at around 550 K and NO reduction started at around 600 K over Pt/ZrO_2, Pt/CeO_2-ZrO_2 and Pt/γ-Al_2O_3. The C_3H_8 and NO conversion behavior was almost the same over these three catalysts in the low conversion region. Above 60% conversion, Pt/ZrO_2 showed the highest activity among the three catalysts. C_3H_8 oxidation began around 600 K and the NO reduction began at around 700 K over Pt/La_2O_3. Pt/La_2O_3 showed the lowest activity for the entire measured temperature range.

The temperature dependences of the fraction of metallic Pt measured on Pt/CeO_2-ZrO_2 and Pt/γ-Al_2O_3 were monotonic compared with those in the reactions of C_3H_6-NO-O_2 and C_3H_6-NO. No sudden changes were observed around 550 - 600 K, the temperature at which the C_3H_8 oxidation and NO reduction started. On the other hand, the fraction of metallic Pt measured on Pt/ZrO_2 showed a relatively steep increase at around 600 K and increased much more than Pt/CeO_2-ZrO_2 and Pt/γ-Al_2O_3 at 750 K. The higher metallic Pt fraction in Pt/ZrO_2 above 650 K could be the reason why Pt/ZrO_2 showed higher catalytic activity compared with Pt/CeO_2-ZrO_2 and Pt/γ-Al_2O_3 over that temperature range.

For Pt/La_2O_3, a relatively sharp increase of the fraction of metallic Pt was seen at around 700 K, the starting temperature for NO reduction. This feature was the same as for Pt/ZrO_2. Over the entire temperature range, the fraction of metallic Pt measured on Pt/La_2O_3 was lower than for the other three catalysts. This lower metallic fraction of Pt in Pt/La_2O_3 should lead to its lower catalytic activity compared with the other three catalysts over the entire temperature range.

3.4 C_3H_8 -NO reactions

The temperature dependencies of C_3H_8 and NO conversions in the C_3H_8-NO reactions, and also the fractions of metallic Pt are shown in Fig. 7. The C_3H_8 oxidation and NO reduction start temperatures of 550 K were almost the same among the reactions over Pt/ZrO_2, Pt/CeO_2-ZrO_2 and Pt/γ-Al_2O_3. The C_3H_8 oxidation and NO reduction start temperature over Pt/La_2O_3 was around 600 K which was the highest among the four catalysts. These were similar to the result in the C_3H_8-NO-O_2 reaction. The impact of the absence of oxygen in the reaction mixture was not as great as the case of the C_3H_6 reaction. C_3H_8 and NO conversions over Pt/γ-Al_2O_3 decreased with increasing temperature between 580 and 620 K. These characteristic temperature dependences were observed only for the C_3H_8-NO reaction over Pt/γ-Al_2O_3. Above 600 K, C_3H_8 and NO conversions over Pt/γ-Al_2O_3 was lowest among the four catalysts. This

characteristic behavior is further discussed in section 4. The temperature dependences of the fraction of metallic Pt, Pt/ZrO_2, Pt/CeO_2-ZrO_2 and Pt/γ-Al_2O_3 showed almost the same profiles over the whole temperature range with sudden changes observed at 550 K, at which temperature C_3H_8 and NO reduction began. The fraction of metallic Pt determined on Pt/La_2O_3 was the lowest among four catalysts over the whole temperature range.

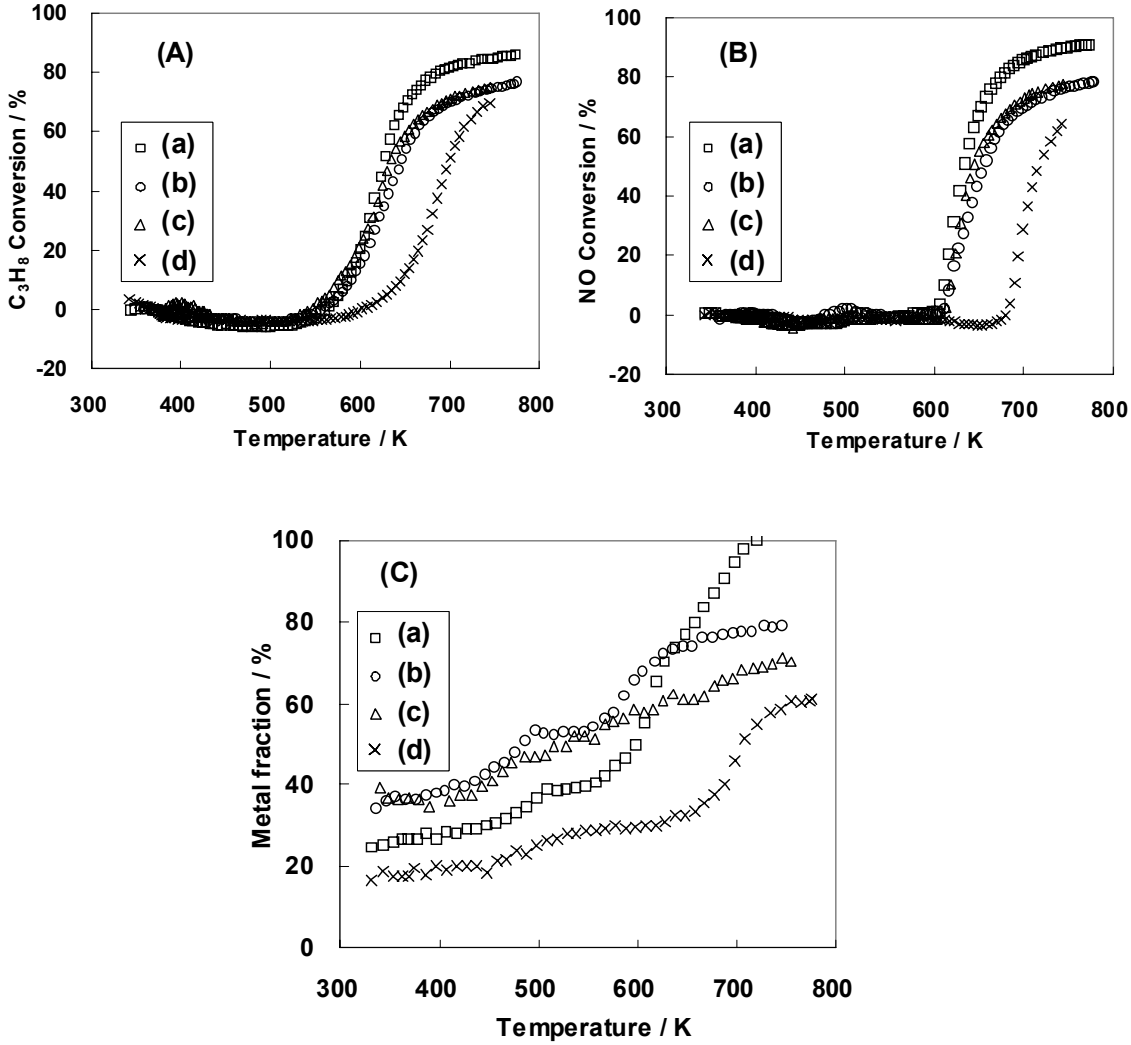

Fig. 6 Temperature dependences of C_3H_8 (A) and NO (B) conversions in the C_3H_8-NO-O_2 reaction over (a) Pt/ZrO_2, (b) Pt/γ-Al_2O_3, (c) Pt/CeO_2-ZrO_2 and (d) Pt/La_2O_3. Temperature dependences of the fraction of metallic Pt (C) determined on (a) Pt/ZrO_2, (b) Pt/γ-Al_2O_3, (c) Pt/CeO_2-ZrO_2 and (d) Pt/La_2O_3 in the C_3H_8-NO-O_2 reaction.

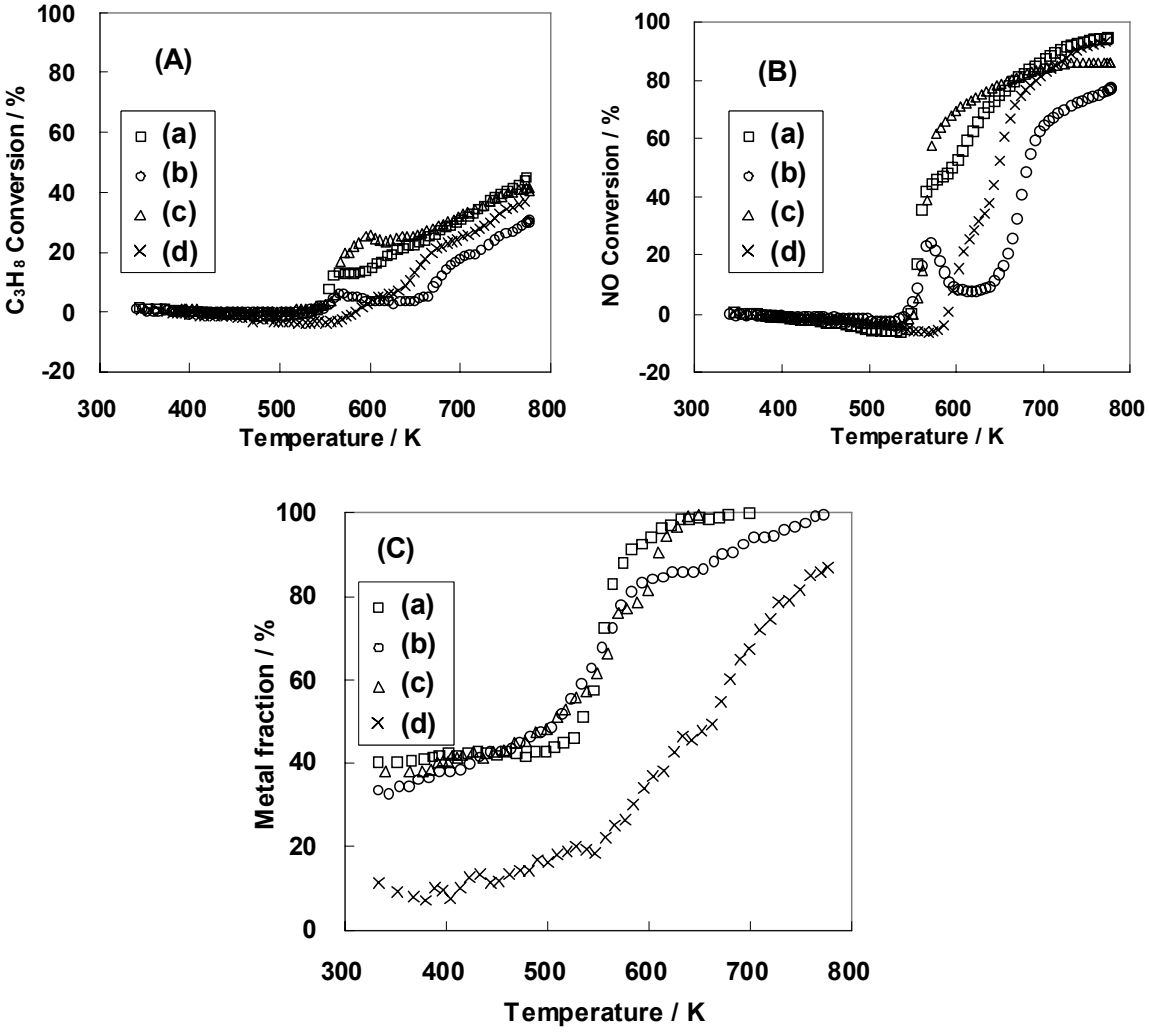

Fig. 7 Temperature dependences of C_3H_8 (A) and NO (B) conversions in the C_3H_8-NO reaction over (a) Pt/ZrO_2, (b) $Pt/\gamma\text{-}Al_2O_3$, (c) Pt/CeO_2-ZrO_2 and (d) Pt/La_2O_3. Temperature dependences of the fraction of metallic Pt (C) determined on (a) Pt/ZrO_2, (b) $Pt/\gamma\text{-}Al_2O_3$, (c) Pt/CeO_2-ZrO_2 and (d) Pt/La_2O_3 in the C_3H_8-NO reaction.

4. Discussion

In this section, the operando experimental results are surveyed with regard to the effect of the oxide support on the catalytic activity of Pt and its oxidation state as a function of temperature. As mentioned in the results section 3.1, the support basicity determined the activity of supported Pt catalyst through the stabilization of oxidized Pt in the C_3H_6-NO-O_2 reaction. In other reaction conditions, the effect of the support on the catalytic activity and also on the stabilization of the oxidized Pt was less clear.

The start-up temperature for the catalytic reaction is important for an automotive catalyst. Because the hydrocarbon was the only reducing agent in the reaction mixture, hydrocarbon oxidation should be activated first. Based on this consideration, HC conversion was used to determine the start-up temperature for the catalytic reaction. In this study, a 20% HC conversion temperature was chosen as the start-up temperature. Below 20% conversion, the reactor is close to differential reactor, in which the concentration of reactant and temperature are almost the same in elsewhere in the reactor. And also mass transport limitation might be small enough to discuss the catalytic reaction rate on the active site. In this condition, almost all active site of Pt should contribute to the catalytic reaction equally and averaged Pt reduction behavior observed by XANES can be discussed in the correlation with start-up behavior of catalytic reaction. A 50% Pt reduction temperature was chosen for the reducibility of the supported Pt based on the following consideration; the dispersions of Pt on Pt/γ-Al_2O_3, Pt/ZrO_2, Pt/CeO_2-ZrO_2 and Pt/La_2O_3, as determined by CO pulse adsorption were 0.55, 0.53, 0.45 and 0.29, respectively. Assuming Pt reduction proceeds from the surface of the Pt particle, a 50% level of Pt reduction means that almost all the surface Pt atoms are reduced to the metallic state. Therefore, at this temperature, almost all the supported Pt should be activated and in the metallic state.

In Fig.8, (A) the 50% Pt reduction temperatures and (B) the 20% HC conversion temperatures for each reaction over each catalyst are plotted versus oxygen O1s binding energy, as determined by XPS measurements. The oxygen O1s binding energy was introduced in our previous work to characterize the Pt-support interaction [44, 45]. In brief, a low value of the O1s binding energy corresponds to strong basicity of the oxide and also high electron density on the oxygen in the support oxide. The 50% Pt reduction temperature decreased with increase of the O1s binding energy, as shown in Fig.8 (A). This trend agreed with our previous results, namely that the oxidized Pt was stabilized on the support with high electron density on oxygen in the support oxide [44, 45]. On the other hand, the 20% HC conversion temperature showed poor correlation with the O1s binding energy, especially in the C_3H_6-NO and C_3H_8-NO reactions. Because a

metallic Pt surface is considered to be more active than oxidized Pt, lowering the Pt reduction temperature should cause a reduction of the catalytic start-up temperature. Based on this consideration, the result in Fig. 8 would suggest that factors other than the creation of metallic Pt active sites must be involved in the catalytic reaction start-up behavior.

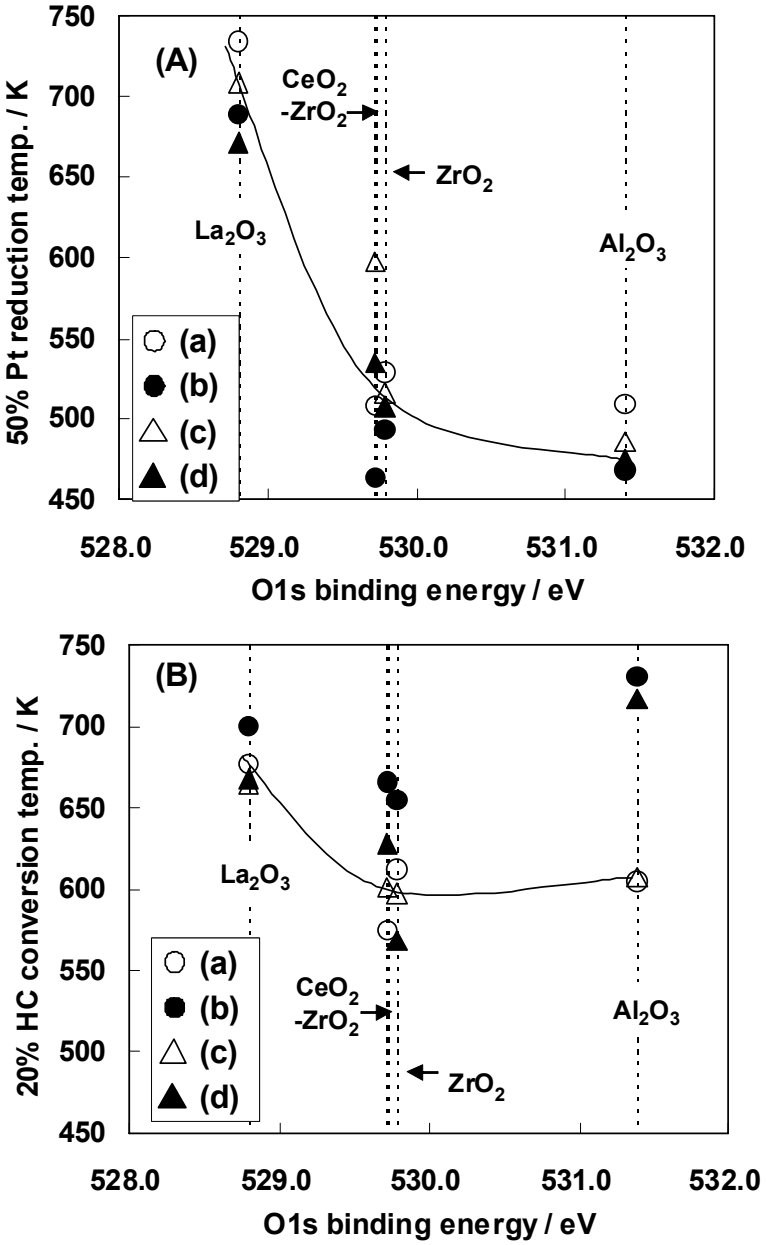

Fig. 8 (A) Correlation between O1s binding energy in the oxide support and 50% Pt reduction temperatures and (B) 20% HC conversion temperatures determined in all 16 reactions. (a) C_3H_6-NO-O_2, (b) C_3H_6-NO, (c) C_3H_8-NO-O_2 and (d) C_3H_8-NO.

To uncover these other factors, the correlation between the 50% Pt reduction and 20% HC conversion temperatures is illustrated in Fig. 9 where a V-shaped correlation is observed. If the creation of metallic Pt active site determines the catalytic start-up temperature, the 20% HC conversion temperature should increase together with the 50% Pt reduction temperature. The right hand side of the V-shaped correlation corresponds to this situation. In this region, the four catalytic reactions over Pt/La_2O_3 and the C_3H_8-NO-O_2 reaction over Pt/ZrO_2 are plotted. In these five reactions, the creation of metallic Pt active site should determine the catalytic start-up temperature, which is shown in the illustration at the right hand side of Figure 9. Because Pt/La_2O_3 was the most basic oxide support of the four catalysts, these results can be satisfactorily explained by the stabilization of the oxidized Pt on basic oxide [30-33, 44, 45]. Some literatures report that oxidized Pt was active state for catalytic reaction [46, 47]. This issue seems still debatable problem because other literatures report metallic Pt was active state for catalytic reaction [48-50]. In our operando study in hydrocarbon - NO -

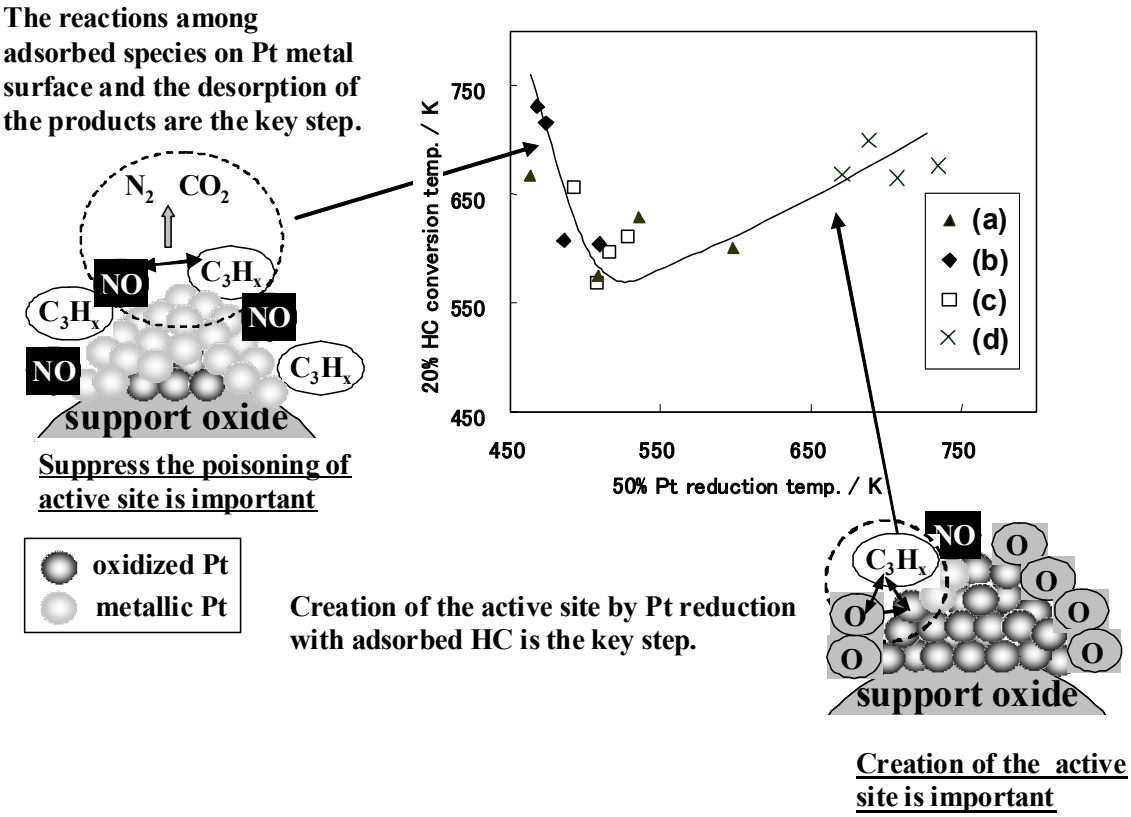

Fig. 9 Correlation between 50% Pt reduction temperature and 20% HC conversion temperatures determined in all 16 reactions. (a) Pt/ZrO_2, (b) Pt/γ-Al_2O_3, (c) Pt/CeO_2-ZrO_2 and (d)Pt/La_2O_3.

O_2 reaction in reducing condition, the creation of metallic Pt was found to be important step for the start-up of catalytic reaction. It should be important to note that the creation of metallic Pt is a requirement for the start-up catalytic reaction but not a sufficient condition as discussed in later.

In the left hand side of the V-shape, the correlation is opposite to the right hand side. This means that a hidden factor is determining the catalytic start-up temperature. The C_3H_6-NO reaction over Pt/γ-Al_2O_3, Pt/ZrO_2, and Pt/CeO_2-ZrO_2 and C_3H_8-NO reaction over Pt/γ-Al_2O_3 appear in this group. These results show that the 20% HC conversion temperatures were much higher than the 50% Pt reduction temperatures. Because the creation of active metallic sites is completed at the catalytic start-up temperature, the catalytic reaction on the metallic Pt surface must be considered in this case. It is well known that C_3H_6 exhibits a self-poisoning effect in the C_3H_6-NO-O_2 and C_3H_6-O_2 reactions on a Pt catalyst, as revealed by kinetic and spectroscopic studies [51-57]. Carbonaceous species derived from C_3H_6 are adsorbed on Pt and inhibit the catalytic reaction by blocking the active site. The cleaning of the carbonaceous species by adsorbed oxygen should determine the catalytic reaction [51-53]. In the C_3H_6-NO reaction over Pt/γ-Al_2O_3, Pt/ZrO_2, and Pt/CeO_2-ZrO_2, the available oxygen on Pt should be very low because oxygen was absent in the feed and Pt was reduced to the metallic state. We consider, therefore, that the C_3H_6 self-poisoning effect determines the catalytic start-up temperature over Pt/γ-Al_2O_3, Pt/ZrO_2, and Pt/CeO_2-ZrO_2. The reaction between adsorbed C_3H_6 and NO on the Pt surface will be the rate determining step in the reaction over Pt/γ-Al_2O_3, Pt/ZrO_2, and Pt/CeO_2-ZrO_2. This situation is illustrated on the left hand side of Fig.9.

In the case of the C_3H_8-NO reaction over Pt/γ-Al_2O_3, very characteristic temperature dependences of HC and NO conversions were observed. These conversions increased around 550 K then decreased with increasing temperature to 650 K. The mechanism of this phenomenon is not clear at the moment but may arise as follows. In the C_3H_8 -NO reactions, the reaction between C_3H_8 and NO began at 550 K over Pt/γ-Al_2O_3, PtZrO_2 and Pt/CeO_2-ZrO_2 and also the reduction of oxidized Pt began almost at the same temperature, as shown Fig.7. The C_3H_8 and NO conversions increased very rapidly at around 550 K over these three catalysts. At this point the adsorbed oxygen on the Pt should be involved in the catalytic reaction between C_3H_8 and NO. This means that the reduction of oxidized Pt and the reaction between C_3H_8 and NO on Pt were coupled through the adsorbed oxygen. This coupling of Pt reduction and C_3H_8-NO reaction on Pt could be the reason for this steep increase of C_3H_8 and NO conversions at 550 K. Because oxygen was absent in the reaction mixture, the available oxygen should

decrease as the Pt reduction proceeds. This reduction of available oxygen should reduce the reaction rate of C_3H_8, and also NO. This limited availability of oxygen could be the reason why the C_3H_8 conversions over Pt/γ-Al_2O_3 decreased between 550 and 650 K. Comparing Pt/ZrO_2 and Pt/CeO_2-ZrO_2, the C_3H_8 conversion over Pt/ZrO_2 showed a small plateau between 550 and 600 K and the C_3H_8 conversion over Pt/CeO_2-ZrO_2 increased gradually with temperature above 550 K. Kotsif et al. showed that oxygen in the oxide support contributes to hydrocarbon oxidation in the absence of gas phase oxygen. The reactivity of oxygen in oxide was in the order CeO_2 > ZrO_2 > γ-Al_2O_3 [58, 59]. This order agreed with the order of C_3H_8 conversion of our results between 550 and 650 K. The difference in conversion behavior between these three catalysts could be caused by the contribution of oxygen in the support oxide and the reactivity of oxygen in the support oxide could determine the catalytic activity in the C_3H_8-NO reaction. Above 600 K, Pt/γ-Al_2O showed even lower catalytic activity than Pt/La_2O_3. This feature was also seen in the C_3H_6-NO reaction. Because oxygen is not included in these reaction mixtures, we presume that the poisoning effect of the carbonaceous species could be enhanced by the acidic property of the γ-Al_2O_3 support.

Around the bottom of the V-shape correlation, the 20% HC conversion temperatures were lower than those on both sides of the V. This means that high catalytic activities were observed in this region. Accordingly, there should be some special factor that promotes high catalytic activity in this region. Viewing from the right-hand side of the correlation, the reduction of the 20% HC conversion temperature may be caused by the lowering of the Pt reduction temperature. The weakening of the basic stabilization effect of the support of the oxidized Pt should be the main reason for this lowering of Pt reduction temperature. On the other hand, viewing from the left-hand side of the correlation, the 20% HC conversion temperatures decreased with increase of Pt reduction temperature. On the left-hand side, as mentioned above, the adsorbed carbonaceous species should inhibit the C_3H_6-NO reaction on metallic Pt and oxygen in the support oxide could contribute to the C_3H_8-NO reaction. This suggests that suppression of the self-poisoning of the carbonaceous species and oxygen reactivity in the catalyst should be important for lowering the 20% HC conversion temperature on this side. Around the bottom of the V-shaped correlation, the Pt reduction temperatures are close to the 20% HC conversion temperatures. In this situation, oxidized and reduced Pt co-exist on the Pt particle surface at the catalytic start-up temperature. Oxygen atoms adsorbed on the oxidized Pt could contribute to the reaction and suppress the self poisoning effect of the adsorbed carbonaceous species, therefore promoting the catalytic reaction on Pt.

Three reaction results over Pt/CeO_2-ZrO_2 (except the C_3H_6-NO) and C_3H_8-NO reactions over Pt/ZrO_2 are plotted around the bottom of the V-shape correlation. In these results, the high oxygen reactivity in CeO_2-ZrO_2 and ZrO_2 should contribute to lowering of the catalytic start-up temperature. The high reactivity of lattice oxygen in CeO_2-ZrO_2 is well known and reported in elsewhere [1-3, 44]. Concerning ZrO_2, some literatures report the high reactivity of lattice oxygen [58-62]. These reactive oxygen in support oxides should contribute to the catalytic reaction and suppress the poisoning effect of carbonaceous species on Pt. Therefore, besides the Pt reduction behavior, high oxygen reactivity in CeO_2-ZrO_2 and ZrO_2 support oxides should also be important in reducing the catalytic start-up temperature by promoting catalytic reaction on Pt.

At the end of discussion section, comparison of catalytic start-up behavior for different supports is discussed in summarizing our findings. In the case of La_2O_3 as support, the stabilizing effect of oxidized Pt by basic oxide was strong and the creation of metallic Pt as active site was important step for catalytic start-up behavior. This means that the use of strong basic oxide as the support for Pt is not appropriate in automotive catalyst to achieve low catalytic start-up temperature, although it has a large benefit for Pt sintering suppression [44, 45]. In the case of γ-Al_2O_3 as the support, the creation of metallic Pt occurred from low temperature and this is not a key step for catalytic start-up behavior. The self poisoning effect of carbonaceous species on Pt should interrupt the catalytic reaction on metallic Pt and should determine the catalytic start-up behavior. In the case of CeO_2-ZrO_2 and ZrO_2, catalytic start-up temperatures were observed lower than that with La_2O_3 and γ-Al_2O_3 support. As mentioned before, the high activity of lattice oxygen in these oxides should contribute to the catalytic reaction and suppress the poisoning effect of carbonaceous species on Pt. This high activity of lattice oxygen in the support oxides should be responsible for the high activity of Pt on CeO_2-ZrO_2 and ZrO_2 at low temperature.

5. Conclusion

An operando XANES study was performed on the HC (C_3H_6, C_3H_8)-NO-O_2 reaction in reducing condition over Pt/γ-Al_2O_3, Pt/ZrO_2, Pt/CeO_2-ZrO_2 and Pt/La_2O_3. This operando study showed a V-shape correlation between catalytic start-up temperature and Pt reduction temperature. In the right hand side of the correlation catalytic start-up temperature increased along with Pt reduction temperature. This result showed that the creation of the metallic Pt as the active site determines the catalytic start-up behavior in the right hand side of the correlation. In the left hand side, lowering of Pt reduction temperature did not promote the catalytic start-up behavior and the self poisoning effect

of adsorbed carbonaceous species on Pt should determine the catalytic start-up behavior. This result suggests an appropriate Pt reduction temperature should exist to lower the catalytic start-up temperature. In addition to the Pt reduction behavior, oxygen in the support oxide can also contribute to the catalytic reaction on Pt and suppress the poisoning effect of adsorbed carbonaceous species. High oxygen reactivity in the support oxide can therefore be another important factor in lowering the catalytic start-up temperature. These operando experimental results suggest that the design of the support oxide to achieve adequate Pt reduction behavior by control of the Pt-support interaction and also high oxygen reactivity in the support oxide are important factors in the development of more efficient automotive catalysts.

References

[1] M. Shelef, R.W. McCabe, Catal. Today 62 (2000) 35.
[2] J. Kašpar, P. Fornasiero, N. Hickey, Catal. Today 77 (2003) 419.
[3] M.V. Twigg, Appl.Catal. B 70 (2007) 2.
[4] M.A. Newton, Chem. Soc. Rev. 37 (2008) 2644.
[5] H. Topsøe, J. Catal. 216 (2003) 155.
[6] B.M. Weckhuysen, Phys. Chem. Chem. Phys. 5 (2003) 4351.
[7] M.A. Banares, Catal. Today 100 (2005) 71.
[8] S.M. Bennici, B.M. Vogelaar, T.A. Nijhuis, B.M. Weckhuysen, Angew. Chem. Int. Ed. 46 (2007) 5412.
[9] T.A. Nijhuis, S.J. Tinnemans, T.Visser, B.M.Weckhuysen, Chem. Eng. Sci. 59 (2004) 5487.
[10] O. Demoulin, M. Navez, E.M. Gaigneaux, P. Ruiz, A. Mamede, P. Granger, E. Payen, Phys. Chem. Chem. Phys. 5 (2003) 4394.
[11] T. Lesage, C. Verrier, P. Bazin, J. Saussey, M. Daturi, Phys. Chem. Chem. Phys. 5 (2003) 4435.
[12] T. Lesage, J. Saussey, S. Malo, M. Hervieu, C. Hedouin, G. Blanchard, M. Daturi, Appl. Catal. B 72 (2007) 166.
[13] F.C. Meunier, A. Goguet, C. Hardacre, R. Burch, D. Thompsett, J. Catal. 252 (2007) 18.
[14] D. Tibiletti, F.C Meunier, A. Goguet, D. Reid, R. Burch, M. Boaro, M. Vicario, A. Trovarelli, J. Catal. 244 (2006) 183.
[15] R.L. Puurunen, B.G. Beheydt, B.M. Weckhuysen, J. Catal. 204 (2001) 253.
[16] R.L. Puurunen, B.M. Weckhuysen, J. Catal. 210 (2002) 418.
[17] A. Bruckner, Phys. Chem. Chem. Phys. 5 (2003) 4461.

[18] M. Hunger, W. Wang, Chem. Commun. (2004) 584.

[19] M. Hunger, T. Horvath, Chem. Commun. (1995) 1423.

[20] C. Lamberti, S. Bordiga, F. Bonino, C. Prestipino, G. Berlier, L. Capello, F. D'Acapito, F.X.L.I. Xamena, A. Zecchina, Phys. Chem. Chem. Phys. 5 (2003) 4502.

[21] M. Caravati, J.D. Grunwaldt A. Baiker, Catal.Today 126 (2007) 27.

[22] M. Tada, S. Murata, T. Asakoka, K. Hiroshima, K. Okumura, H. Tanida, T. Uruga, H. Nakanishi, S. Matsumoto, Y. Inada, M. Nomura, Y. Iwasawa, Angew. Chem. Int. Ed. 46 (2007) 4310.

[23] M.A. Newton, A.J. Dent, S.G. Fiddy, B. Jyoti, J. Evans, Catal. Today 126 (2007) 64.

[24] C. Mondelli, D. Ferri, J.D.Grunwaldt, F. Krumeich, S. Mangold, R. Psaro, A. Baiker, J. Catal. 252 (2007) 77.

[25] 23 A.M. Beale, A.M.J. van der Eerden, K. Kervinen, M.A.Newton, B.M. Weckhuysen, Chem. Commun (2005) 3015.

[26] S.J. Tinnemans, J.G. Mesu, K. Kervinen, T. Visser, T.A. Nijhuis, A.M. Beale, D.E. Keller, A.M.J. van der Eerden, B.M. Weckhuysen, Catal. Today 113 (2006) 3.

[27] D. Ferri, M. S. Kumar, R. Wirz, A. Eyssler, O. Korsak, P. Hug, A. Weidenkaff, M.A. Newton, Phys. Chem. Chem. Phys. 12 (2010) 5634.

[28] N. Guo, B.R. Fingland, W.D. Williams, V.F. Kispersky, J. Jelic, W.N. Delgass, F.H. Ribeiro, R.J. Meyer, J.T. Miller, Phys. Chem. Chem. Phys. 12 (2010) 5678.

[29]Y. Yazawa, N. Kagi, S. Komai, A. Satsuma, Y. Murakami, T. Hattori, Catal. Lett. 72 (2001) 157.

[30] Y. Yazawa, N. Takagi, H. Yoshida, S. Komai, A. Satsuma, T. Tanaka, S. Yoshida, T. Hattori, Appl. Catal. A 233 (2002) 103.

[31] Y. Yazawa, H. Yoshida, S. Komai, T. Hattori, Appl. Catal. A 233 (2002) 113.

[32] Y. Yazawa, H. Yoshida, T. Hattori, Appl. Catal. A 237 (2002) 139.

[33] H. Yoshida, Y. Yazawa, T. Hattori, Catal. Today 87 (2003) 19.

[34] M.G. Samant and M. Boudart, J. Phys. Chem. 95 (1991) 4070.

[35] B.L. Mojet, J.T. Miller, D.E. Ramaker, D.C. Koningsberger, J. Catal. 186 (1999) 373.

[36]D.C. Koningsberger, J. de Graaf, B.L. Mojet, D.E. Ramaker, J.T. Miller, Appl. Catal. A 191 (2000) 205.

[37] T. Tanabe, Y. Nagai, K. Dohmae, N. Takagi, N. Takahashi, H. Shinjoh, Top. Catal. 52 (2009) 1433.

[38] T. Tanabe, Y. Nagai, T. Hirabayashi, N. Takagi, K. Dohmae, N. Takahashi , S.

Matsumoto, H. Shinjoh, J. N. Kondo, J. C. Schouten, H. H. Brongersma, Appl. Catal. A 370 (2009) 108.

[39] J.A. Anderson, R.A. Daley, S.Y. Christou, A.M. Efstathiou, Appl. Catal. B 64 (2006) 189.

[40] K. Okumura, K. Kato, T. Sanada, M. Niwa, J. Phys. Chem. C 111 (2007) 14426.

[41] A.N. Mansour, J.W. Cook, D.E. Sayers, J. Phys. Chem. A 88 (1984) 2330.

[42] J. A. Anderson, B. Bachiller-Baezaa, M. Ferna´ndez-Garcı´a, Phys. Chem. Chem. Phys. 5 (2003) 4418.

[43] J. A. Anderson, Z. Liu , M. Ferna´ndez-Garcı´a, Catal. Today 113 (2006) 25.

[44] Y. Nagai, T. Hirabayashi, K. Dohmae, N. Takagi, T. Minami, H. Shinjoh, S. Matsumoto, J. Catal. 242 (2006) 103.

[45] T. Tanabe, Y. Nagai, K. Dohmae, H. Sobukawa, H. Shinjoh, J. Catal. 257 (2008) 117.

[46] E.M.C. Alayon, J. Singh, M. Nachtegaal, M. Harfouche, J.A. van Bokhoven, J. Catal. 263 (2009) 228.

[47] J.Singh, E.M.C. Alayon, M. Tromp, O.V. Safonov, P. Glatzel, M. Nachtegaal, R. Frahm, J. A. van Bokhoven, Angew. Chem. Int. Ed. 47 (2008) 9260.

[48] F.J. Gracia, L. Bollmann, E.E. Wolf, J.T. Miller, A.J. Kropf, J. Catal. 220 (2003) 382.

[49] B.L.M. Hendriksen, J.W.M. Frenken, Phys. Rev. Lett. 89 (2002) 046101.

[50] M.D. Ackermann, T.M. Pedersen, B.L.M. Hendriksen, O. Robach, S.C. Bobaru, I. Popa, C. Quiros, H. Kim, B. Hammer, S. Ferrer, J.W.M. Frenken, Phys. Rev. Lett. 95 (2005) 255505.

[51] R. Burch, Anita Ramli, Appl. Catal. B 15 (1998) 63.

[52] P. Denton, A. Giroir-Fendler, Y. Schuurman, H. Praliaud, C.M.M. Primet, Appl. Catal. A 220 (2001) 141.

[53] R. Burch and T.C. Watling, Catal. Lett. 43 (1997) 19.

[54] R. Burch, J.A. Sullivan, J. Catal. 182 (1999) 489.

[55] Yu Yao Y-F, J. Catal. 87（1984）152.

[56] D.J. Burnett, A.M. Gabelnick, A.L. Marsh, D.A. Fischer, J.L. Gland, Surf. Sci. 553 (2004) 1.

[57] A.M. Gabelnick, A.T. Capitano, S.M. Kane, J.L. Gland, D.A. Fischer, J. Am. Chem. Soc. 122 (2000) 143.

[58] A. Kotsif, D. I. Kondarides, X.E. Verykios, Appl. Catal. B 72 (2007) 136.

[59] A. Kotsif, D. I. Kondarides, X.E. Verykios, Appl. Catal. B 80 (2008) 260.

[60] J. Zhu, J. G. van Ommen, L.Lefferts, Catal. Today 112 (2006) 82.

[61] A.G. Steghuis, J. G. van Ommen, L.Lefferts, Catal. Today 46 (1998) 91.

[62] J. Zhu, J. G. van Ommen, H.J.M. Bouwmeester, L. Lefferts, J. Catal. 233 (2005) 434.

Chapter 5

Pt sintering suppression and catalytic activity of Pt supported catalyst

5.1 Sintering and redispersion behavior of Pt on Pt/MgO

Abstract

Sintering–redispersion of Pt and deterioration–regeneration of catalytic activity on Pt/MgO as automotive exhaust catalyst was studied. No Pt sintering was observed after air aging up to 1173 K. Pt L_3-edge extended X-ray absorption fine structure results revealed the formation of an Mg_2PtO_4-like compound at the MgO surface and stabilization of oxidized Pt after air aging. Interaction between Pt and MgO involved in the formation of this Mg_2PtO_4-like compound likely provides an anchoring effect that prevents Pt sintering. After redox aging at 1073 K, Pt particles of ca. 20 nm were observed by X-ray diffraction and transmission electron microscopy (TEM). TEM images revealed that sintered Pt redispersed into smaller Pt particles of 2–5 nm on sequential oxidation–reduction treatment at 1073 K. Interactions involved in the formation of the Mg_2PtO_4-like compound should be the driving force for this redispersion. The redispersion behavior led to regeneration of the catalytic activity of Pt/MgO in a simulated automotive exhaust reaction.

Keywords; Platinum, MgO, Redispersion, Regeneration, Sintering, X-ray absorption fine structure, Electron microscopy, Automotive catalyst, Turnover frequency

1. Introduction

Supported noble metal (Pt, Rh and Pd) catalysts are widely used to control automotive emissions by converting carbon monoxide, hydrocarbons and nitrogen oxides to carbon dioxide, water and nitrogen in the exhaust gas [1, 2]. Deterioration of catalytic activity is one of the main problems in maintaining low emissions during automotive life. The noble metal loading is thus designed to provide sufficient catalytic performance to maintain low emission levels even after deterioration with long-term usage. If catalyst deterioration can be improved, the noble metal loading can be decreased, leading to more efficient use of natural resources. One of the main causes of deterioration is sintering of the supported noble metals in the catalyst [3–12]. Because Pt easily agglomerates at high temperature (above ca. 1023 K) in the presence of

oxygen [4, 5], inhibition of Pt sintering is one of the key issues in developing efficient automotive catalysts with low Pt loading. In the last two decades, the mechanism of Pt sintering has been investigated extensively with experimental techniques [4-8, 10] and modeling work [8, 9, 11, 12]. Flynn and Wanke developed a model of supported Pt sintering based on the molecular migration of Pt along the surface [8, 9]. In that model, single atoms or molecular cluster escaped from the particles, moved along the surface and were captured by other particles. Through this process the particle size increased and the total surface area of Pt decreased. Dadyburjor et al. also proposed a similar model, but suggested that the internal stress in the Pt particle might have an effect on the multi atom escape from the Pt particle [11, 12]. Völter et al. showed experimentally that the species migrating on the support surface should be oxidized Pt species [10]. This kind of species has been also suggested by Flynn and Wanke [8]. Based on these studies, the more severe Pt sintering observed in oxidative atmospheres should be caused by the production of oxidized Pt species that migrate on the support surface. Besides sintering, the redispersion of supported noble metals has also been studied for a long period. An oxy-chlorination treatment was effective for Pt redispersion and used to regenerate catalytic activity of supported Pt catalysts [13–19]. In those studies, oxy-chlorination was needed to oxidize the Pt crystallites and produce the mobile species including Pt [16, 19]. The oxidized Pt species were deduced by in situ X-ray absorption spectroscopy to be a complex containing oxygen and chlorine [17]. In this redispersion process, that mobile species migrated and were trapped on support sites and decomposed to smaller Pt particles. Redispersion of noble metals on supported catalysts in oxidative atmospheres was also reported in some papers [20-30]. Baker at al. showed the redispersion of sintered Ir on Al_2O_3 via the formation of iridates with Group IIA-oxides [20]. They proposed that redispersion proceeded with the capture of mobile, molecular iridium oxide species by Group IIA-oxides on the support surface. Nishihata et al. studied on $LaFe_{0.57}Co_{0.38}Pd_{0.05}O_3$ perovskite-based catalysts with X-ray diffraction and absorption [21]. They suggested the reversible movement of Pd into and out of the perovskite lattice in oxidative and reductive atmosphere cycles that were likely responsible for the high durability of this catalyst and called this phenomenon self-regeneration. Concerning Pt, the redispersion under oxidative atmosphere were reported mainly on Pt/Al_2O_3 catalysts with moderate treatment temperature of around 773 K [22-31]. Pt redispersion under oxidative atmosphere is closely connected to sintering phenomena. Wanke et al. showed that oxidative atmosphere treatment of Pt/Al_2O_3 at 823 K caused Pt redispersion and higher temperature than 873 K caused Pt sintering. They proposed a molecular migration mechanism of oxidized Pt for Pt

sintering and redispersion in Pt/Al_2O_3 [22]. In this mechanism, the oxidized species migrated on the surface and were trapped at surface sites in redispersion or were captured in Pt crystallites in sintering. Some experimental studies showed that oxidized Pt was stabilized by forming a complex with the Al_2O_3 support in redispersion [23, 26]. Although slightly different mechanisms were proposed, e.g. oxide film formation [28, 29] or particles splitting model [30, 31] for redispersion, the molecular migration and trapped oxidized Pt species on surface sites was common [22-27]. Based on this mechanism, oxidation of Pt and the interaction between oxidized Pt and the support surface sites are important for redispersion.

Nagai et al. recently investigated the interaction between Pt and the support oxide in terms of the inhibition mechanism for Pt on ceria-based oxides [32]. The authors reported that the interaction between Pt and the support oxide inhibited Pt sintering at 1073 K under oxidizing conditions, and that the oxygen 1s core electron level in the support oxide was important for this interaction. The oxidized Pt stabilization was observed on oxides with a lower oxygen 1s core electron level. This oxidized Pt had strong interaction with support and this interaction inhibited the Pt sintering. The oxygen 1s core electron level correlates with the electron density on oxygen and the low core electron level corresponds to high electron density [33]. Higher electron density on oxygen means more electron localization on oxygen rather than covalency. This trend is usually discussed with electronegativity of the element and the acid-base properties of oxide. So, low oxygen 1s core electron level corresponds to more basic property of oxides with lower electronegativity cations. The stabilization of oxidized Pt on basic oxides was already reported and discussed in terms of electronegativity [34]. From this viewpoint, oxygen core electron level should be an experimental parameter to describe the acid-base oxide property and have parallelism with electronegativity. In the present study, we attempted to regenerate the activity of an aged Pt catalyst by redispersion of sintered Pt using the interaction between Pt and the support oxide at high temperature mentioned above. A typical basic oxide (MgO) was chosen as the support because more basic cation in the oxide has a lower oxygen 1s core electron level [32], for which a stronger interaction is expected. MgO is also favorable as a support oxide because of its high surface area. γ-Al_2O_3 was also investigated for comparison. Although Pt redispersion was observed on Al_2O_3 at moderate temperature, it is thought to interact weakly with Pt at high temperature [22, 32]. Comparative investigation of these two oxides should provide some insights into the role of the interaction between Pt and the support oxide for Pt redispersion.

2. Experimental

2.1 Catalyst preparation and aging tests

Pt/MgO and Pt/γ-Al_2O_3 were prepared by the usual impregnation method. MgO (Ube Material Industries) and γ-Al_2O_3 (Nikki Universal) were impregnated with $Pt(NH_3)_2(NO_2)_2$ (Tanaka Kikinzoku Kogyo K.K). The impregnated catalyst was dried in an oven at 383 K for 24 h and calcined in flowing air at 773 K for 5 h. The Pt loading was controlled at 1 wt.%. The catalyst powders were pressed into disks, crushed and sieved to yield pellets of 0.5–1.0 mm for aging and catalytic reaction tests.

Aging tests were performed under two atmospheric conditions. In one aging test, catalyst pellets were placed in a quartz tube and heated at 973, 1073 or 1173 K for 5 h in an air flow (hereafter referred as the air aging test). In the other test, catalyst pellets were placed in a quartz tube and heated at 1073, 1173 or 1273 K for 5 h in a flow cyclically switched every 5 min between 5% O_2 in N_2 and 10% H_2 in N_2 (referred to as the redox aging test). The total flow rate was controlled at 1 L/min in both aging tests.

2.2 Characterization

X-ray diffraction (XRD) was used to evaluate the Pt particle size in each catalyst after aging tests. Measurements were performed using a Rigaku SX instrument with Co K_α radiation (λ=1.7903 Å) operated at 30 kV and 30 mA at a scan speed of 0.125 deg/min. The particle size was estimated from the width at half-height (β) of the XRD line of Pt(311) using the Scherrer equation $L=K\lambda/\beta\cos\theta$ (K=1, λ=1.7903 Å).

The Pt dispersion was determined by CO pulse chemisorption at 323 K using an Ohkura Riken R6015-S instrument. The sample was heated to 673 K in flowing O_2 and held at this temperature for 15 min. After purging with He, the sample was reduced in H_2 for 15 min and then cooled to 323 K in flowing He. A CO pulse was injected into the sample at 323 K until the adsorption reached saturation. The amount of CO adsorbed was calculated as the difference between total amount of CO injected and the outlet from the sample. Metal dispersion was calculated by assuming a CO/surface Pt atom ratio of 1:1 [35].

Transmission electron microscopy (TEM) was performed on a JEOL JEM2000-EX system at an acceleration voltage of 200 kV to observe Pt particles in the catalysts.

Pt L_3-edge (11.5 keV) X-ray absorption fine structure (XAFS) measurements were carried out using the BL01B1 and BL16B2 beamlines at the SPring-8 facility (Hyogo, Japan) to investigate the local coordination structure around Pt and its chemical state after aging tests. Standard samples of Pt foil and PtO_2 were also measured as references for Pt metal and Pt oxide. The storage ring energy was operated at 8 GeV with a typical current of 100 mA. XAFS spectra at the Pt L_3-edge were measured using a Si(111)

double-crystal monochromator in transmission mode at room temperature in air. XAFS data reduction was carried out as described elsewhere [36]. Curve-fitting analysis of extended XAFS (EXAFS) spectra was performed for inverse Fourier transforms on the Pt–oxygen and Pt–cation (cations Pt and Mg) shells using theoretical parameters calculated by McKale et al. [37].

X-Ray photoelectron spectroscopy (XPS) measurements were carried out using a PHI model 5500MC instrument with Mg K_α radiation. Oxygen 1s core electron levels in the support oxides were recorded to evaluate the chemical properties of the support. Binding energies were calibrated with respect to Pt $4f_{7/2}$ at 71.4 eV [32]. The spectrum of Pt $4f_{7/2}$ was also measured to evaluate the valence state of Pt. To calculate the proportion of each valence state, spectral deconvolution was performed.

2.3 Catalytic reaction test

Catalytic reaction tests were carried out in a tubular fixed-bed reactor at atmospheric pressure with a simulated automotive exhaust gas using a conventional flow system [38]. A quantity of 1.0 g of catalyst was used and the total flow rate was 3.3 L/min (W/F=0.009 g·s·mL^{-1}). The conversion of hydrocarbon (HC), carbon monoxide (CO) and NO_x over the catalysts was measured as a function of temperature between 373 and 773 K using a simulated exhaust gas containing 0.7% CO, 0.23% H_2, 0.053% C_3H_6, 0.12% NO, 0.646% O_2, 10% CO_2, and 3% H_2O in N_2. This gas composition resembles the exhaust gas of a gasoline fueled automotive internal combustion engine operating under a stoichiometric air/fuel ratio. Samples were pretreated in situ in the simulated exhaust gas at 773 K for 15 min and then cooled to 373 K before catalytic reaction tests. The concentrations of HC, CO and NO_x in the outlet were measured using an exhaust gas analysis system (MEXA8120, Horiba) as a function of the reaction temperature.

3. Results and discussion

3.1 Air aging

Since previous work [32] revealed that interaction between Pt and the support oxide should occur under oxidizing conditions, the effect of air aging on the catalyst was investigated as a first step. Fig.1 shows the temperature dependences of HC conversion for Pt/γ-Al_2O_3 in (a) and Pt/MgO in (b), before and after air aging tests at 973, 1073 and 1173 K. The catalytic activity of Pt/γ-Al_2O_3 deteriorated severely after air aging tests while the activity of Pt/MgO changed little. As the characteristic temperature dependence of the catalytic reaction in automotive exhaust, the conversion showed very sharp increase in a narrow temperature region and shifted to higher temperature after aging. To evaluate this kind of catalytic activity, the temperature at which 50% HC

conversion occurs (referred as T_{50}) has been frequently used as the indicator of catalytic activity [15] and chosen also in this work. Thus, HC conversion reaches 50% at T_{50} and a lower value of T_{50} indicates higher catalytic activity. Fig. 2 shows T_{50} values for Pt/γ-Al_2O_3 and Pt/MgO, before and after air aging tests at 973, 1073 and 1173 K. T_{50} for Pt/MgO did not change, whereas T_{50} for Pt/γ-Al_2O_3 increased by approximately 200 K after air aging tests. This result indicates that Pt/MgO had higher stability than Pt/γ-Al_2O_3 under oxidizing conditions at high temperature, although its catalytic activity was not as high as that of Pt/γ-Al_2O_3 before the aging test.

The Pt particle size in Pt/MgO and Pt/γ-Al_2O_3 determined by XRD measurements after air aging tests is shown in Table 1. No Pt sintering was observed in Pt/MgO, although the Pt particle size in Pt/γ-Al_2O_3 was ca. 30 nm. The oxygen 1s binding energy measured by XPS for MgO and γ-Al_2O_3 was 529.6 and 531.4 eV, respectively. According to these XPS results, the stability of Pt against sintering agreed with previous results in terms of the oxygen 1s core electron level [32]. This stability of Pt on MgO against sintering corresponded to the stable catalytic performance of Pt/MgO after air aging tests.

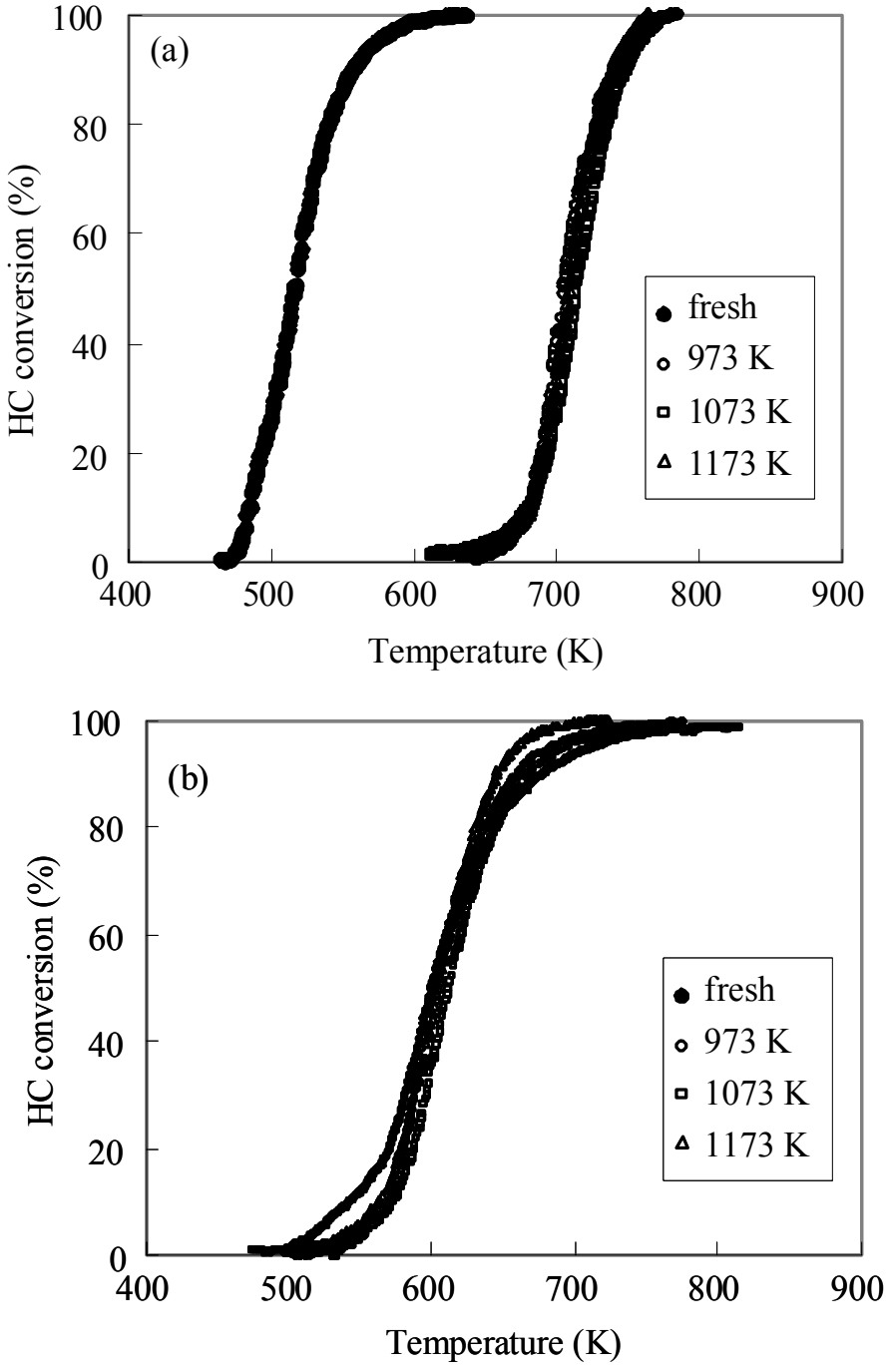

Fig.1 Temperature dependences of hydrocarbon conversion in simulated exhaust reactions over fresh and air aged catalysts. (a) Pt/ γ -Al_2O_3, (b) Pt/MgO. Air aging temperature; 973, 1073 or 1173K.

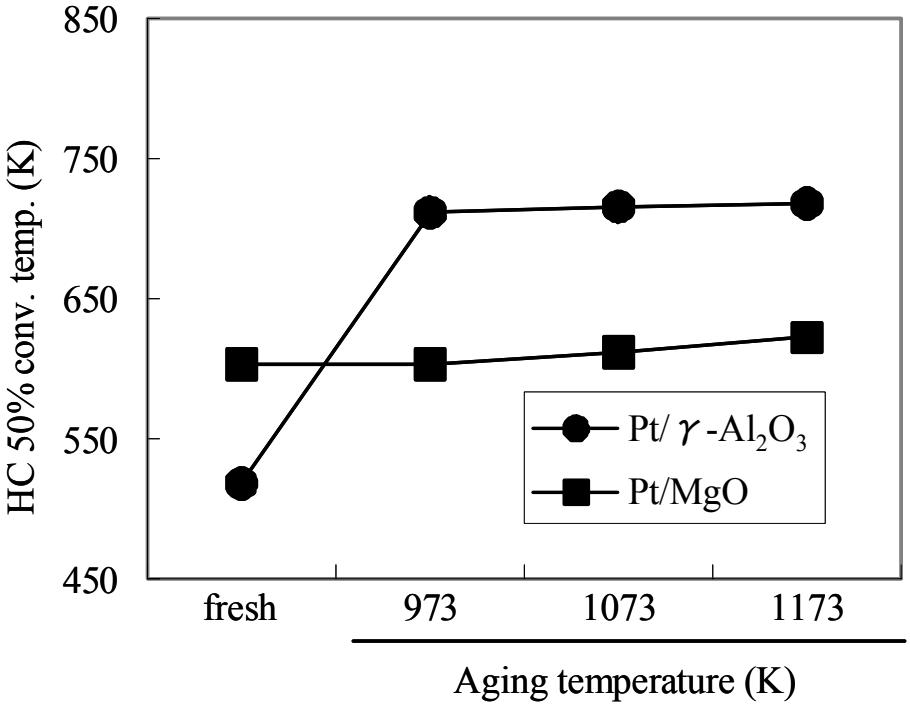

Fig. 2 Hydrocarbon 50% conversion temperatures (T_{50}) in simulated exhaust reactions over Pt/MgO and Pt/ γ -Al_2O_3 before and after air aging tests.

Table 1 Pt particle size determined by XRD in Pt/ γ -Al_2O_3 and Pt/MgO after air aging test

Aging temperature (K)	Pt particle size (nm)	
	Pt/ γ -Al_2O_3	Pt/MgO
973	30	N.D
1073	34	N.D
1173	35	N.D

ND: not detected.

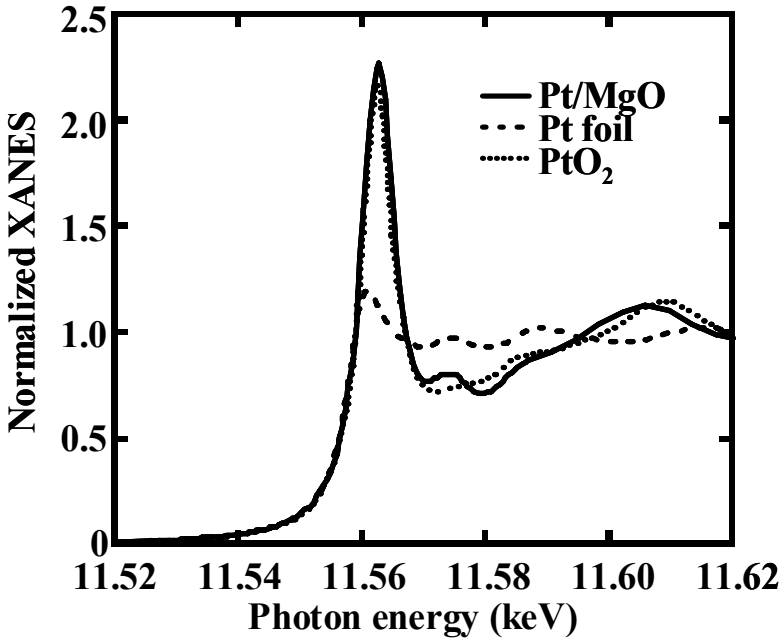

Fig. 3 Pt L_3-edge XANES spectra of Pt/MgO after 1073 K air aging test, together with standard samples of Pt foil and PtO_2 powder.

To investigate the state of Pt in Pt/MgO after air aging tests, XAFS measurements were performed. Fig. 3 shows the X-ray absorption near edge structure (XANES) spectra at L_3-edge for Pt/MgO after air aging at 1073 K with the spectra of standard samples of Pt foil and PtO_2. In the case of Pt L-edge XANES, the white line absorption intensity reflects the vacancy of Pt 5d orbital [39] and is used to estimate the Pt oxidation state [40]. The white line absorption intensity of Pt/MgO after air aging at 1073 K showed comparable or even higher intensity than standard sample of PtO_2. This result indicated that Pt existed in the Pt^{4+} oxidation state in Pt/MgO after air aging at 1073 K. Fig. 4 shows the Fourier-transformed Pt L_3-edge EXAFS spectrum for Pt/MgO after air aging at 1073 K, with spectra of standard samples of Pt foil and PtO_2 shown as references for bulk Pt metal and Pt oxide. Quantitative curve-fitting analysis of the EXAFS spectra was performed for inverse Fourier transforms on the Pt–oxygen and Pt–cation (cation = Pt and Mg) shells. The results of curve-fitting were summarized in Table 2. The FTs are not corrected for phase shift; therefore, the peaks in the FTs are shifted to lower R values. The values of bond length in the text and table are corrected for phase shift. In the FT spectrum of Pt foil, the peak at 2.76 Å is assigned to the Pt–Pt bond. In the FT spectrum of PtO_2, the peaks at 2.04 and 3.10 Å are assigned to the Pt–O and Pt–O–Pt

bonds, respectively. The spectrum of Pt/MgO is clearly different from that of bulk Pt

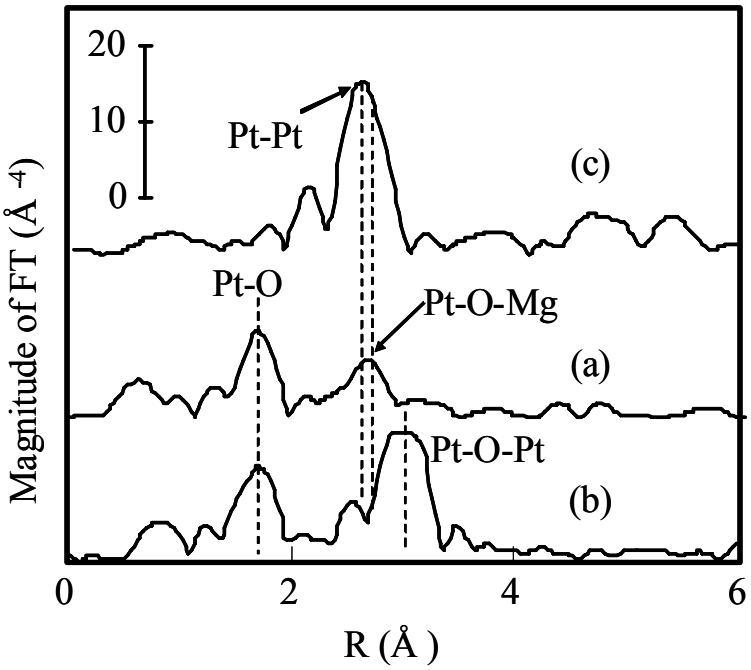

Fig. 4 Fourier-transformed spectra of Pt L_3-edge EXAFS for (a) Pt/MgO after 1073 K air aging tests, and standard samples of (b) PtO_2 powder and (c) Pt foil.

foil and PtO_2. No peak corresponding to the Pt–Pt bond, which should appear at 2.76 Å, was observed in the EXAFS spectrum of Pt/MgO after air aging at 1073 K. The first peak at 2.04 Å was close to that of PtO_2 and it was fitted with the Pt–O bond. The second evident peak at 3.02 Å was not observed in both Pt foil and PtO_2. A curve-fitting simulation of this second peak was carefully performed. Fig. 5 shows the results based on the supposition that the second neighboring atom was Mg or Pt. An excellent fitting result for the simulation of Mg was obtained. In contrast, an appropriate fit could not be obtained for Pt, because the EXAFS oscillation pattern of Pt was very different than that of the experimental data. From this fitting, this second peak was assigned to Pt–O–Mg bond with a distance of 3.02 Å and its coordination number (CN) was 6.2. These XANES and EXAFS results on Pt/MgO after air aging tests at 1073 K indicated that Pt was dispersed at the atomic level as Pt^{4+} and was surrounded by six oxygen atoms in Pt/MgO and that its state was different from that of bulk PtO_2. Muller et al. reported that PtO_2 reacts with MgO to form an inverse spinel-type oxide of Mg_2PtO_4 at an oxygen pressure of 150–200 atm at 1123 and 1173 K [43]. Such a high oxygen pressure was needed to stabilize oxidized Pt because PtO_2 is easily reduced to the metallic state above

Table 2 Results of curve-fitting analysis for the Pt/MgO after 1073 K air aging test and the standard samples

Sample	Shell	CN	*R* (Å)	σ^2 (Å^2)
Pt foil [a]	Pt-Pt	12.0	2.76	0.0045
Pt/MgO	Pt-O	5.9	2.04	0.0041
	Pt-Mg	6.2	3.02	0.0027
PtO_2 [a]	Pt-O	5.7	2.04	0.0026
	Pt-Pt	5.3	3.10	0.0019

CN; coordination number, R; bond distance, σ;Debye-Waller factor

[a] The curve-fitting analysis for the standard samples were performed by reference to [41, 42].

900 K in air. In this inverse spinel structure, Pt is surrounded by six oxygen atoms at octahedral sites. Asakura et al. reported an Pt L_3-edge EXAFS analysis on Pt/MgO catalyst [44], in which the very similar values for Pt local structure were found; the first neighbor was Pt-O with 2.03 Å distance and CN=6.2, the second neighbor was Pt-Mg (oct) with 3.01 Å distance and CN=6.0 and third neighbor was Pt-Mg (tetra) with 3.45 Å distance and CN=4.0. They discussed these results on the basis of a formation of spinel type oxide of Mg_2PtO_4 and proposed that Pt^{4+} ion substituted for Mg^{2+} in the top layer of MgO lattice and its structure distorted to this spinel-like structure. Based on the literature and present XAFS results, we concluded that Pt reacted with MgO to form an Mg_2PtO_4-like compound in air aging tests and existed as atomically dispersed Pt^{4+} ions than sintered metallic Pt particles. The formation of a binary oxide including Pt in supported catalysts was already proposed by Yoshida et al [34]. They discussed Pt L_3-edge XANES results with thermochemical data and showed that electrophobic oxides, such as alkali and alkaline earth oxides, promote noble metal oxidation and the formation of binary oxides including noble metal. The present results and conclusion agree with that proposed mechanism since MgO is a typical electrophobic oxide. This Mg_2PtO_4-like compound is considered to be restricted to the MgO surface [44], because its formation starts on the MgO surface and the Mg/Pt atomic ratio (>2) was much too

great for bulk Mg_2PtO_4. The formation of this Mg_2PtO_4-like compound should act as an anchor for Pt at the MgO surface and should be responsible for inhibiting Pt sintering in air aging tests.

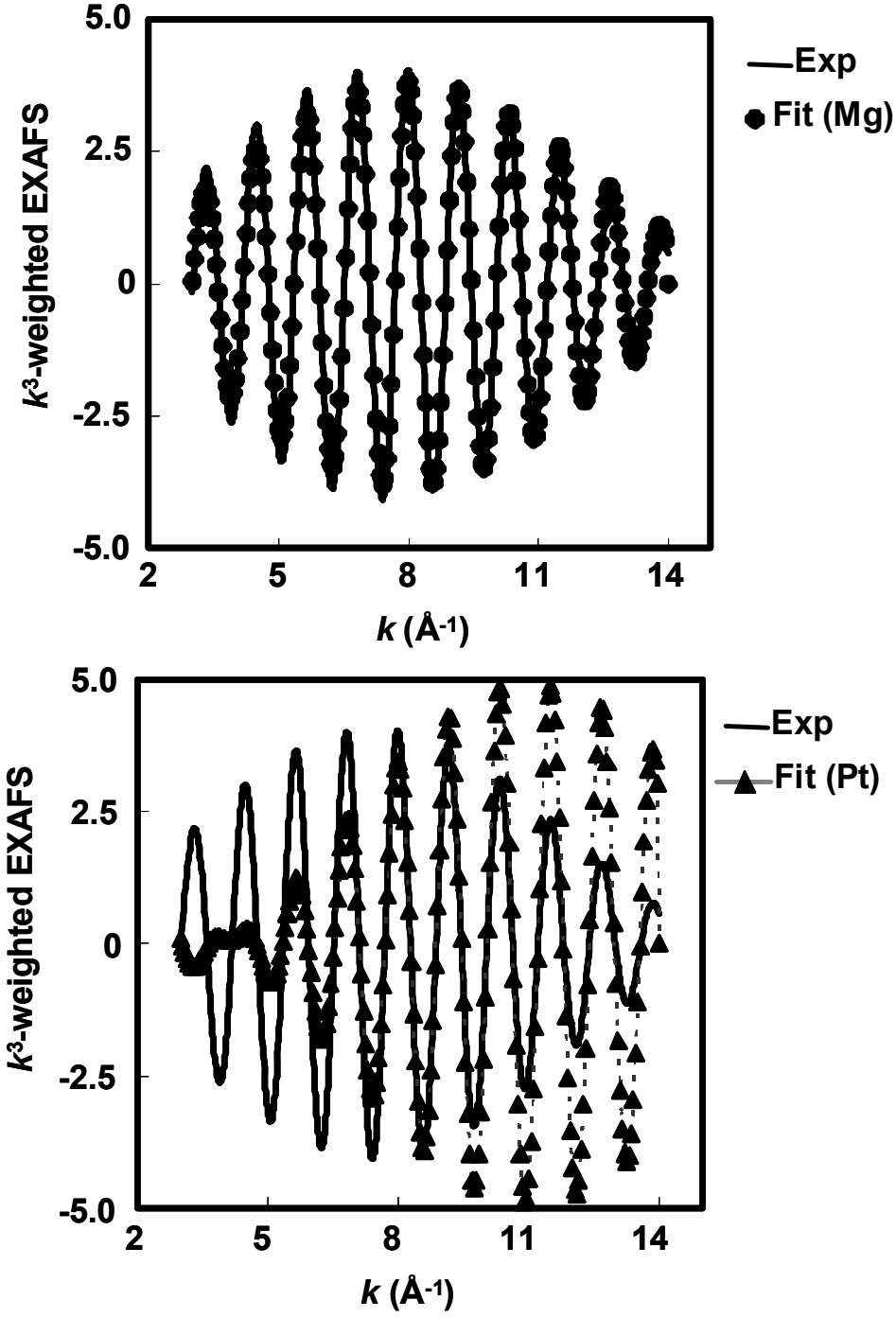

Fig. 5 Curve-fitting analysis on the inverse Fourier-transform of the second peak on the Pt/MgO after 1073 K air-aging test in Fig. 4 and the corresponding curve-fit. (A) Experimental (–) and curve-fit on Mg atom (●). (B) Experimental (–) and curve-fit on Pt atom (··▲··)

3.2 Redox aging

In real situations, automotive catalysts are exposed not only to oxidizing, but also to reducing conditions, because combustion is controlled at a stoichiometric condition between oxidizing and reducing atmospheres to achieve highly efficient catalytic purification of the exhaust gas [1, 2]. To simulate this situation, redox aging tests were performed. The temperature dependences of HC conversion are shown in Fig. 6 for Pt/γ-Al_2O_3 in (a) and Pt/MgO in (b), before and after air aging tests at 1073, 1273 and 1273 K. The conversion curve of Pt/γ-Al_2O_3 shifted almost monotonously to higher temperature with increase of redox aging temperature. In the case of Pt/MgO, although the conversion curve of the aged catalyst shifted to higher temperature from that of fresh catalyst, the changes within the aged catalysts were not as simple as that of Pt/γ-Al_2O_3. The temperature dependence of conversion of the catalyst aged at 1273 K was less steep than those of other aged catalysts. At lower reaction temperature, Pt/MgO aged at 1273 K showed higher activity than those aged at 1173 or 1073 K. The conversion increased less steeply than other aged catalysts and showed lower activity at high reaction temperature. T_{50} for HC conversions after redox aging tests at 1073, 1173 and 1273 K are shown in Fig. 7 for the comparison of catalytic activity. In contrast to air aging tests, T_{50} for Pt/MgO increased after redox tests, although it did not depend on the aging temperature. Pt/MgO showed comparable catalytic activity to that of Pt/γ-Al_2O_3 after redox aging tests at 1073 K. After redox tests at 1173 and 1273 K, Pt/MgO showed higher catalytic activity than Pt/γ-Al_2O_3. This trend was the same if the overall conversion curve was compared among these catalysts. XRD measurements revealed sintered Pt in both catalysts after redox aging, as shown in Fig. 8. The Pt particle size in both catalysts increased with the aging temperature, and the Pt particle size was comparable in Pt/MgO and Pt/γ-Al_2O_3 after redox aging tests at all temperature. These XRD results are not consistent with the catalytic activity results in the viewpoints of the difference between Pt/γ-Al_2O_3 and Pt/MgO, and also the aging temperature dependence of Pt/MgO.

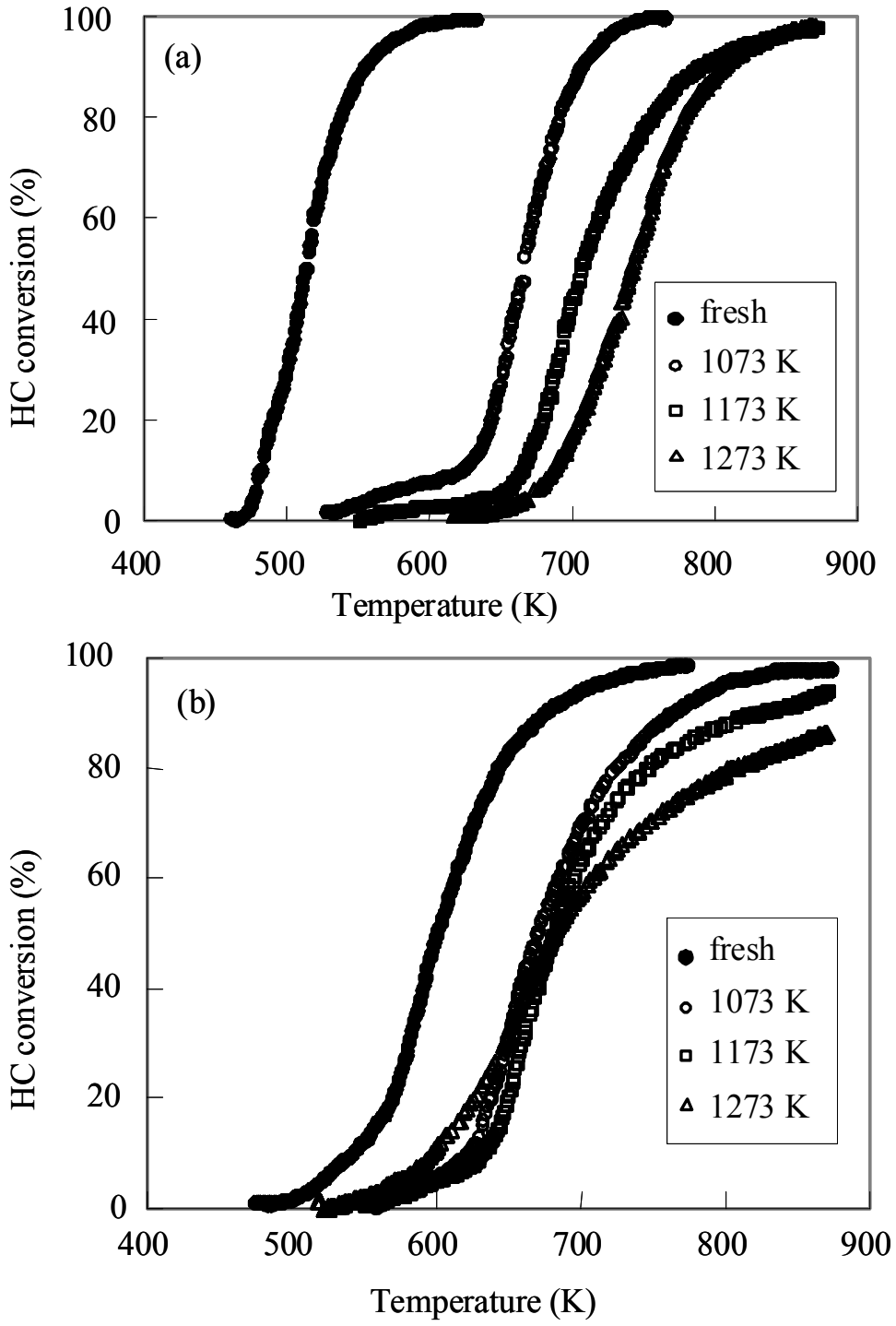

Fig. 6 The temperature dependences of hydrocarbon conversion in simulated exhaust reactions over fresh and redox aged catalysts. (a) Pt/ γ - Al_2O_3, (b) Pt/MgO. Redox aging temperature; 1073, 1173 or 1273K.

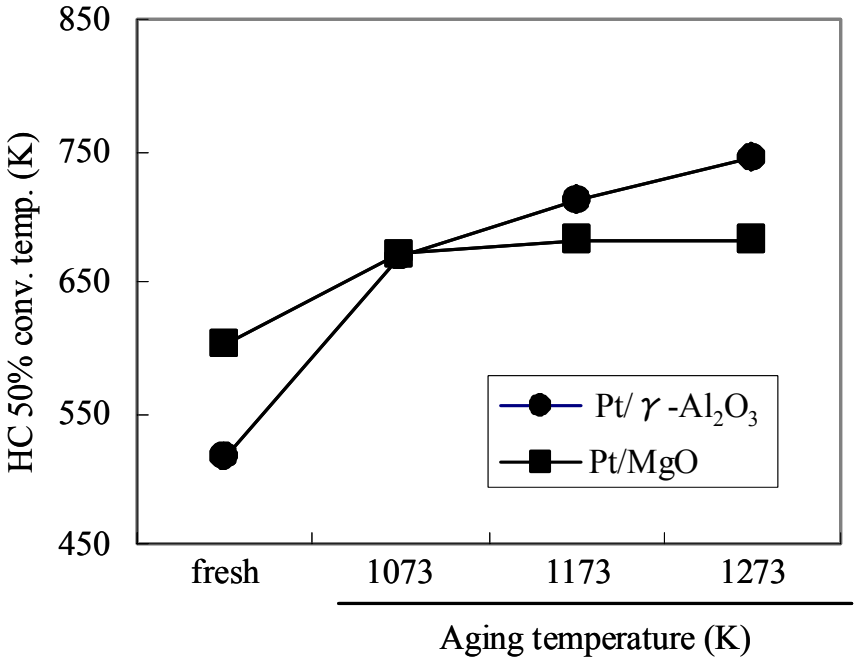

Fig.7 Hydrocarbon 50% conversion temperatures (T_{50}) in simulated exhaust reactions over Pt/MgO and Pt/ γ -Al_2O_3 before and after redox aging tests.

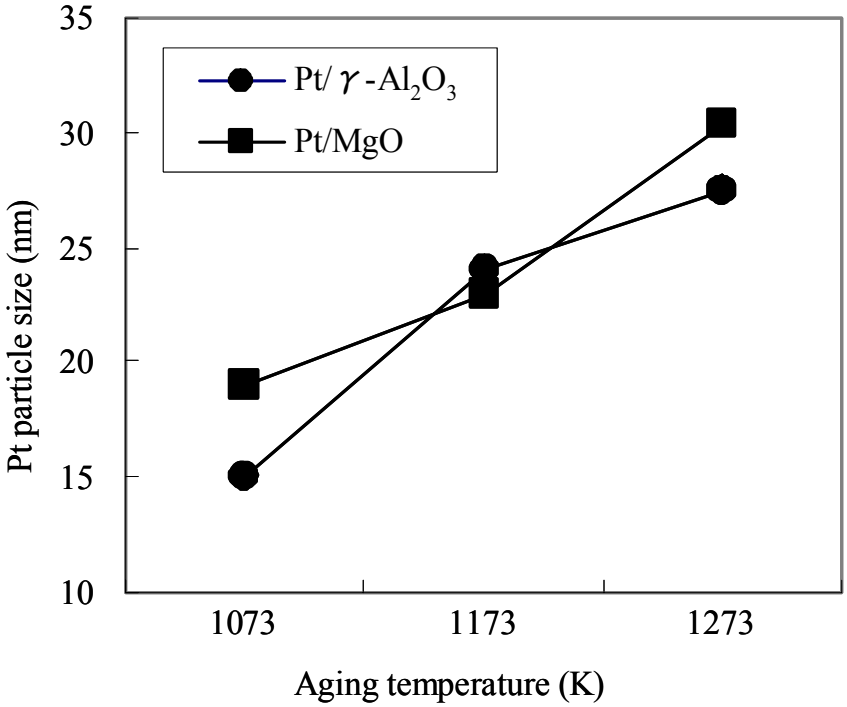

Fig. 8 Particle size of Pt in Pt/MgO and Pt/ γ -Al_2O_3 determined by XRD after redox aging tests.

To investigate this discrepancy in more detail, CO pulse adsorption measurements were used. The Pt dispersions determined by this method are shown in Fig. 9. Pt dispersion in Pt/MgO was almost constant after the redox aging tests. After redox aging at 1073 K, the Pt dispersion in Pt/MgO was comparable to that of Pt/γ-Al_2O_3. After redox tests at 1173 and 1273 K, the Pt dispersion in Pt/MgO was greater than that in Pt/γ-Al_2O_3. This trend for Pt dispersion after redox aging tests is fairly consistent with the catalytic activity. Because Pt dispersion is considered to be a direct measure of the number of active sites in the Pt-supported catalyst, the higher Pt dispersion in Pt/MgO should be responsible for its higher catalytic activity compared to Pt/γ-Al_2O_3. Using these Pt dispersion results, turnover frequency (TOF) of these catalysts were estimated at a reaction temperature of 673 K. The temperature of 673 K was chosen because that temperature was necessary to get enough conversion with Pt/γ-Al_2O_3 redox aged at 1273 K, which showed the lowest activity. The conversions over some catalysts, especially the fresh catalysts, were too high at 673 K to estimate TOF. In such a case, the TOF was estimated from the extrapolation of the conversions at lower temperature with an assumption of Arrhenius-type temperature dependence. The Pt dispersions of fresh Pt/γ-Al_2O_3 and Pt/MgO were determined as 55 and 21 %, respectively by CO pulse adsorption and used to estimate the TOF of fresh catalysts. The results are shown in Fig. 10. The TOF of fresh Pt/γ-Al_2O_3 was much higher than that of fresh Pt/MgO. TOF of Pt/γ-Al_2O_3 decreased and that of Pt/MgO increased after redox aging. The TOFs of redox aged catalysts were almost the same among six Pt/γ-Al_2O_3 and Pt/MgO catalysts. The large TOF difference between fresh Pt/γ-Al_2O_3 and Pt/MgO is likely caused by a support effect on the fresh catalyst. The catalyst on the more basic support showed lower activity for hydrocarbon oxidation and this effect was attributed to the stabilization of oxidized Pt on the oxide [34], After aging tests, the TOFs of the aged catalysts were almost the same regardless of the support or the Pt particle size. This means that the reaction was structure-insensitive.

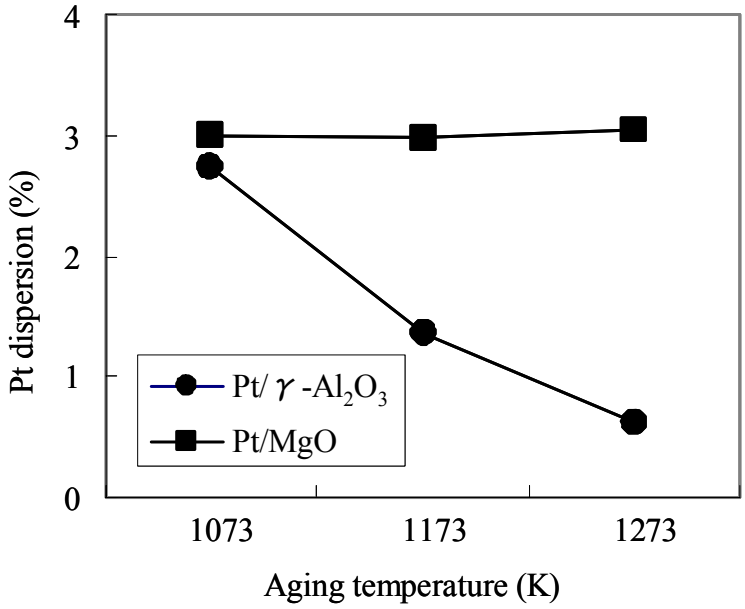

Fig. 9 Dispersions of Pt in Pt/MgO and Pt/ γ -Al_2O_3 determined by CO pulse adsorption after redox aging tests.

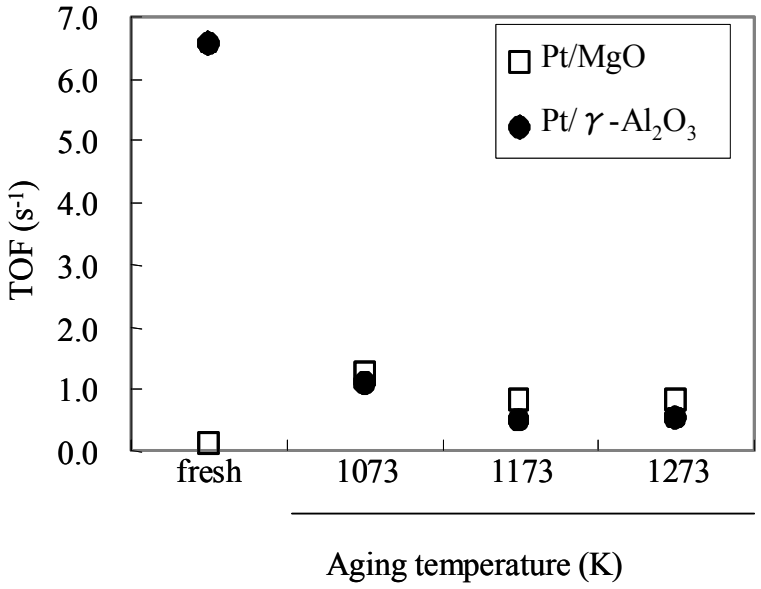

Fig. 10 Turn over frequencies (TOF) of fresh and redox aged Pt/ γ -Al_2O_3 and Pt/MgO. TOF was estimated at 673 K reaction temperature. The values for Pt/ γ -Al_2O_3 aged at 1173 and 1273 K were experimental and for others were estimated from the conversions at lower temperature with an assumption of Arrhenius-type temperature dependence. Pt dispersions in Fig. 9 were used for aged catalysts. Pt dispersion of fresh Pt/ γ -Al_2O_3 and Pt/MgO determined by CO pulse adsorption were 55 and 21 %, respectively and used to estimate the TOFs of fresh catalysts.

The discrepancy between the Pt particle size determined by XRD and the Pt dispersion determined by CO adsorption should be attributed to the difference in Pt particle size distribution in these catalysts, because the experimental results give only an average value over the distribution. The number of Pt particles smaller than ca. 5 nm, which are not observable by XRD measurement, should be greater on Pt/MgO than on Pt/γ-Al_2O_3. These small Pt particles contribute to the CO adsorption and catalytic activity. The larger number of small Pt particles on Pt/MgO could be caused by strong interaction between Pt and MgO under oxidizing conditions, as mentioned in Section 3.1. Even among the aged Pt/MgO, the Pt particle size estimated by XRD increased with increasing aging temperature although the Pt dispersions were almost constant after any aging temperature. This result would indicate the Pt particle size distribution change in Pt/MgO with increasing aging temperature. A bimodal type distribution would account for these results [25], in which the large Pt particles sintered to larger particles and the number of Pt particles smaller than ca 5 nm increased with increasing aging temperature. This Pt particle size distribution change might be a reason for the change of the temperature dependence of the conversion of aged Pt/MgO.

3.3 Regeneration after redox aging

If the interaction between Pt and MgO under oxidizing conditions is effective after redox aging of samples, this interaction could be a driving force for the redispersion of sintered Pt particles. Thermal treatment in air at 1073 K could cause a reaction between Pt particles and MgO to form an Mg_2PtO_4-like compound on the MgO surface. This reaction could cause atomic-level redispersion of Pt on the MgO surface under oxidizing conditions. To investigate this hypothesis, Pt/MgO was submitted to a redox aging test at 1073 K, after which it was treated in air for 5 h at 1073 K. The catalyst was then reduced in a flow of 10% of H_2 in N_2 for 5 h at 1073 K. The size of the Pt particles after each treatment was investigated by TEM and XRD. TEM images of the catalyst after each treatment are shown in Fig. 11. After the redox aging test, Pt particles of ca. 20 nm were observed in TEM images (Fig. 11A), which is comparable to the size estimated from XRD measurements. After thermal treatment in air at 1073 K, large Pt particles almost disappeared (Fig. 11B) and no Pt diffraction peak was observed in the XRD pattern. After this oxidizing treatment, Pt particles were considered to have been redispersed at the atomic level, with the formation of Mg_2PtO_4-like compound on the MgO surface. After reduction by 10% H_2/N_2 at 1073 K, many Pt particles of 2–5 nm appeared (Fig. 11C). After this reducing treatment, Pt atoms segregated as metallic Pt particles from the Mg_2PtO_4-like compound. These results demonstrated that sequential oxidation and reduction treatments at 1073 K led to redispersion of sintered Pt into

smaller Pt particles, and the interaction between Pt and MgO was effective at high temperature, even after redox aging tests. During this sequential treatment, the oxidation state of the supported Pt was investigated by XPS. Pt/γ-Al_2O_3 was also investigated for comparison. XPS measurements were made on both samples after redox aging tests, oxidizing treatment and reducing treatment. The percentage of Pt in high valence states (summation of $Pt^{2+}$and Pt^{4+}) is summarized in Table 3. On Pt/γ-Al_2O_3, supported Pt was found to be in the Pt^0 (metallic) state after every treatment, and no high valence state was observed. Because Pt was sintered as large particles on Pt/γ-Al_2O_3 after redox aging tests, almost all the Pt atoms should exist as large Pt particles in the metallic state. On the other hand, a high valence state (Pt^{2+} or Pt^{4+}) was observed on Pt/MgO, even after redox aging, although large Pt particles were confirmed both in TEM images and from XRD measurements. This result suggests that some Pt atoms interacted strongly with MgO and not all Pt atoms existed as large particles, even after redox aging. The percentage of Pt in high valence states increased to 80% after oxidizing treatment and decreased to 30% after reducing treatment. A proportion of Pt after reducing treatment could be transformed to high valence states during sample transfer in air at room temperature for XPS measurements. The present redispersion results agreed well with the redispersion mechanism [22-27] in which oxidized Pt species migrated along surface and were trapped at surface sites. The XPS observation of a high valence state Pt in Pt/MgO after oxidizing treatment revealed the presence of oxidized Pt species in the redispersion. The Mg_2PtO_4-like compound should be the trap site for oxidized Pt species and should be a driving force for the redispersion.

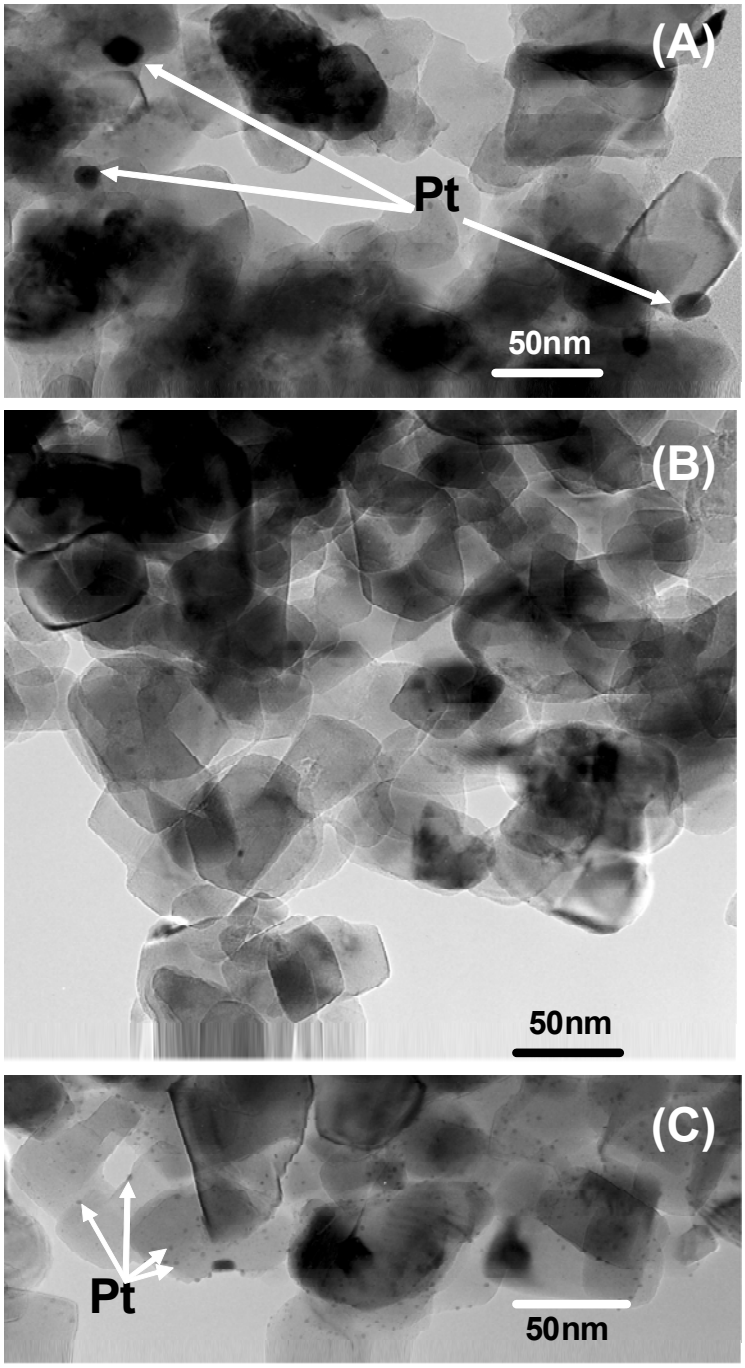

Fig. 11 TEM image of Pt/MgO (A) after a redox aging test at 1073 K, (B) after thermal treatment at 1073 K in air for 5 h and (C) after reduction at 1073 K for 5 h in 10% H_2/N_2.

To determine if the regeneration of catalytic activity can be attributed to this Pt redispersion, a catalytic activity test was performed on Pt/MgO using a simulated exhaust gas. For comparison, Pt/γ-Al_2O_3 was treated in the same manner and its catalytic activity was also tested. Fig. 12 shows T_{50} for the catalytic reaction. As mentioned in Section 3.2, Pt/γ-Al_2O_3 showed much higher activity than Pt/MgO before aging. T_{50} for both Pt/MgO and Pt/γ-Al_2O_3 increased to comparable values after the redox aging test. T_{50} for Pt/MgO decreased after sequential oxidation–reduction treatment at 1073 K after redox aging tests, whereas T_{50} for Pt/γ-Al_2O_3 increased further. Since the number of active sites dominantly determined catalytic activity after redox aging tests mentioned in Sec. 3.2, this catalytic regeneration was considered to be caused by the redispersion of Pt. These results demonstrated that deactivated Pt in Pt/MgO catalyst could be regenerated via redispersion of the agglomerates by sequential oxidation–reduction treatment at 1073 K, whereas the activity of Pt/γ-Al_2O_3 further deteriorated after the same treatment. The results indicate that a strong interaction between Pt and the support oxide is essential for catalyst regeneration.

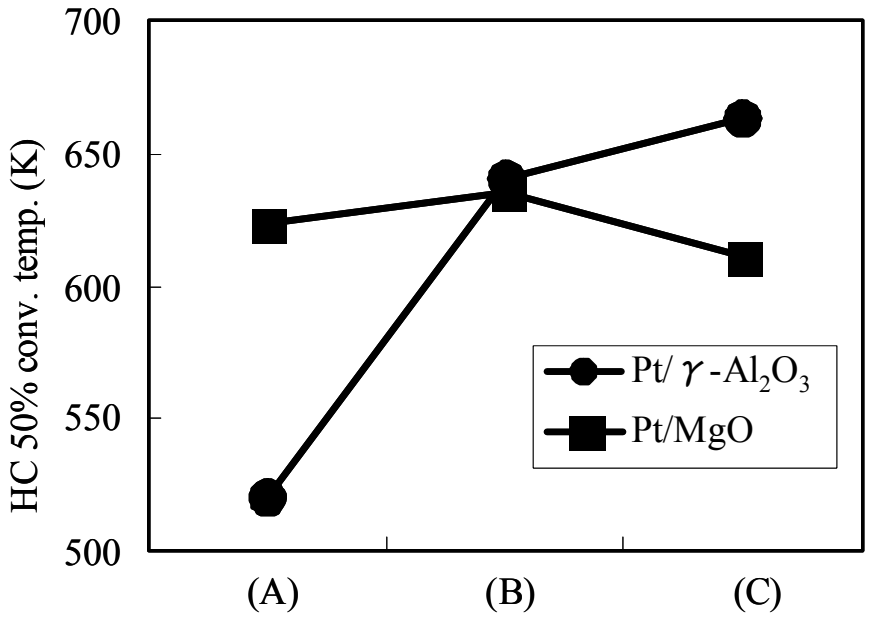

Fig. 12. Hydrocarbon 50% conversion temperatures (T_{50}) in simulated exhaust reactions over Pt/MgO and Pt/ γ -Al_2O_3: (A) before aging; (B) after a redox aging test at 1073 K; and (C) after sequential oxidation for 5 h in air and reduction for 5 h in 10% H_2/N_2 at 1073 K.

4. Conclusions

After redox aging tests at above 1073 K, the catalytic activity of Pt/MgO deteriorated

and Pt agglomerates of ca. 20 nm were observed by XRD and TEM. TEM images revealed that the sintered Pt redispersed into smaller particles of 2–5 nm on sequential treatment in 20% O_2/N_2 followed by 5% H_2/N_2 at 1073 K. This redispersion of Pt led to regeneration of the catalytic activity of Pt/MgO to a value almost the same as that before the aging test. In contrast the same sequential treatment caused further deterioration of Pt/γ-Al_2O_3 after redox aging at 1073 K. EXAFS and XPS results revealed oxidized Pt species and the formation of Mg_2PtO_4-like compound on the MgO surface after oxidizing treatment at 1073 K. This Mg_2PtO_4-like compound formation should be the driving force for the redispersion.

Acknowledgements

We thank Mr. N. Suzuki for TEM observations, Mr. N. Isomura for XPS measurements, and Mr. N. Takahashi for fruitful discussions.

References

[1] S. Matsumoto, Catal. Today 90 (2004) 183.
[2] H.C. Yao, Y.F. Yao, J. Catal. 86 (1984) 254.
[3] C.H. Bartholomew, Appl. Catal. A Gen. 212 (2001) 17.
[4] R.M. J. Fiedorow, B.S. Chahar, S.E. Wanke, J. Catal. 51 (1978) 193.
[5] S.A. Hassan, F.H. Khalil, F.G. El-Gamal, J. Catal. 44 (1976) 5.
[6] F. Oudet, A. Vejux, P. Courtine, Applied Catal. 50 (1989) 79.
[7] P.C. Flynn, S.E. Wanke, J. Catal. 37 (1975) 432.
[8] P.C. Flynn, S.E. Wanke, J. Catal. 34 (1974) 390.
[9] P.C. Flynn, S.E. Wanke, J. Catal. 34 (1974) 400.
[10] H. Lieske, G. Lietz, H. Spindler, J. Völter, J. Catal. 81 (1983) 8.
[11] E. Ruckenstein, D.B. Dadyburjor, J. Catal. 48 (1977) 73.
[12] D.B. Dadyburjor, S.P. Marsh, M.E. Glicksman, J. Catal. 99 (1986) 358.
[13] H. Birgersson, L. Eriksson, M. Boutonnet, S. G. Jaras, Appl. Catal. B Environ. 54 (2004) 193.
[14] F.C. Galisteo, R. Mariscal, M.L. Granados, J.L.G. Fierro, R.A. Daley J.A. Anderson, Appl. Catal. B Environ. 59 (2005) 227.
[15] M.J. D'Aniello, D.R. Monroe, C.J. Carr, M.H. Krueger, J. Catal. 109 (1988) 407.
[16] K. Foger, H. Jaeger, Appl. Catal. 56 (1989) 137.
[17] F.L. Normand, A. Borgna, T.F. Garetto, C.R. Apesteguia, B.D Moraweck, J. Phys. Chem. 100 (1996) 9068.
[18] A. Monzón. T.F. Garetto, A. Borgna, Appl. Catal. A Gen. 248(2003) 279.

[19] K. Foger, H. Jaeger, J. Catal. 92 (1985) 64.
[20] G.B. McVicker, R.L. Garten, R.T.K. Baker, J. Catal. 54 (1978) 129.
[21] Y. Nishihata, J. Mizuki, T. Akao, H. Tanaka, M. Uenishi, M. Kimura, T. Okamoto, N. Hamada, Nature 418 (2002) 164.
[22] R.M.J. Fiedorow, S. E. Wanke, J. Catal.43 (1976) 34.
[23] T.J. Lee, Y.G. Kim, J. Catal. 90 (1984) 279.
[24] J. Adamiec, R.M.J. Fiedorow, S.E. Wanke, J. Catal. 95 (1985) 492.
[25] J.M. Rickard, L. Genovese, A. Moata, S. Nitsche, J. Catal. 121 (1990) 141.
[26] K. Otto, W.H. Weber, G.W. Graham, J. Z. Shyu, Appl. Surf. Sci. 37 (1989) 250.
[27] G. Lietz, H. Lieske, H. Spindler, W. Hanke, J. Völter, J. Catal. 81 (1983) 17.
[28] E. Ruckenstein, Y.F. Chu, J. Catal. 59 (1979) 109.
[29] I.Sushumna, E. Ruckenstein, J. Catal. 108 (1987) 77.
[30] R.Gollob, D.B. Dadyburjor, J. Catal. 68 (1981) 473.
[31] D.B. Dadyburjor, J. Catal. 57 (1979) 504.
[32] Y. Nagai, T. Hirabayashi, K. Dohmae, N. Takagi, T. Minami, H. Shinjoh, S. Matsumoto, J. Catal. 242 (2006) 103.
[33] G.A. Somorjai, Introduction to surface chemistry and catalysis, John Wiley & Sons, Inc., New York, 1994, p 388.
[34] H. Yoshida, Y. Yazawa, T. Hattori, Catal. Today 87 (2003) 19.
[35] J.A. Anderson, R.A. Daley, S.Y. Christou, A.M. Efstathiou, Appl. Catal. B Environ. 64 (2006) 189.
[36] T. Tanaka, H. Yamashita, R. Tsutitani, T. Funabiki, S. Yoshida, J. Chem. Soc. Faraday Trans. 84 (1988) 2987.
[37] A.G. McKale, B.W. Veal, A.P. Paulikas, S.K. Chan, G.S. Knapp, J. Am. Chem. Soc. 110 (1988) 3763.
[38] A. Morikawa, T. Suzuki, T. Kanazawa, K. Kikuta, A. Suda, H. Shinjoh, Appl. Catal. B Environ. 78 (2008) 210.
[39] A.N. Mansour, J.W. Cook, D.E. Sayers, J. Phys. Chem. A 88 (1984) 2330.]
[40] H. Yoshida, S. Nonoyama, Y. Yazawa, T. Hattori, Phys. Scr. T 115 (2005) 813.
[41] M. Vaarkamp, Catal. Today 39 (1998) 271.
[42] A.F. Lee, K.Wilson, R.M. Lambert, C.P. Hubbard, R.G. Hurley, R. W. McCabe, H. S. Gandhi, J. Catal. 184 (1999) 491.
[43] O. Muller, R. Roy, Mater. Res. Bull. 4 (1969) 39.
[44] K. Asakura, H. Nagahiro, N. Ichikuni,Y. Iwasawa, Appl. Catal. A Gen. 188 (1999) 313.

5.2 Low temperature CO pulse adsorption for the determination of Pt particle size in a Pt/cerium-based oxide catalyst

Abstract

Unexpectedly large amounts of CO adsorption have resulted from a pulse adsorption experiment at 323 K, giving about 300 % Pt dispersion in a Pt/cerium-based oxide catalyst. An in-situ diffuse reflectance infrared Fourier transform spectroscopic investigation on a Pt/cerium-based oxide during CO adsorption has revealed that carbonate species on the cerium oxide surface are responsible for the unrealistically large CO adsorption at 323 K, as a result of CO spillover. Lowering the temperature to 195 K considerably diminished the amount of CO adsorption. The size of the Pt particles in the Pt/cerium-based oxide catalyst was determined by CO pulse adsorption at 195 K and showed good agreement with the particle size determined by X-ray diffraction and low energy ion scattering. This indicates that CO pulse adsorption at 195 K is a useful technique to reliably estimate the Pt particle size in a Pt/cerium-based oxide catalyst.

Keywords; Pt particle size, cerium-based oxide, CO adsorption, X-ray diffraction, Low Energy Ion Scattering

1. Introduction

Supported noble metal (Pt, Pd and Rh) catalysts are used for the control of emissions in automotive exhausts by converting carbon monoxide (CO), hydrocarbons and nitrogen oxides to carbon dioxide (CO_2), water and nitrogen in the exhaust gas [1,2]. The suppression of the catalyst deterioration is one of the major issues in the development of efficient catalysts that use sufficiently small quantities of a noble metal. Because sintering of the noble metal is one of the major reasons for the catalyst deterioration, suppression of the sintering is very important. The sintering of the supported noble metal, especially Pt, has been extensively studied over recent decades [3-10]. Because knowledge about the Pt particle size in the catalyst is essential to quantify the level of Pt sintering, different physical/chemical techniques have been employed for particle size determination [11-17]. One technique is the direct observation of the noble metal particles by transmission electron microscopy (TEM). Other physical techniques include X-ray diffraction (XRD) line broadening, small angle X-ray scattering and X-ray absorption fine structure (XAFS). Chemical characterization techniques are based on selective adsorption of probe molecules on the noble metal and

CO or H_2 are frequently used for this. The advantages and the limitations of these techniques have been reviewed in the literature [11, 12].

In the practical development of automotive catalysts, CO adsorption is the most widespread characterization technique because it is relatively easy and requires only a simple experimental set-up [12]. The CO adsorption technique covers the particle size range of 1 to 10 nm, which is highly relevant for automotive catalysts.

To ensure a high conversion efficiency of pollutants, industries often use cerium-based oxides in three-way automotive catalysts (TWC) to keep the catalyst surface at nearly stoichiometric conditions by its oxygen storage/release function, even when the engine's exhaust air-to-fuel-ratio fluctuates [2]. The presence of cerium-based oxide makes it difficult to determine the Pt particle size in the catalyst [12]. There are reports that the CO adsorption measurement gives extremely large values for the amount of CO adsorption in the cerium-based oxide containing catalyst. The CO uptake of the cerium-based oxide itself is considered as the main reason for the extraordinary large amount of CO adsorption [11-19]. Holmgren et al. investigated the interaction of CO with Pt/CeO_2 [18, 19]. They suggested that the extraordinary large amount of CO adsorbed by the Pt/CeO_2 is caused by the formation of carbonate species on the CeO_2 support surface.

Komai et al. showed that CO pulse adsorption on Pt/CeO_2, after a mild reduction pretreatment from 373 to 573 K, gave a reasonable Pt dispersion that agreed well with the Pt particle size determined by TEM observations [13]. Takeguchi et al. proposed that the CO_2 adsorption pretreatment suppressed the CO adsorption on the CeO_2 surface; O_2-CO_2-H_2-CO pulse sequencing was used to determine the amount of adsorbed CO on the platinum [14]. A similar result was reported using a combination of infrared (IR) absorption spectroscopy of the chemisorbed CO and TEM observations of the Pt/CeO_2 [15]. In these studies, the combination of surface pretreatment and pulse sequencing has been used to obtain a reasonable amount of CO adsorption. Because many variations of cerium-based oxides are used in catalyst development, an appropriate pretreatment protocol has to be found for each type of cerium-based oxide. Holmgren et al. reported that the formation of carbonate species on a CeO_2 support surface was suppressed by lowering the adsorption temperature to 195 K [18, 19]. Their studies showed a decrease of the amount of CO adsorbed by lowering the temperature from 298 to 195 K. However, it is not clear whether this approach can be applied to the determination of the Pt particle size.

Another approach used IR absorption spectroscopy during CO adsorption on Pt/cerium-based oxides [16, 17]. The IR absorption band of CO linearly bonded on the

Pt atom can be distinguished from other adsorbed CO species, such as carbonates, on the catalyst. The integrated absorption band intensity of this linearly bonded CO gives the amount of the chemisorbed CO on the platinum atoms. Although this approach is a straightforward way of determining the amount of CO adsorbed on to the Pt, a calibration curve is still necessary for each catalyst, correlating the integrated band intensity and the CO adsorption.

Based on these considerations, the aim of this study was to develop a simple and readily applicable technique to determine the Pt particle size in Pt/cerium-based oxide catalysts. CO adsorption at low temperature was chosen for this study because this technique was considered as the simplest of the techniques mentioned above. To demonstrate the feasibility of this technique for determination of Pt particle size, a comparative study with other methods such as XRD and low energy ion scattering (LEIS) is necessary. LEIS is a surface science technique that can be used to quantify the chemical composition of the outermost surface of a material [20 -23]. In this study, LEIS was used to estimate the size of Pt particles smaller than about 5 nm because this is considered the lowest limit that can be quantified by XRD.

2. Experimental

2.1 Catalysts

CeO_2 was supplied by Anan Kasei and used as received. CeO_2-ZrO_2 (50 mol% Ce) was prepared by conventional precipitation. $Ce(NO_3)_3 \cdot 6H_2O$ and $ZrO(NO_3)_2 \cdot 2H_2O$ were dissolved in distilled water and then aqueous NH_3 was added to cause the precipitation. The filtered precipitate was dried at 383 K and then calcined at 773 K in air. The oxide powders were impregnated with $Pt(NH_3)_2(NO_2)_2$ (Tanaka Kikinzoku Kogyo K.K). The impregnated catalysts were dried in an oven at 383 K for 24 h and then calcined in flowing air at 773 K for 5 h. The Pt loading was controlled at 1 wt.%. Pt/CeO_2-ZrO_2 catalysts were treated in a nitrogen flow containing 3% CO and 3% H_2O at a temperature between 1073 and 1323 K for 5 h for sintering of Pt. The addition of 3% of H_2O was achieved by bubbling the nitrogen gas flow through water.

2.2 In situ diffuse reflectance infrared Fourier transform spectroscopy (in situ DRIFTS)

In situ diffuse reflectance infrared Fourier transform spectroscopy (DRIFTS) measurements were performed using a JASCO FT-IR spectrometer (FT/IR-8400) with an in situ DRIFTS cell. The gas flow set-up was connected to the FT-IR spectrometer; a gas mixture of O_2, H_2, CO and N_2 generated by means of mass flow controllers was introduced into the in situ cell after the catalyst powder was placed in the cell. The

catalyst was heated to 673 K in a gas flow of 7 % O_2 in N_2 and held at this temperature for 15 min. After purging with nitrogen for 5 min, the catalyst was reduced in a gas flow of 7 % H_2 in N_2 at 673 K for 15 min. After purging again with nitrogen for 5 min, the catalyst was cooled to the measurement temperature in a nitrogen flow. The measurements were performed at 323 and 195 K. In the measurement at 323 K, the temperature was controlled by the heater in the in situ cell. In the measurement at 195 K, cooled N_2 gas was introduced to flow through the cooling water pipe in the in situ cell instead of cooling water. This cooled N_2 was obtained by passing it through the pipe in the Dewar-bottle filled with liquid N_2. It took about 50 min for cooling to 195 K. This was about 4 times longer than the time needed for the measurement at 323 K. At the measurement temperature, a FT-IR spectrum was recorded and then the gas flow was switched to 0.28 % CO in N_2 for CO adsorption. Then the FT-IR spectra of the adsorbed CO were recorded. The difference spectra were obtained by subtracting the spectra recorded during nitrogen flow from the spectra obtained after the introduction of 0.28 % CO in N_2 at different measurement temperatures (323 and 195 K).

2.3 CO pulse adsorption

CO pulse adsorption measurements were performed using an Ohkura Riken R6015-S instrument modified for CO adsorption at low temperature. The sample was heated to 673 K in an oxygen flow and held at this temperature for 15 min. After purging with He, the sample was reduced in H_2 for 15 min and then cooled to the measurement temperature in a helium flow. CO pulses were injected at that temperature until the adsorption reached saturation. The measurement temperature was varied between 323 and 195 K. For the temperature variation measurement, the adsorption temperature was controlled by the heater in the flow of cooled N_2 gas that was obtained by the evaporation of liquid nitrogen. In the case of the constant temperature at 195 K, dry ice-ethanol bath cooling was also employed instead of with N_2 gas cooling because of the convenience of the experiment, since it became easy to obtain the stability of temperature. The concentration of the CO pulse was determined by a thermal conductivity detector (TCD). The outlet gas was monitored also by a mass spectrometer (ULVAC, MMC-200). The amount of CO adsorption was calculated as the difference between the total amount of CO injected and the amount measured at the outlet from the sample. The metal dispersion was calculated by assuming a CO to surface metal atom ratio of 1:1 [24]. The Pt particle size was estimated using the cubic Pt particle model with the calculated Pt metal dispersion.

2.4 X-ray diffraction

XRD measurements were performed using a RINT-1500V instrument (Rigaku) with

Cu K_α radiation (λ=0.15418 nm) operating at 40 kV and 350 mA at a scan speed of 0.125°/min. The Pt particle size (L) was estimated from the full width at half maximum (β) of the XRD line of Pt(111) using the Scherrer equation $L=K\lambda/\beta\cos\theta$ (K=1, λ=0.15418 nm).

2.5 Transmission electron microscopy

TEM graphs were obtained on a JEOL JEM2000-EX system at an acceleration voltage of 200 kV to observe the Pt particles in the catalysts.

2.6 Low energy ion scattering

LEIS measurements were performed in the UHV Calipso LEIS setup [20 -23]. In this setup, the primary ion beam is directed perpendicular to the surface. In the double toroidal energy analyzer, all ions scattered over 145^0 with respect to the incoming beam are detected. Integration of the signal over the full azimuth and parallel energy detection gave a high detection sensitivity, thus allowing static analysis of highly dispersed insulating catalysts. At first, the catalysts were pretreated in an atomic oxygen beam to remove any traces of environmental contaminations. The cleaned catalysts were then heated in a hydrogen flow to a temperature of 573 K. The temperature ramp rate was controlled at 10 K/min. In this procedure, the hydrogen pressure was kept at 20 kPa and the flow rate was kept at 80 ml/min. The maximum temperature of 573 K was maintained for 10 min. After this treatment, the pre-treatment chamber was evacuated and the catalyst sample was transported to the LEIS analysis chamber. The base pressure of this chamber was below 10^{-8} Pa. After the reduction pretreatment, hydrogen atoms remain on the surface of the catalyst. This LEIS technique is only sensitive to the outermost atomic layer of the material [20-23]. Therefore the remaining hydrogen affected the LEIS spectra and the scattered intensity decreased. To remove these hydrogen atoms from the sample, we sputtered the reduced catalyst with 3 keV Ne^+ ions. An ion dose of 1.0×10^{15} Ne^+ ions /cm^2 was needed to obtain a completely hydrogen-free surface. Between a dose of 1.0×10^{15} and 1.4×10^{15} Ne^+ ions /cm^2, the surface composition and the elemental LEIS yields of the catalysts remained unchanged. In this “depth window”, the quantification of Pt was performed.

A Pt (100) single crystal was used to calibrate the LEIS spectra to relate it to the density of Pt atoms on the surface. The Pt (100) single crystal specimen was cleaned with an atomic oxygen beam. Subsequently, the surface was sputtered with 3 keV Ne^+ ions, which removed 2 to 3 monolayers of material. 3 keV He^+ LEIS measurements were used to check whether all oxygen atoms had been sputtered off the specimen. Finally, the specimen was annealed to obtain an atomically smooth surface.

3. Results and discussion

3.1 DRIFTS study during CO adsorption

The adsorbed species on the Pt/CeO_2 catalyst sample during CO adsorption were studied by in situ DRIFTS measurements. Holmgren et al. reported the FT-IR results of CO adsorption on the Pt/CeO_2 catalyst and showed that minor contamination of the catalyst, for example with chlorine, considerably changed the CO adsorption behavior [19]. Figure 1 shows the DRIFT spectra of the adsorbed CO on the Pt/CeO_2 catalyst. The spectra are presented as the difference spectra obtained by subtracting the spectra before and after CO adsorption at the same temperature. In the spectrum measured at 323 K (Fig. 1 (A)), a strong absorption band is observed between 1700 and 1200 cm^{-1}. This is the typical absorption band of carbonate species adsorbed on oxides [16, 17, 19]. The absorption band near 2050 cm^{-1} corresponds to CO linearly bonded on Pt. This result indicates that the CO was not only adsorbed on the Pt but also on the CeO_2 surface by forming the carbonate species at 323 K. As suggested by Holmgren et al., this adsorbed carbonate species is responsible for the extraordinary large quantity of adsorbed CO measured at 323 K. This species can be generated by the spillover process from the CO adsorbed on Pt. A basic site such as O^{2-} on CeO_2 oxide will react with the spillover CO to form the carbonate species (Fig. 2). Since this spillover process and the successive reaction with lattice oxygen on the CeO_2 surface are activated processes, they can be suppressed at low temperature. The spectrum measured at 195 K is shown in Fig. 1 (B). The absorption band corresponding to the carbonate species has noticeably diminished, while the intensity of the band due to CO bonded to Pt did not change significantly. This result revealed that the CO spillover process and the reaction to form carbonate species were suppressed at this temperature, and the CO adsorbed on Pt is the dominant species on the catalyst. These results agree well with the results obtained by Holmgren et al. Following the discussion in sections 3.2 and 3.3, the amount of CO adsorption decreased a lot by lowering the temperature to 195 K; the Pt particle size determined by the amount of CO adsorption at 195 K agreed well with the size determined by other methods. These results indicate that the spillover process was suppressed well at 195 K and that the amount of carbonate species observed in DRIFTS at 195 K should be sufficiently small to estimate the Pt particle size. A weak band was observed at about 2150 cm^{-1}, which most probably corresponds to CO co-adsorbed on Pt with oxygen atoms [25, 26]. The oxygen source could be a small contamination in the nitrogen flow. It took about 50 minutes for cooling to 195 K after pre treatment at 673 K; this about 4 times longer than was needed for the measurement at 323 K. This longer duration of the nitrogen flow after the pretreatment may have caused the small

amount of oxygen adsorption on Pt and is most probably the reason why this weak band was observed only in the measurement at 195 K.

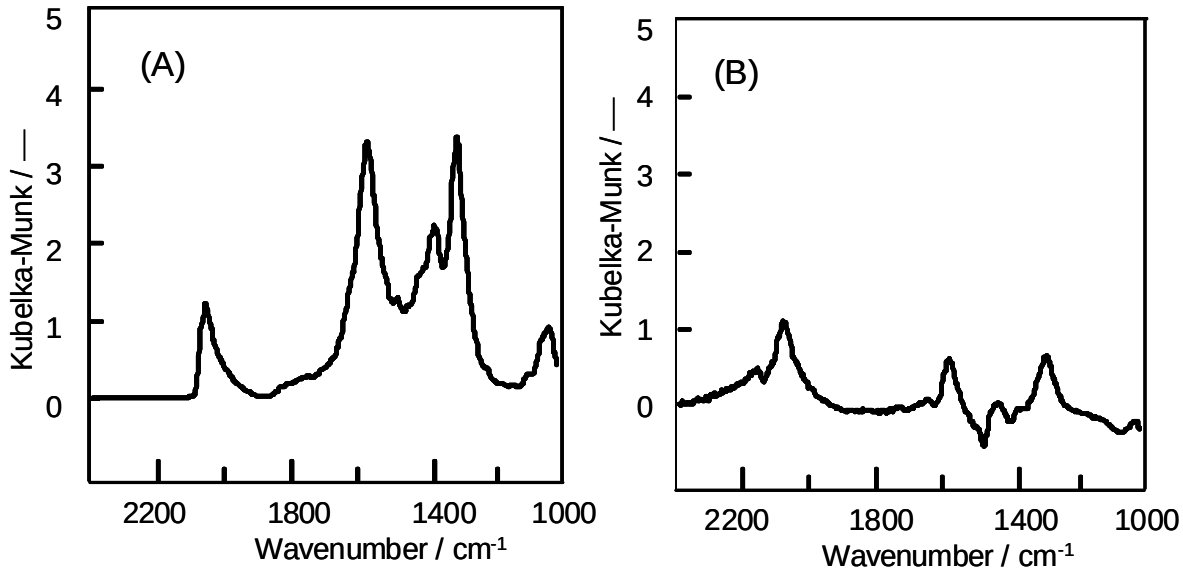

Fig. 1 DRIFT spectra of adsorbed CO on Pt/CeO_2: (A) 323 K, (B) 195 K. The spectra are shown as the difference spectra of adsorbed CO and are obtained by subtracting the spectra in nitrogen flow from the spectra obtained after introduction of 0.28 % CO/N_2.

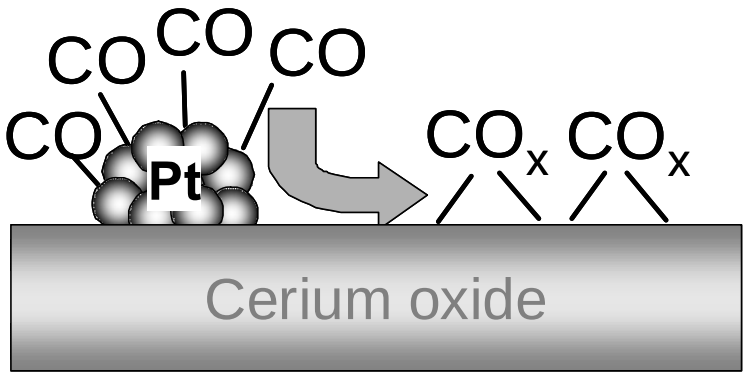

Fig.2 Schematic illustration of CO spillover from Pt to the CeO_2 surface with carbonate species.

3.2 CO pulse adsorption at low temperature

CO pulse adsorption measurements at low temperature were carried out to determine the Pt dispersion in the Pt/CeO_2 and Pt/CeO_2-ZrO_2 catalysts. Figure 3 shows the CO concentration as a function of time in the outlet gas during the pulse adsorption experiments on Pt/CeO_2 at 323 K and 195 K. About 20 pulses were required to saturate the catalyst by adsorption of CO at 323 K. At this temperature the large degree of adsorption at the first pulse and the continuing adsorption after the second pulse point to two processes taking place: that is, CO adsorption on Pt and CO spillover onto the CeO_2 surface (Fig.3 (A)). At 195 K, saturation takes place at the second pulse, pointing to CO adsorption on the Pt only, without spillover (Fig. 3 (B)). The outlet gas was also monitored by a mass spectrometer. No CO_2 evolution was observed in the outlet gas. So, the spillover will be the main process in the CO adsorption at 323 K. The amounts of CO adsorption and Pt dispersion were estimated from the pulse adsorption measurements at both temperatures (Table 1). The dispersion of Pt at 323 K is unrealistically high and exceeds 100%, while the Pt dispersion at 195 K is 27%, illustrating the feasibility of the method at this lower temperature.

On the Pt/CeO_2-ZrO_2 catalyst, the amount of CO adsorption was determined at different temperatures (Fig. 4). It decreases with decreasing temperature from 323 K to 220 K and then remains constant below 220 K. This result indicates that a temperature of 195 K is suitable to perform CO pulse adsorption experiments on the Pt/CeO_2-ZrO_2 catalyst. To simplify the experiment, we chose a temperature of 195 K for the remaining experiments because 195 K can be reached with dry ice-ethanol cooling and is thus more convenient than cooling with N_2 gas.

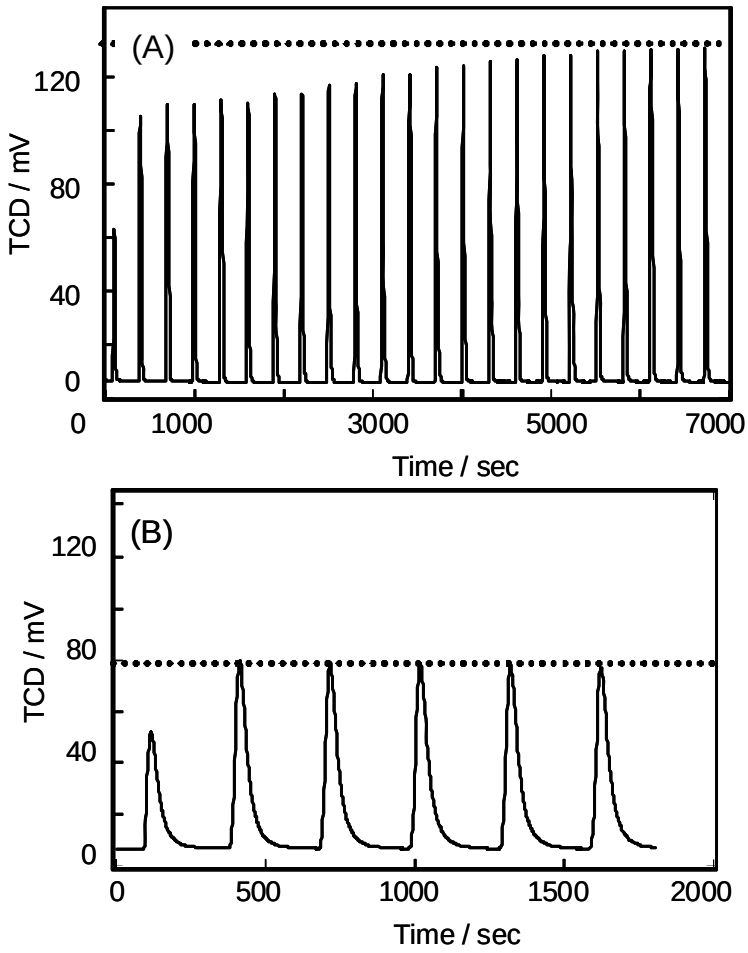

Fig. 3 CO adsorption as a function of time on Pt/CeO_2: (A) 323 K, (B) 195 K.

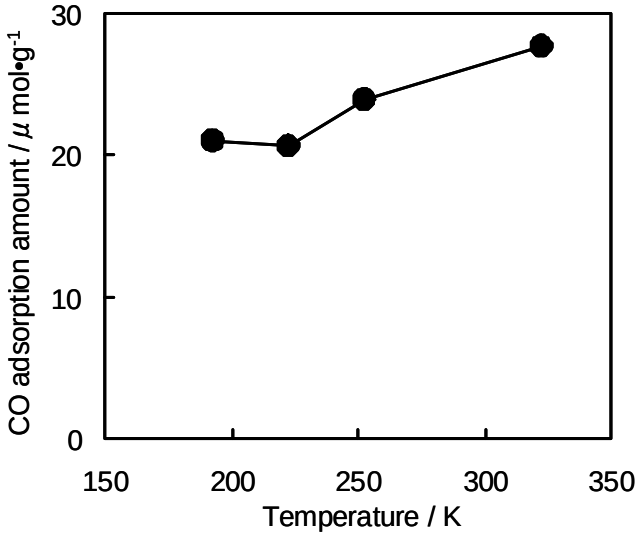

Fig. 4 Temperature dependence of CO adsorption on Pt/CeO_2-ZrO_2.

3.3 Comparative study on the Pt particle size

A comparative study was carried out to investigate the validity of the CO pulse adsorption at 195 K in order to estimate the Pt particle size in the Pt/cerium-based oxide catalysts. Catalyst samples with different Pt particle sizes were prepared for this study. In general, the size of supported Pt particles in actual catalyst samples may show a size distribution. To avoid wide particle size distributions, we kept the heat treatment temperatures as low as possible to avoid sintering of the particles, leading to wide size distributions. Concerning Pt sintering, it is known that Pt easily sinters to form larger particles with a wide particle size distribution after heat treatment in oxidizing atmospheres [6, 7]. In our work, the reducing heat treatment was employed to avoid the wide particle size distribution caused by oxidizing heat treatment. A temperature higher than 1073 K was needed for Pt sintering to take place during reducing heat treatment. Only Pt/CeO_2-ZrO_2 samples were used in this study, because the thermal stability of CeO_2 as the support was not sufficient under these conditions. TEM images of Pt/CeO_2-ZrO_2 samples after heat treatment at 1323, 1223 and 1073 K are shown in Fig. 5. Pt particles as large as 100 nm are observed for the sample treated at 1323 K (Fig. 5 (A)). This sample is therefore not suitable for the CO pulse adsorption measurement because the amount of CO adsorption on this sample will be too low. In the sample treated at 1223 K, the Pt particle size was about 5 nm and its particle size distribution was sufficiently narrow, as can be seen in Fig. 5 (B). Relatively uniformly sized Pt particles, approximately 2 to 3 nm diameter, are observed in the sample treated at 1073 K (Fig. 5 (C)). Based on these TEM observations, 1123, 1173 and 1223 K were chosen as the heat treatment temperatures for the comparative studies between XRD and low temperature CO pulse adsorption. LEIS measurements were applied to the sample treated at 1073 K, because the particle size was smaller than the XRD measurement limit. CO pulse adsorption measurements at 195 K were performed on all samples. Figure 6 shows the LEIS spectrum of the Pt/ CeO_2-ZrO_2 sample treated at 1073 K. Three peaks corresponding to Zr, Ce, and Pt are observed in the spectrum. The outermost surface composition can be estimated from the peak intensity [20], as seen in Table 2. The intensity corresponding to Pt measured on the Pt (100) surface of a Pt single crystal is also shown in Table 2. Because the surface density of Pt atoms on the Pt (100) surface can be calculated from the crystal structure, the intensity corresponding to Pt measured on the Pt (100) surface was used as the calibration to estimate the accessible Pt atoms in the Pt/CeO_2-ZrO_2 sample (see Table 3). The Pt particle size was calculated from the number of accessible Pt atoms with the cubic Pt particle model [22]. In this model the accessible Pt atoms are considered to be located at the surface of the

cubic Pt. The XRD patterns of Pt(111) measured on the Pt/CeO_2-ZrO_2 sample treated at 1123, 1173 and 1223 K are shown in Figure 7. The Pt particle size estimation from XRD data was carried out using the Scherrer equation with the full width at half maximum (Table 4). In Fig. 8, a good agreement is shown between the Pt particle sizes determined by LEIS, XRD and CO pulse adsorption at 195 K. This confirms the reliability of the CO pulse adsorption measurements at 195 K for the size of Pt particles in the Pt/CeO_2-ZrO_2 catalyst.

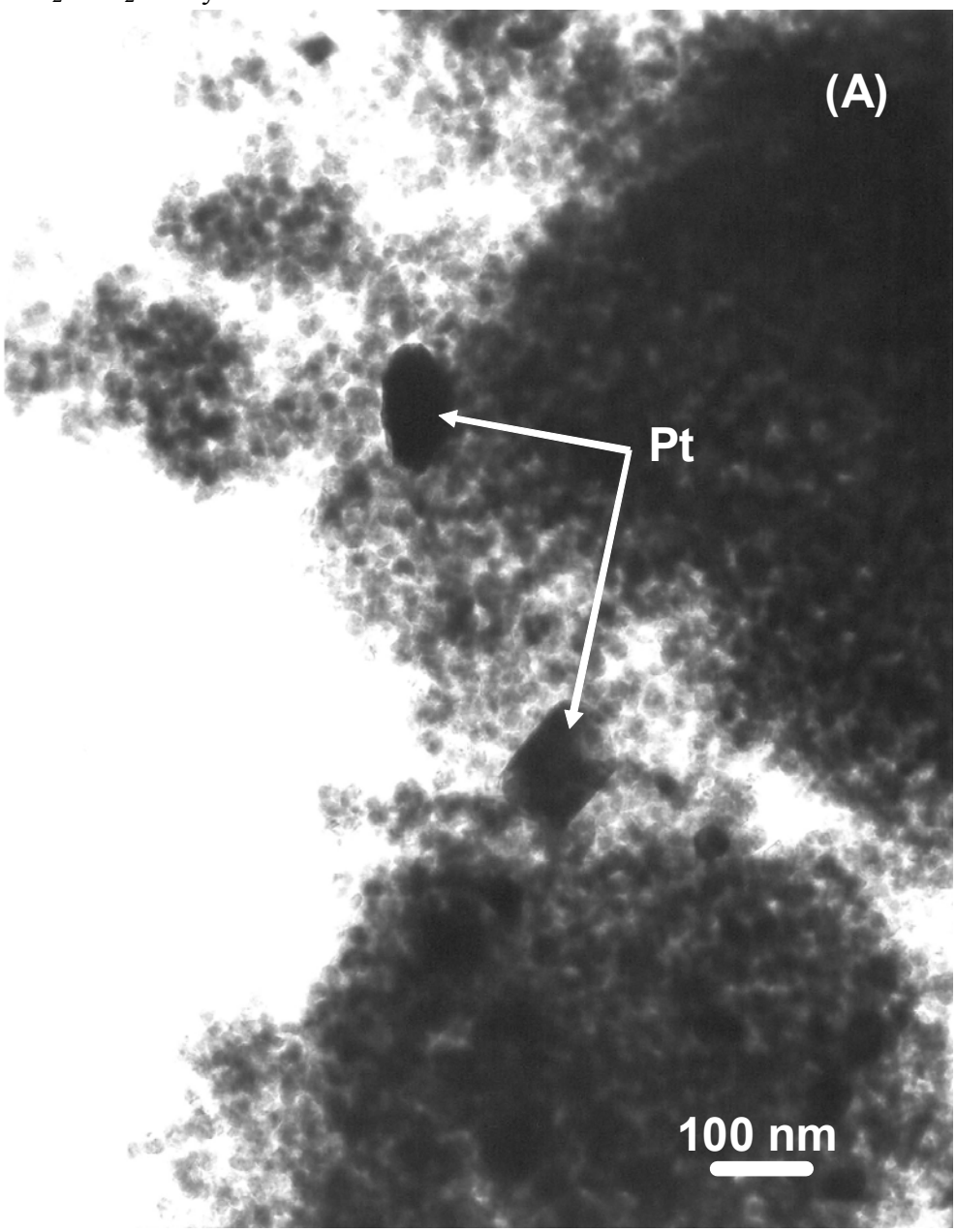

Fig. 5-(A) TEM image of Pt/CeO_2-ZrO_2 after heat treatment at 1323 K.

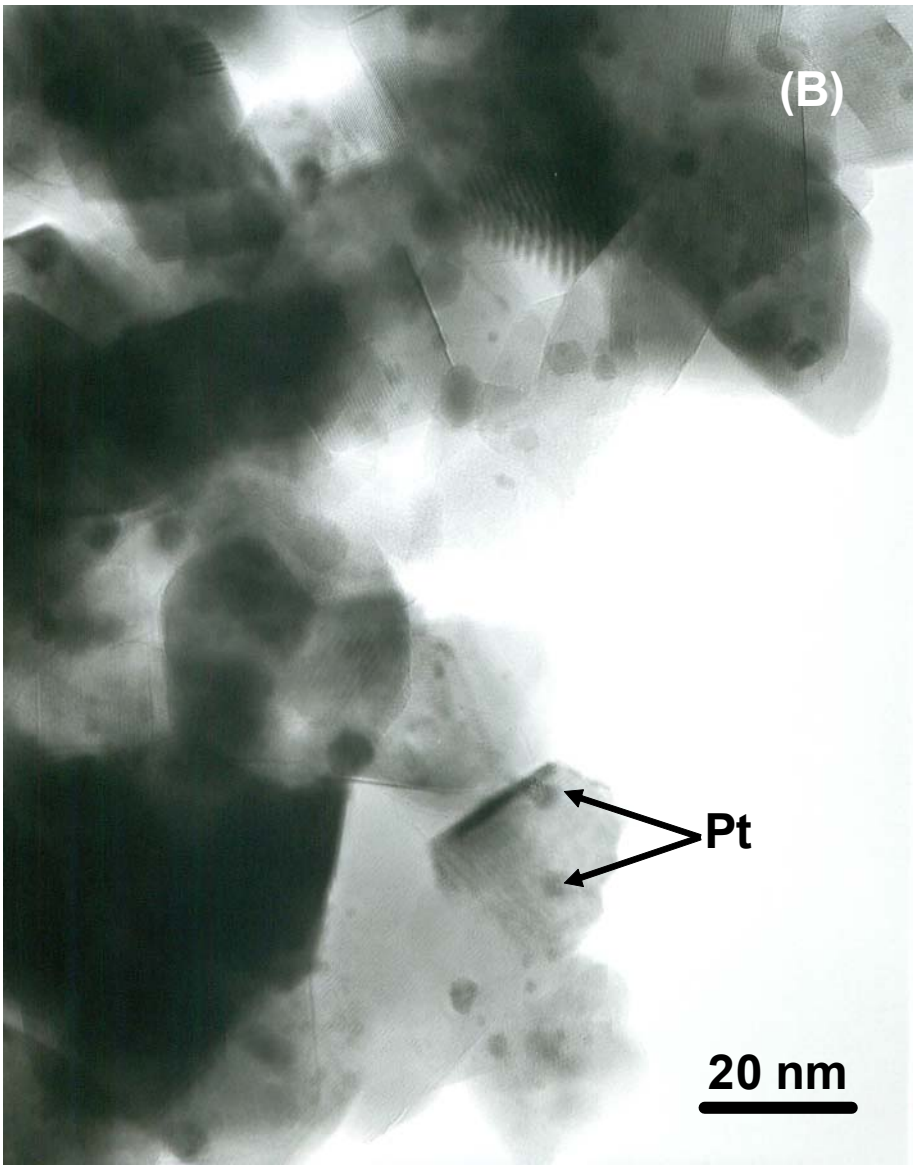

Fig. 5-(B) TEM image of Pt/CeO_2-ZrO_2 after heat treatment at 1223 K.

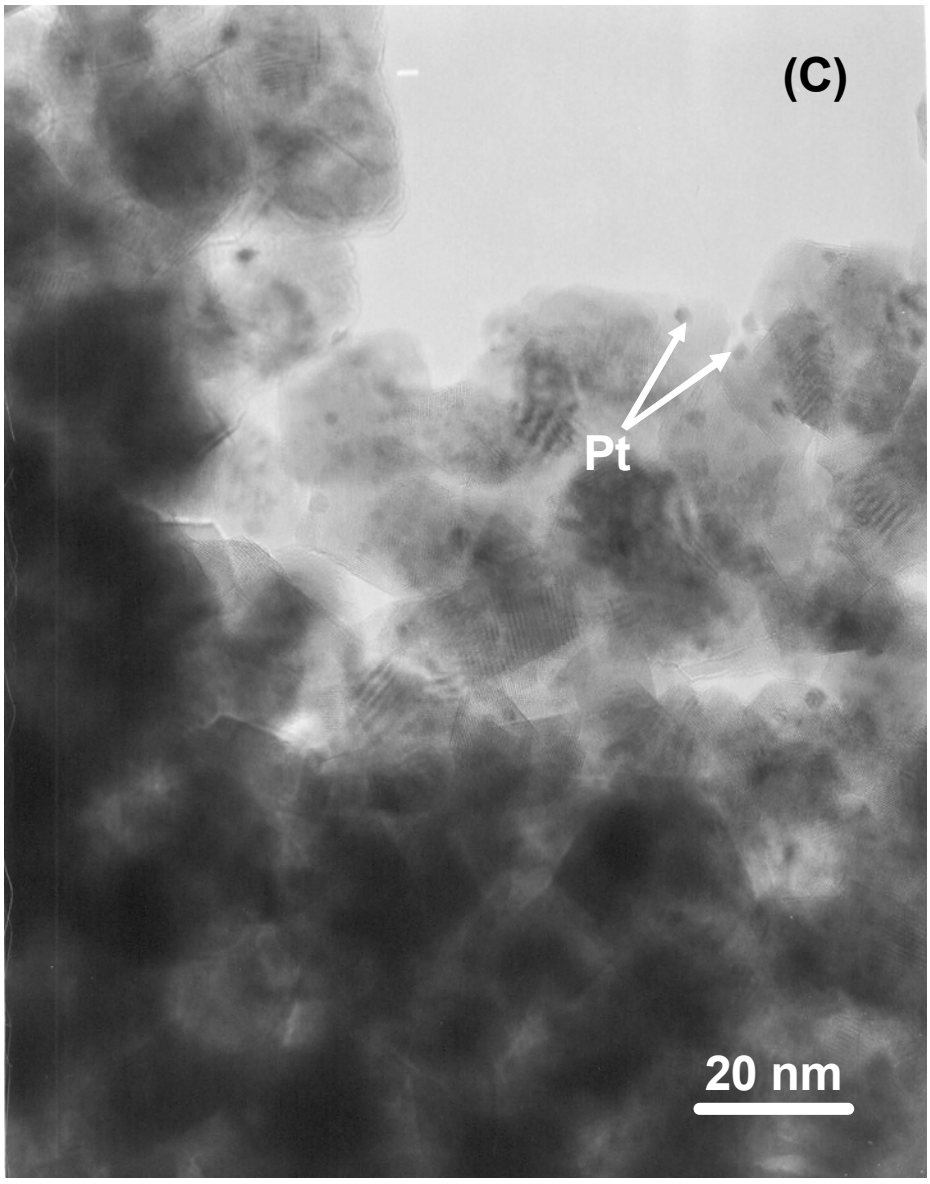

Fig. 5-(C) TEM image of Pt/CeO_2-ZrO_2 after heat treatment at 1073 K.

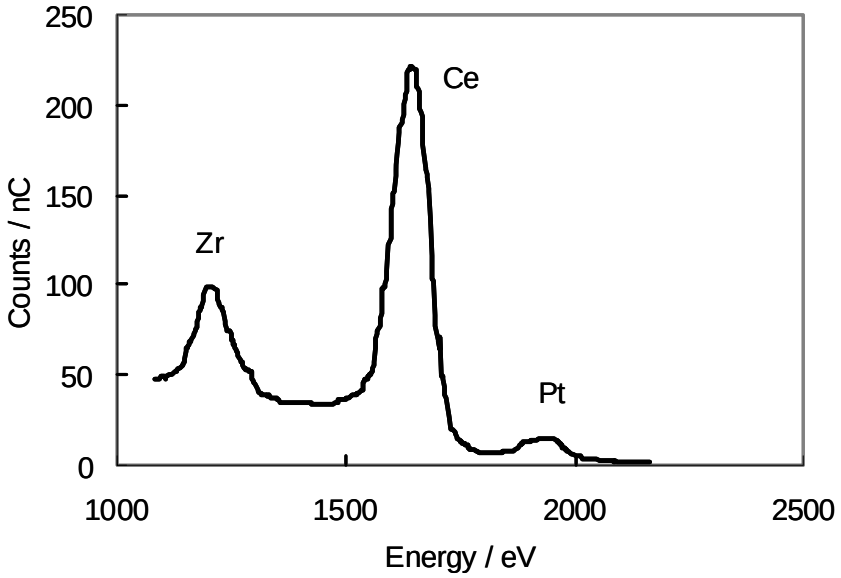

Fig. 6 LEIS spectrum of Pt/CeO_2-ZrO_2 measured with 3 keV Ne^+ ions. With these heavy ions and the large scattering angle (145^0) a high mass resolution is obtained.

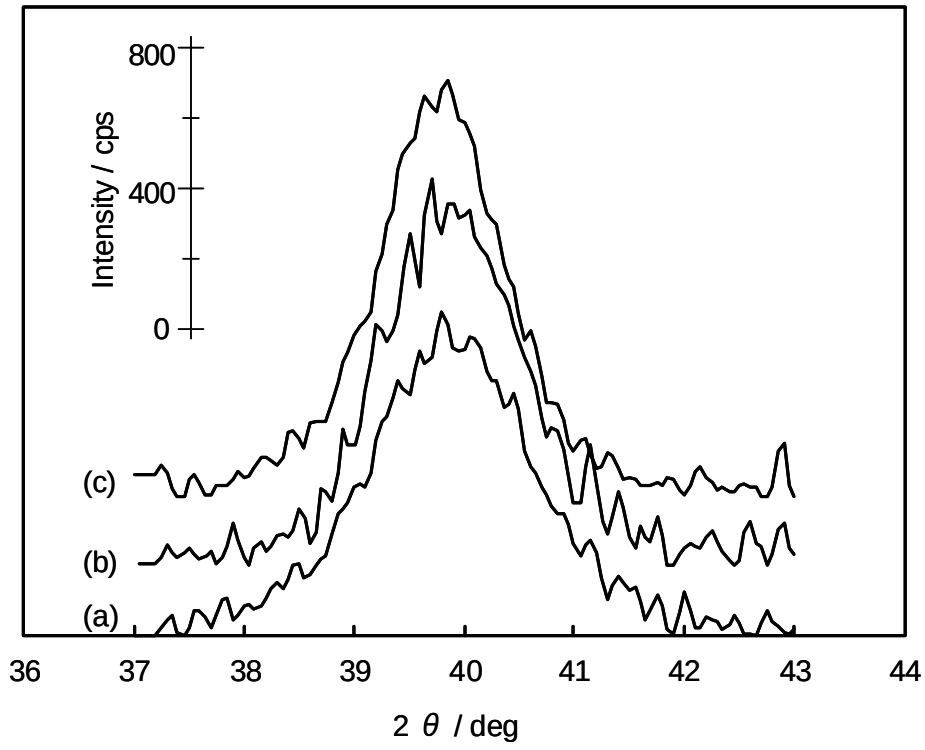

Fig. 7 XRD patterns at Pt(111) diffraction line measured on Pt/CeO_2-ZrO_2 treated in 3% CO and 3% H_2O in nitrogen at (a) 1123, (b) 1173 and (c) 1223 K.

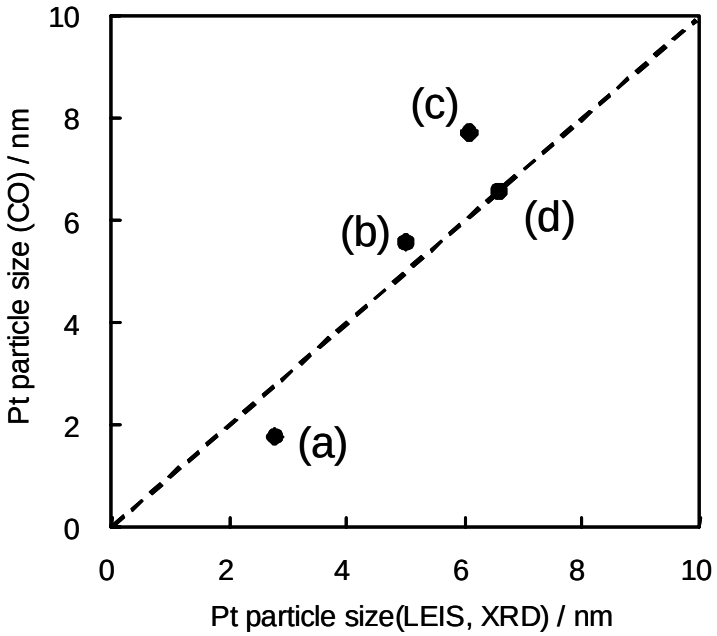

Fig. 8 Pt particle size in Pt/CeO_2-ZrO_2 treated in 3% CO and 3% H_2O in nitrogen at (a) 1073, (b) 1123, (c) 1173 and (d) 1223 K. Pt particle size was determined by CO pulse adsorption at 195 K and determined by LEIS (a) and XRD (b, c, and d).

4. Conclusion

Carbonate species on CeO_2 are responsible for the unrealistically large amounts of CO adsorption on Pt/CeO_2 at 323 K. Realistic platinum dispersion is obtained at the lower adsorption temperature of 195 K, indicating that CO spillover is taking place from Pt to the support at higher temperatures. In comparative studies of CO pulse adsorption at 195 K, XRD and LEIS showed good agreement between the respective Pt particle sizes. This method of CO pulse adsorption at 195 K is therefore considered as a simple and reliable method to determine Pt particle sizes in practical automotive catalysts containing cerium-based oxides.

Acknowledgement

The authors would like to acknowledge the valuable contributions to the early stages of the work presented in this paper by the late dr.ir. Jozef Hoebink, at that time associate professor at Eindhoven University of Technology, who passed away in 2005.

References

[1] S. Matsumoto, Catal. Today 90 (2004) 183-190.

[2] H.C. Yao, Y.F. Yao, J. Catal. 86 (1984) 254-265.

[3] P. C. Flynn, S. E. Wanke, J. Catal. 34 (1974) 390-399.
[4] P. C. Flynn, S. E. Wanke, J. Catal. 34 (1974) 400-410.
[5] P. C. Flynn, S. E. Wanke, J. Catal. 37 (1975) 432-448.
[6] S. A. Hassan, F. H. Khalil, F. G. El-Gamal, J. Catal. 44 (1976) 5-14.
[7] R.M.J. Fiedorow, B.S. Chahar, S.E. Wanke, J. Catal. 51 (1978) 193-202.
[8] H. Lieske, G. Lietz, H. Spindler, J. Völter, J. Catal. 81 (1983) 8-16.
[9] F. Oudet, A. Vejux, P. Courtine, Appl. Catal. 50 (1989) 79-86.
[10] C.H. Bartholomew, Appl. Catal. A Gen. 212 (2001) 17-60.
[11]S. Bernal, J.J. Calvino, M.A. Cauqui, J.M. Gatica, C. Larese, J.A. PeÂrez Omil, J.M. Pintado, Catal. Today 50 (1999) 175-206.
[12] V. Perrichon, L. Retailleau, P. Bazin, M. Daturi, J.C. Lavalley, Appl. Catal. A Gen. 260 (2004) 1-8.
[13]S. Komai, Y. Yazawa, A. Satsuma, T. Hattori, J. Jpn. Petrol. Inst. 48 (2005) 173-177.
[14]T. Takeguchi, S. Manabe, R. Kikuchi, K. Eguchi, T. Kanazawa, S. Matsumoto, W. Ueda, Appl. Catal. A Gen. 293 (2005) 91-96.
[15] S. Bernal, G. Blanco, J. M. Gatica, C. Larese, H. Vidal, J. Catal. 200 (2001) 411-415.
[16] J. L. Duplan, H. Praliaud, Appl. Catal. 67 (1991) 325-335.
[17] M. Primet, M. E. Azhar, R. Frety, M. Guenin, Appl. Catal 59 (1990) 153-163.
[18] A. Holmgren, B. Anderson, J. Catal. 178 (1998) 14-25.
[19] A. Holmgren, B. Anderson, D. Duprez, Appl. Catal. B Environ. 22 (1999) 215-230.
[20] H.H. Brongersma, M. Draxler, M. de Ridder, P. Bauer, Surf. Sci. Rep. 62 (2007) 63-109.
[21] J.M.A. Harmsen, W.P.A. Jansen, J.H.B.J. Hoebink, J.C. Schouten, H.H. Brongersma, Catal. Lett. 74 (2001) 133-137.
[22] W. P. A. Jansen, J. M. A. Harmsen, A. W. D. v. d. Gon, J. H. B. J. Hoebink, J. C. Schouten, H. H. Brongersma, J. Catal. 204 (2001) 420-427.
[23] H.R.J. ter Veen, T. Kim, I.E. Wachs, H.H. Brongersma, Catal. Today 140 (2009) 197-201.
[24] J.A. Anderson, R.A. Daley, S.Y. Christou, A.M. Efstathiou, Appl. Catal. B Environ. 64 (2006) 189-200.
[25] T. Jin, Y. Zhou, G. J. Mains, J. M. White, J. Phys. Chem. 91 (1987) 5931-5937.
[26] D. W. Daniel, J. Phys. Chem. 92 (1988) 3891-3899.

Chapter 6

Development of highly durable Rh supported catalyst ～combining Rh sintering suppression and its metallization～

Abstract

To suppress sintering of Rh supported on an oxide, the interaction between Rh and the support oxide was investigated. To eliminate the structural instability effect of the support oxide on Rh sintering, ZrO_2 doped with a rare earth element was used in this study. La doping was found to be most effective for maintaining a specific surface area and the tetragonal phase of ZrO_2 after the aging test at 1273 K in air. On this stabilized La-ZrO_2 surface, Nd_2O_3 was introduced, with the aim of investigating its interaction with the supported Rh. Transmission electron microscopy observation with energy dispersive X-ray analysis showed that Nd enrichment existed around the surface of the primary particle of La-ZrO_2. Investigations with Hydrogen-temperature programmed reduction and extended X-ray absorption fine structure revealed that the supported Rh interacted with Nd_2O_3 on the surface of the La-ZrO_2 and Rh−O−Nd bond formation in oxidizing atmosphere was the origin of the interaction. After a redox aging test at 1273 K, it was found that Rh sintering behavior depended on the Nd_2O_3 surface enrichment amount and sintering suppression was obtained with a 1−2 wt% Nd_2O_3 surface enrichment amount. This improvement was caused by the anchoring effect of the Nd_2O_3-enriched surface layer against supported Rh sintering. This study sets out a way to suppress Rh sintering by an adequate control of the interaction between supported Rh and Nd_2O_3 on the surface of stabilized ZrO_2.

Keywords; Rh sintering, Rh-support interaction, Nd, ZrO_2, anchoring effect

1. Introduction

Noble metals such as Pt, Pd, and Rh are used as catalysts in automobiles for the abatement of pollutants in the automotive exhaust. Because of the increase in automobile use in emerging countries such as China and the strengthening of legislation regarding automotive emissions in the world, the usage of these noble metals is increasing very much. Because of the scarcity of these noble metals, the decrease of usage amount is strongly demanded. Among these noble metals, Rh is the scarcest, and more than 80% of its production is for the purpose of manufacturing automotive catalysts [1, 2]. So far no alternative material has been found that can serve as a

substitute for Rh, which significantly reduces nitrogen oxides (NOx) in a three-way automotive catalyst. From a practical point of view, reducing the deterioration of the catalyst is an important issue in decreasing the usage of Rh because the amount of Rh used in the automotive catalyst is designed to achieve consistently high performance over the whole life of the automobile.

The deterioration of supported Rh in automotive catalysts has been studied for some time. Those studies mainly investigated the deterioration of a Rh/Al_2O_3 catalyst in an oxidizing atmosphere [3-10]. It was found that supported Rh strongly interacted with Al_2O_3 and irreducible Rh was formed during aging tests at high temperature. Because metallic Rh is an active component of a supported Rh catalyst [11, 12], the formation of the irreducible Rh species resulted in the deterioration of the supported-Rh catalyst. Some works claimed that diffusion of Rh into an alumina support or the formation of a Rh-aluminate compound corresponds to the irreducible state of oxidized Rh [6-9]. In those studies, an ionic Rh species was proposed in the deactivated state rather than agglomerated Rh oxide particle. The occlusion of supported Rh by alumina has also been reported for the deactivated state of supported Rh [10]. Supported Rh was occluded in the pores of alumina or in thin films of alumina-covered supported Rh, and the presence of alumina blocked the access of the reactant onto the Rh surface. The extent of this deterioration depended on the crystalline phase of the Al_2O_3. The compound γ-Al_2O_3 had the strongest interaction with supported Rh, while α-Al_2O_3 was found to have weak interaction with supported Rh and to suppress the deterioration in an oxidizing atmosphere [10, 13]. Because the loading of Rh is restricted by its low surface area, the practical use of α-Al_2O_3 would not be feasible [10].

Based on these studies, material other than alumina was investigated as an Rh support. Recently Machida et al. investigated various metal phosphates as possible support material for an Rh-supported catalyst. They reported that $Rh/AlPO_4$ (aluminum phosphate) showed high thermal resistance in three-way automotive catalytic activity after an aging test at 1173 K in air with H_2O [14, 15]. Among the four types of $AlPO_4$ polymorphs – berlinite, cristobalite, tridymite, and microporous AlPO-5 – only tridymite-type $AlPO_4$ was effective for Rh sintering suppression and supported Rh was in an easily reducible state after the aging test. They concluded that the sintering suppression of Rh in an easily reducible state was responsible for high activity of Rh supported catalyst after the aging test at 1173 K. They stated that the slow grain growth of tridymite-type $AlPO_4$ should be responsible for the sintering suppression of supported Rh. They also suggested the epitaxial effect between the (001) face of tridymite-type $AlPO_4$ and orthorhombic Rh_2O_3 might be an additional factor in the sintering

suppression.

Cerium-based oxide has also been studied as a possible support for an Rh catalyst. S. Suhonen et al. reported that Rh sintering was suppressed on CeO_2−ZrO_2 compared to that on γ-Al_2O_3 and also that Rh supported on CeO_2−ZrO_2 was more readily reduced than Rh supported on alumina. They claimed that direct contact between the Rh and CeO_2−ZrO_2 was important to obtain these effects [16]. Concerning cerium-based oxide, many studies were conducted on the catalytic activity and oxygen storage/release performance of Rh supported catalysts rather than on Rh sintering behavior [17-20] because the redox function of cerium-based oxide is very important in an automotive three-way catalyst.

We have previously reported that Pt sintering was suppressed by the anchoring effect of the Pt−O−Ce interaction on cerium-based oxides in an oxidizing atmosphere [21-25]. This anchoring effect is based on the chemical interaction between Pt and the support oxide. A support oxide with higher electron density of oxygen more strongly interacted with the supported Pt. This interaction stabilized Pt in a high oxidation state and anchored the supported Pt against sintering [21]. At the beginning of our study on Rh sintering, a preliminary survey of Rh sintering behavior was conducted on various support oxides in air at 1273 K [Supplementary Information 1]. In this survey, Rh dispersion after the aging test, which was determined by the CO chemisorption method, depended on the electron density of oxygen in the oxide support material. This result was very similar to those of Pt sintering behavior found in our previous work. In an oxidizing atmosphere, Rh strongly interacted with the support that had a high electron density of oxygen and the high oxidation state of the supported Rh was stabilized by this interaction. This interaction anchored the supported Rh against sintering in an oxidizing atmosphere. During this investigation, we found that Rh dispersion in the aged catalysts that supported on γ-Al_2O_3 and Nd-containing ZrO_2 increased significantly by increasing the reduction pretreatment temperature before the CO chemisorption. This result suggests that a part of a decrease in Rh dispersion during the aging test in air at 1273 K would be caused by the formation of poorly reducible Rh rather than by physical aggregation of Rh on these two support materials. Both γ-Al_2O_3 and Nd-containing ZrO_2 had strongly interacted with the supported Rh more than would be expected by the electron density of oxygen in those two support oxides. Concerning γ-Al_2O_3, a very similar phenomenon was already reported by Hu et al. [8]. They concluded that Rh-aluminate was produced after air-aging at high temperature and the reduction of Rh-aluminate at 1173 K created highly dispersed metallic Rh on γ-Al_2O_3. On the other hand, supported Rh had little interaction with ZrO_2 and could more easily

be reduced with ZrO_2 than it could with γ-Al_2O_3 [13]. There are few works concerning the strong interaction between Rh and ZrO_2 in the literature. Based on these findings, we focused on the interaction between supported Rh and Nd-containing ZrO_2 in relation to suppression of Rh sintering at high temperature.

The aim of this study was to find a way to suppress Rh sintering using the interaction between supported Rh and a ZrO_2 support containing Nd. To investigate the interaction, the concept of an enriched surface layer of Nd_2O_3 was introduced on ZrO_2. This concept was not involved in our previous study on Pt sintering suppression [21-25] and introduced to control the interaction. An adequate control of the interaction should be important in suppressing Rh sintering in order to avoid the formation of poorly reducible Rh. This investigation revealed that a Nd_2O_3-enriched surface layer interacted with the supported Rh and adequate control of the interaction suppressed Rh sintering on the zirconium-based oxide supports.

2. Experimental

2.1 Preparation and characterization of ZrO_2-based oxides

A ZrO_2-based oxide was prepared using a conventional precipitation method by the hydrolysis of $ZrO(NO_3)_2$ with aqueous NH_3. Nitrates of rare earth elements were added to the precipitate to improve the thermal stability of the ZrO_2. Sc, Y, Pr, Nd, or La was employed as the rare earth element and the amount added was controlled at Re_2O_3/ZrO_2 = 3 mol% (Re: rare earth element dopant). Pure Nd_2O_3 was also prepared by the hydrolysis of an aqueous solution of $Nd(NO_3)_3 \cdot 6H_2O$ with aqueous NH_3. The precipitate was filtered, dried at 373 K overnight, and finally calcined in air at 773 K. An aging test was performed at 1273 K for 5 h in air to investigate the thermal stability of the prepared ZrO_2-based oxides. X-ray diffraction (XRD) was performed using a RINT-1500V (Rigaku) with Cu Kα radiation (λ = 0.15418 nm) operating at 40 kV and 350 mA. Transmission Electron Microscope (TEM) observation was conducted using Hitachi HF-2000 with an energy dispersive X-ray (EDX) analyzer for the characterization of the ZrO_2-based oxides. Specific surface area (SSA) was determined by N_2 adsorption, employing the Brunauer−Emmett−Teller (BET) method.

2.2 Preparation of an Nd_2O_3-enriched surface layer onto ZrO_2-based oxides and characterization

The prepared ZrO_2-based support oxide was impregnated with $Nd(NO_3)_3 \cdot 6H_2O$ at loading levels of 2, 5, and 10 wt% as Nd_2O_3 and then calcined in air at 773, 973, or 1173 K. TEM-EDX analysis was performed on the Nd-impregnated ZrO_2-based oxide to investigate the structure and Nd distribution in the oxide. X-ray photoelectron

spectroscopy was conducted using a PHI model 5500MC instrument with Mg Kα radiation to estimate the chemical composition near the surface of the prepared ZrO_2-based oxide support. The amount of Nd_2O_3 surface-enrichment was determined by the amount of Nd_2O_3 that dissolved when the support oxide powder was stirred for 1 h in a 0.1 N HNO_3 aqueous solution at room temperature. The amount of the dissolved Nd_2O_3 in the HNO_3 aqueous solution was determined by Inductively Coupled Plasma-Atomic Emission Spectrometry (ICP-AES) after filtering the insoluble ZrO_2-based oxide.

2.3 Preparation of a Rh-supported catalyst, aging test and characterization

A 0.5 wt% Rh catalyst was prepared using a conventional method of impregnating the support material with rhodium nitrate, as described in Section 2.2. The catalyst was calcined in air at 773 K after the impregnation. An aging test was performed at 1273 K in the cyclic flow of reducing and oxidizing gas, which was switched every 5 min and which continued for 5 h. The reducing composition was 2% H_2 - 10% CO_2 - 3% H_2O in N_2 and the oxidizing gas composition was 1% O_2 - 10% CO_2 - 3% H_2O in N_2.

Rh dispersion was determined using the CO pulse adsorption method with an Ohkura Riken R6015-S instrument. The sample was heated to 673 K in an oxygen flow and held at this temperature for 15 min. After purging with He, the sample was reduced in H_2 for 15 min and then cooled to 323 K in a helium flow. CO pulses were injected until the adsorption reached saturation. The amount of CO adsorption was calculated as the difference between the total amount of CO injected and the amount measured at the outlet from the sample. The metal dispersion was calculated by assuming a CO-to-surface metal atomic ratio of 1:1 [26].

Hydrogen temperature programmed reduction (H_2-TPR) was performed on the aged Rh catalysts to investigate Rh reducibility. For the pretreatment, the sample was heated to 873 K in a flow of 20% O_2 in Ar, kept at this temperature for 15 min, then cooled to 323 K. The flow was switched to a flow of 1% H_2 in Ar at this temperature. The sample was heated from 323 to 873 K in a flow of 1% H_2 in Ar. The H_2 consumption was monitored by a mass spectrometer (MMC-200, ULVAC) during the heating. The total flow rate was 20 mL/min and 0.5 g of catalyst was employed in the H_2-TPR experiment.

Rh K-edge (23.3 keV) X-ray absorption fine structure (XAFS) measurements were carried out using the BL33XU beamline at the SPring-8 facility (Hyogo, Japan) to investigate the local coordination structure around Rh and its chemical state after aging tests. Standard samples of Rh foil and Rh_2O_3 were also measured as references for Rh metal and Rh oxide. The storage ring energy was operated at 8 GeV with a typical current of 100 mA. XAFS spectra at the Rh K-edge were measured using a Si (220)

double-crystal monochromator in transmission mode at room temperature in air. Background subtraction and normalization were performed using the REX2000 program Ver.2.5.9 (Rigaku Corp.). Curve-fitting analysis of extended XAFS (EXAFS) spectra was performed for inverse Fourier transforms on the Rh-oxygen and Rh-cation (cations Rh and Nd) shells using theoretical parameters calculated by McKale et al. [27]

3. Results and Discussion

3.1 Thermal stability of rare earth doped ZrO_2 oxide supports

Sufficiently high thermal stability of the support is important in order to investigate the interaction between the Rh and the support oxide because structural instability of support itself affects Rh sintering behavior. To obtain this thermal stability, the doping effect of rare earth elements into ZrO_2 was investigated. Fig. 1 shows powder X-ray diffraction patterns of the rare earth element doped ZrO_2. The powder X-ray diffraction patterns were shown around the diffraction of tetragonal ZrO_2 (111). The diffraction corresponding to tetragonal phase of ZrO_2 was dominant on all samples and minor monoclinic phase of ZrO_2 was found in Y and Sc doped samples. The diffraction peak of tetragonal ZrO_2 (111) shifted to a lower angle along with an increase of the ionic radius of the rare earth dopant. This indicates that a doping of large ionic radius ion increase lattice parameter corresponding to larger unit cell volume. Therefore, the doped rare earth element has been incorporated into the ZrO_2 crystal lattice and should substitute for the Zr position. The results of the as-prepared SSA before and after the aging test in air at 1273 K are shown in Fig. 2. The SSA of the ZrO_2 support post-aging increased as the ionic radius of the doped element increased, although the as-prepared SSA was almost constant around 100 m^2/g. La doping was most effective in maintaining high SSA after the aging test. As-prepared SSA of undoped ZrO_2 was 100 m^2/g and it decreased to 9 m^2/g after the aging test. The SSA of undoped ZrO_2 after the aging test was comparable to the SSA of Y or Yb doped ZrO_2 and higher than that of Sc doped ZrO_2. The SSA of undoped ZrO_2 after the aging test is off the trend shown in Fig. 2. After the aging test, the main crystalline phase of the undoped ZrO_2 was monoclinic phase although tetragonal phase was main phase in the doped ZrO_2. This difference in crystalline phases could be the reason why the result of the undoped ZrO_2 is off the trend of the doped ZrO_2. Fig. 3 shows the TEM graphs of La-doped and undoped ZrO_2 after the aging test. The primary particle size of the La-doped ZrO_2 was 20−50 nm, which was much smaller than that of undoped ZrO_2. The sintering of the primary ZrO_2 particle was suppressed by La doping and this suppression caused the high SSA after the aging test.

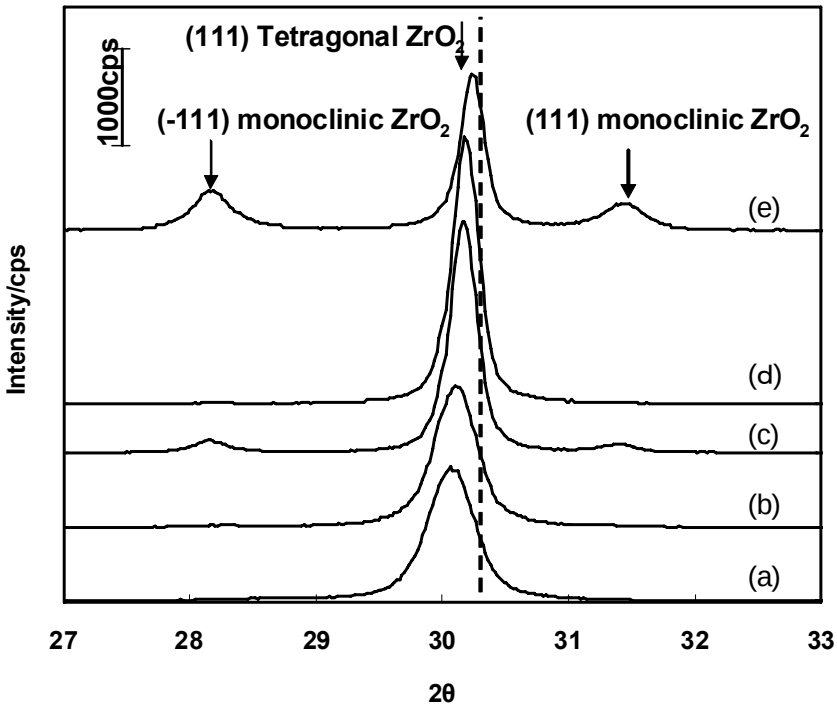

Fig. 1 X-ray diffraction patterns measured on rare earth (RE) element-doped ZrO_2. The doped element was (a) La, (b) Nd, (c) Y, (d) Yb, (e) Sc and the doped amount was $RE_2O_3/ZrO_2 = 0.03$. The dashed line indicate (111) diffraction position of undoped tetragonal ZrO_2 [29].

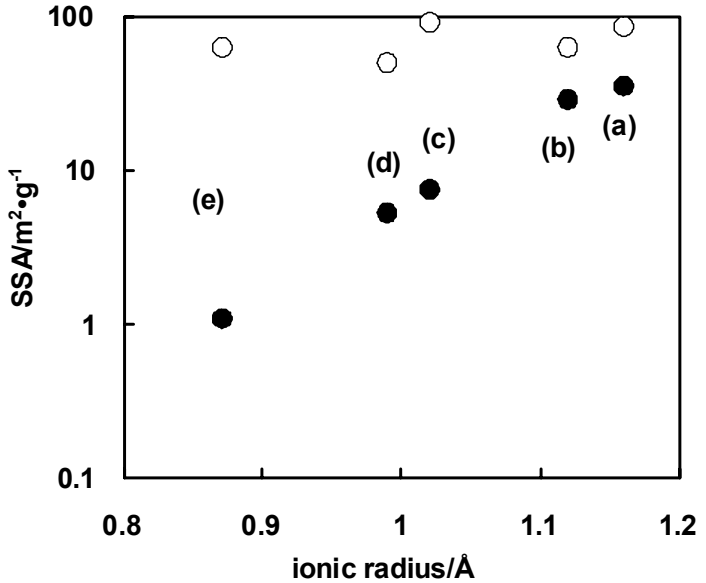

Fig. 2 Specific surface area of rare earth (RE) element doped ZrO_2 before (○) and after (●) aging test at 1273 K in air for 5 h. The doped rare earth was (a) La, (b) Nd, (c) Y, (d) Yb, (e) Sc and the doped amount was $RE_2O_3/ZrO_2 = 0.03$.

It is well known that doping of a trivalent cation into ZrO_2 stabilizes the tetragonal phase and suppresses grain growth of the ZrO_2 crystal [28]. The doped trivalent cation substitute Zr ion position in ZrO_2 lattice and decreases the cation diffusion in trivalent cation-doped ZrO_2 [28]. This effect should be the main reason for the stabilizing effect on ZrO_2 because the phase transition and grain growth involve the cation diffusion in the lattice. The large ionic radius cation should block more effectively than small ionic radius cation by its steric effect [28, 29]. This effect should be the most probable explanation for ionic radius dependence of post-aging SSA. The results we obtained for the La-doping effect on ZrO_2 are well explained by this discussion.

The effect of the La-doping amount on the SSA after the aging test was investigated and the results are shown in Fig. 4, which shows that 3 mol% of La_2O_3/ZrO_2 was most effective in maintaining the high surface area. Similar results were reported by Mercera at al. [28]. They reported that 2.7 mol% was the optimum amount of La_2O_3 to use with ZrO_2. The production of a $La_2Zr_2O_7$-mixed oxide was found in a post-aging sample with a high doping amount. This production should be the reason that a high doping amount was not as effective in improving the thermal stability of ZrO_2.

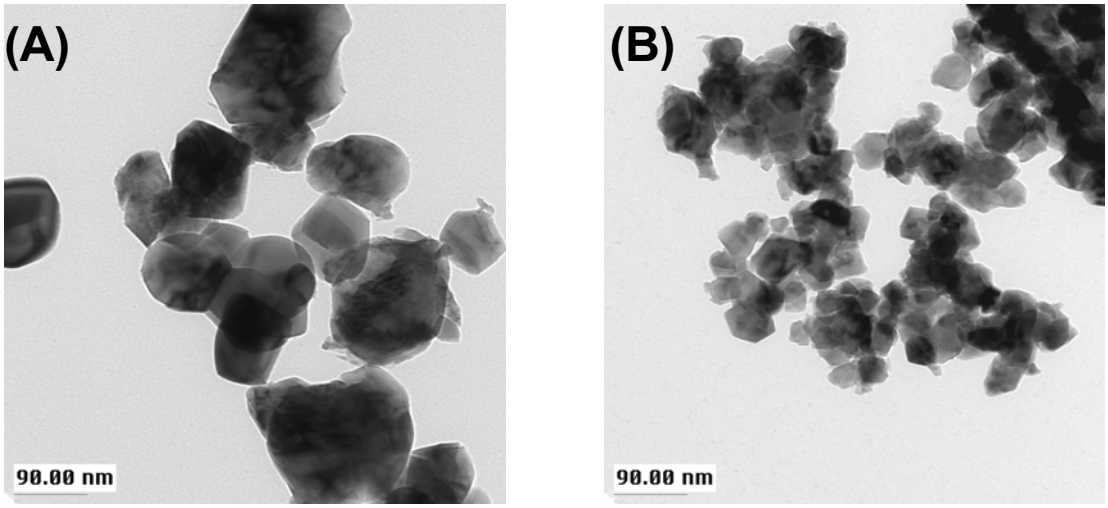

Fig. 3 Transmission electron micrograph of (A) ZrO_2 and (B) La-doped ZrO_2 after aging test at 1273 K in air for 5 h. La-doped amount was $La_2O_3/ZrO_2 = 0.03$.

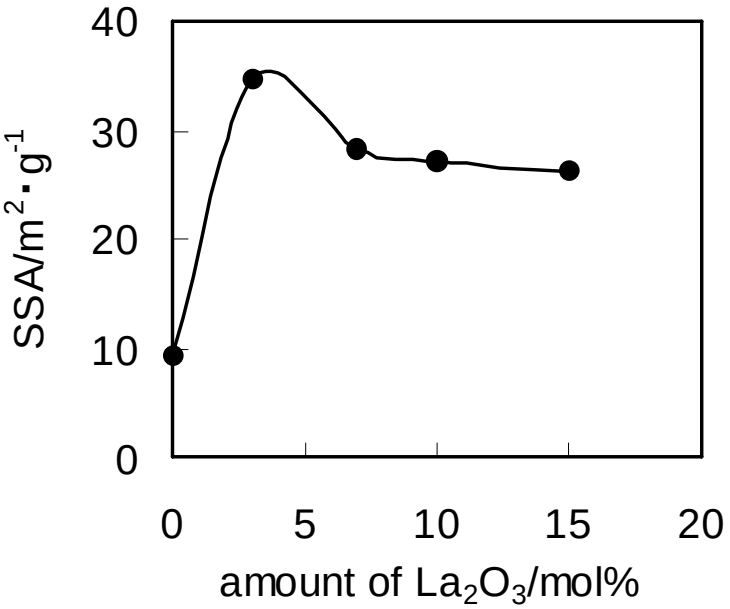

Fig. 4 La-doping amount-dependence of specific surface area of La-doped ZrO_2 after aging test at 1273 K in air for 5 h.

3.2 Characterization of Nd_2O_3 enriched surface layer

Based on the results discussed in Section 3.1, 3 mol% of La_2O_3-doped ZrO_2 was used as the base material for the subsequent preparation of the Nd_2O_3-enriched surface layer. To characterize the amount of Nd_2O_3 surface enrichment in the prepared material, the amount of Nd_2O_3 dissolved in aqueous nitric acid was measured. Bulk compositions of Nd_2O_3, the preparation temperatures, and the amount of Nd_2O_3 dissolved in aqueous nitric acid are summarized in Table 1. In this table, dissolved amount of Nd into aqueous nitric acid was calculated as the weight of Nd_2O_3 and summarized as the weight ratio of Nd_2O_3 to ZrO_2. The amount of dissolved Nd_2O_3 depended on the Nd_2O_3 bulk composition and also the preparation temperature. The amount of dissolved Nd_2O_3 was lower than the Nd_2O_3 bulk composition. At the same bulk composition, the amount of dissolved Nd_2O_3 decreased with the increase in preparation temperature. This means that some part of the impregnated Nd diffused into the bulk phase of the ZrO_2 at high preparation temperatures and this diffused Nd did not dissolve in the acidic solution. The dissolved Nd should remain around the surface as Nd_2O_3, which should be easily dissolved with aqueous nitric acid.

XPS measurements were performed on some samples to determine the Nd/Zr atomic ratio around the surface of the prepared support oxide. Fig. 5 shows the correlation between the Nd/Zr atomic ratio determined by XPS and the amount of dissolved Nd_2O_3.

Table 1 Nd_2O_3 bulk composition, Nd_2O_3 surface enrichment amount and Rh dispersion of Rh supported catalyst with Nd_2O_3 enriched surface layer.

Nd_2O_3 bulk composition / wt%	Preparation temperature / K	Nd_2O_3 surface enrichment amount (1) / wt%	Rh dispersion (2) / %
0	-	-	16.4
2	773	1.44	18.7
5		4.99	13.8
10		8.91	2.7
2	973	1.11	18.9
5		3.77	14.3
10		8.35	3.4
2	1173	0.56	16.2
5		2.34	1.7
10		7.89	5.9

(1) Nd_2O_3 surface enrichment amount was determined by the amount of Nd dissolved into acid solution..
(2) Rh dispersion was determined by CO pulse chemisorption after redox aging test at 1273 K..

The Nd/Zr atomic ratio almost linearly correlated with the amount of dissolved Nd_2O_3. This good correlation suggests that the amount of dissolved Nd_2O_3 should provide a fairly accurate estimation of the amount of Nd_2O_3 around the surface of support oxide.

To characterize the Nd_2O_3-enriched surface layer on an atomic scale, TEM-EDX observation was performed on the sample of 2 wt% of Nd_2O_3 bulk composition at a preparation temperature of 773 K. Fig. 6 shows the TEM graph and the Nd concentration at each analysis spot (indicated by the circle in the TEM graph) that was determined by EDX analysis. The Nd concentration determined around the surface of the primary ZrO_2 particle was higher than that of the bulk composition, and also the Nd concentration determined at the center of the primary ZrO_2 particle was lower than that of the bulk composition. This observation suggests that Nd was concentrated on the surface of the primary ZrO_2 particle, forming an enriched surface layer.

These characterization results suggested that the Nd_2O_3-enriched surface layer should exist around the surface of the primary ZrO_2 particle and the amount of dissolved Nd_2O_3 into aqueous nitric acid solution can be used as the Nd_2O_3 surface-enrichment amount.

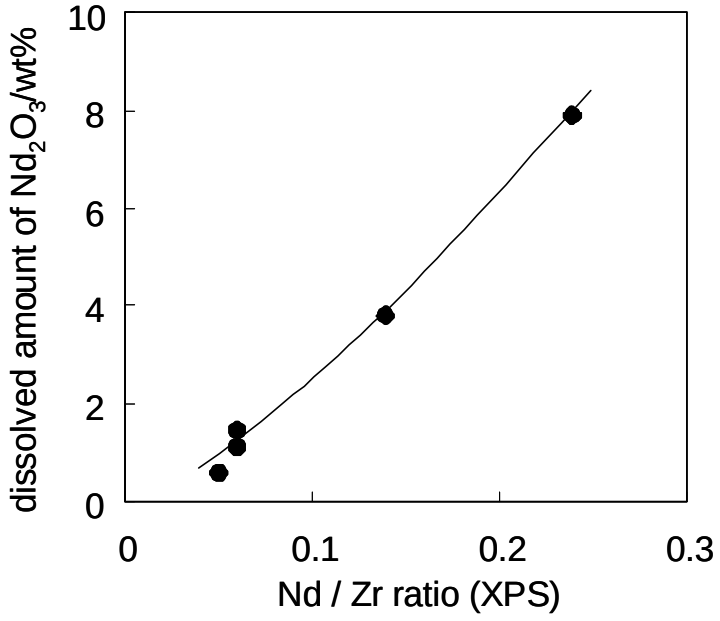

Fig. 5 The correlation between the Nd/Zr atomic ratio as determined by XPS and the dissolved amount of Nd_2O_3 in a 0.1 mol% HNO_3 aqueous solution. Dissolved amount of Nd_2O_3 was calculated as the weight ratio to ZrO_2 from the concentration of Nd in a 0.1 mol% HNO_3 aqueous solution.

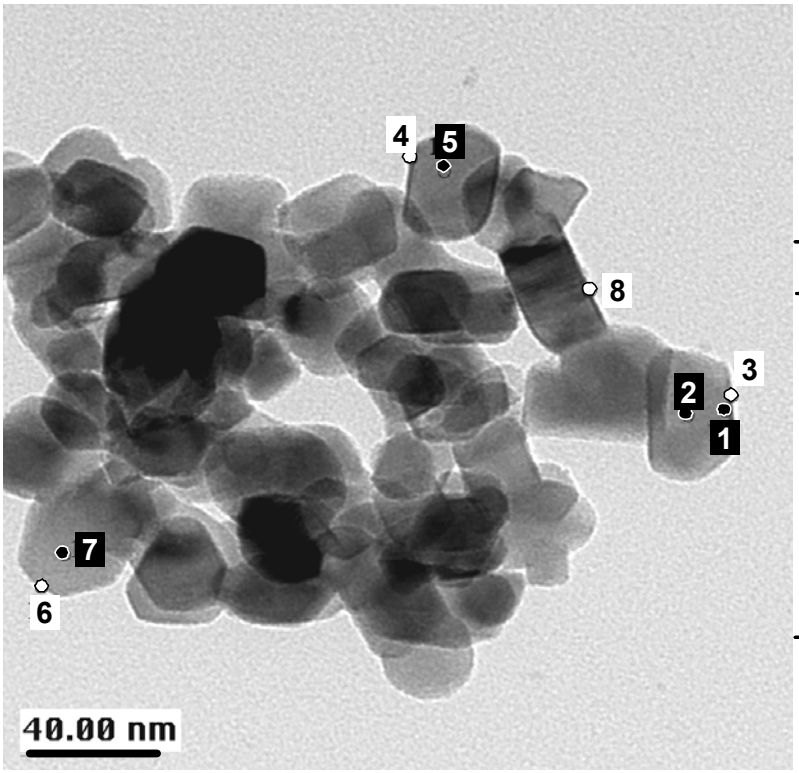

Spot	Nd/at%
1	0.39
2	0.24
3	**1.29**
4	**0.91**
5	0.50
6	**2.27**
7	0.0
8	**1.48**

Nd bulk composition
0.8 at% (Nd_2O_3 2wt%)

Fig.6 Transmission electron micrograph (TEM) of ZrO_2 with Nd_2O_3enriched surface layer and Nd composition determined by energy dispersive X-ray (EDX) analysis during TEM observation. Small circle indicates the EDX analysis point. The underlined bold value in the table indicates the analysis point around the surface of the primary ZrO_2 particle.

3.3 Rh sintering and reduction behavior on Nd_2O_3-enriched surface layer

An Nd_2O_3-enriched surface layer was prepared on a ZrO_2 support oxide aiming at the interaction with supported Rh. Rh sintering behavior on the supported catalyst was investigated from the view point of the Rh−Nd_2O_3 interaction. Fig.7 shows the change of Rh dispersion with Nd_2O_3 surface-enrichment amounts after the redox aging test. The broken line shows the Rh dispersion without Nd_2O_3 surface-enrichment. The Rh dispersion strongly depended on the amount of Nd_2O_3 surface-enrichment and an improvement of Rh dispersion was obtained with a 1 to 2 wt% Nd_2O_3 surface-enrichment amount. The SSA of these catalysts after aging was almost constant around 35 m^2/g and independent of the amount of Nd_2O_3 surface-enrichment. Also, no structural change of the ZrO_2 support oxide was found with the Nd_2O_3 surface-enrichment. These results indicate that the main cause of the change in Rh dispersion should be the interaction between the supported Rh and the Nd_2O_3-enriched surface layer.

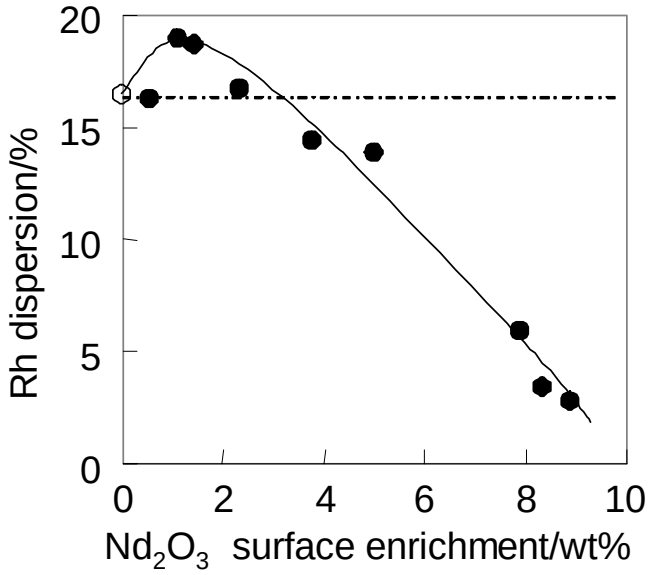

Fig. 7 The change of Rh dispersion in Rh-supported catalysts with Nd_2O_3 surface enrichment amount. Rh dispersion was determined by CO pulse chemisorption after redox aging test at 1273 K for 5 h.

Although there is very little literature on the chemistry between Nd and Rh, Taniguchi et al. reported the formation of the compounds using these two elements [30]. They reported that the reaction between Rh_2O_3 and Nd_2O_3 in oxygen at 1373−1573 K resulted in a production of a $NdRhO_3$ perovskite-type oxide. Taniguchi's work means that Rh_2O_3 and Nd_2O_3 have a strong affinity in an oxidizing atmosphere to form a

compound between Rh_2O_3 and Nd_2O_3. Based on this fact and on the results of the redox aging test in our work, a supported Rh and a Nd_2O_3-enriched surface layer should strongly interact in an oxidizing atmosphere. This interaction should anchor the supported Rh against sintering on the support and improve Rh dispersion with adequate Nd_2O_3 surface-enrichment amount. This mechanism is similar to that seen in Pt sintering suppression with the Pt−O−Ce anchoring effect that was reported in our recent works.

To clarify the anchoring effect of a Nd_2O_3-enriched surface layer, H_2-TPR was conducted to investigate the Rh-support interaction. Fig. 8 shows H_2-TPR profiles of a redox-aged Rh supported catalyst with various Nd_2O_3 surface-enrichment amount. Since no H_2 consumption was observed on Nd_2O_3/ZrO_2 support only, observed H_2 consumption can be attributed to the reduction of supported Rh. Two reduction peaks are observed at 360 K and 400 K for all samples. A surface-enrichment sample of 7.89 wt% Nd_2O_3 showed another reduction around 440 K that was not observed in the other

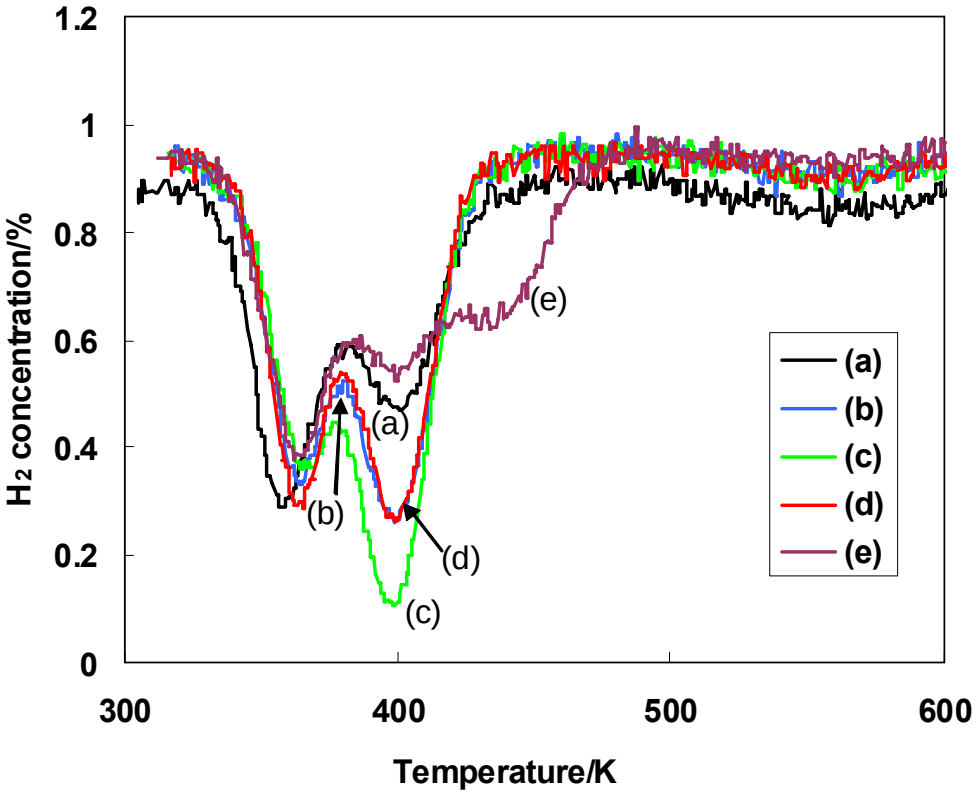

Fig. 8 H_2- TPR profiles of Rh supported catalysts with Nd_2O_3 surface enrichment. The measurement were carried out on the samples after redox aging test at 1273 K. Nd_2O_3 surface enrichment amount; (a) non-surface enrichment, (b) 0.56 wt%, (c) 1.11wt%, (d) 1.44 wt%, (e) 7.89 wt%.

samples. No Rh reduction peak was observed at temperatures higher than 500 K. This result means that no irreducible Rh was formed in any of the samples during the redox aging test at 1273 K. Two reduction peak temperatures of 360 K and 400 K were almost independent of Nd_2O_3 surface-enrichment. The reduction peak height at 400 K changed significantly with Nd_2O_3 surface-enrichment amount while the peak height at 360 K did not change significantly. The detail of the Rh support interaction will be discussed in the next section.

3.4 The interaction between supported Rh and Nd_2O_3-enriched surface layer

To discuss the TPR results shown in Fig. 8 in terms of the interaction between Rh and the Nd_2O_3-enriched surface layer, the Rh dispersion effect and Rh−Nd_2O_3 interaction effect on H_2-TPR had to be estimated independently. To see these two effects, two sets of H_2-TPR experiments were carried out.

The first set was conducted on Rh/ZrO_2 to evaluate the Rh dispersion effect. In this investigation, pure ZrO_2 without any dopant was used as the support to see only the Rh dispersion effect. The dispersion was changed by the time of redox aging test at 1273 K for from 2 to 50 hours. Fig. 9 shows Rh dispersions and those H_2-TPR profiles of Rh/ZrO_2 after redox aging test at 1273 K. The Rh dispersion decreased from approximately 8% to 2% with an increase in aging time from 2 to 50 h. Concerning H_2-TPR, two reduction peaks were observed at 360 K and 420 K on all samples. Those peak temperatures did not change significantly and only the peak height decreased with the decrease of Rh dispersion. Similar two Rh reduction peaks at ca 360 K and 400K were observed on Rh supported catalysts after thermal treatment [31-33]. In their discussion, the lower temperature reduction peak was attributed to the reduction of three dimensional Rh_2O_3 crystallite that has little interaction with support and the higher reduction peak was attributed to the reduction of two dimensional Rh_2O_3 that interacted with support. Based on this discussion, the same assignment can be applied to our results shown in Fig. 9, the reduction peak around 360 K is attributed to the reduction of three dimensional Rh_2O_3 and the reduction at 420 K is attributed to the reduction of two dimensional Rh_2O_3. With increasing aging test time, the peak at 360 K decreased first and the reduction peak at 420 K decreased later. This result suggests that three dimensional Rh_2O_3 agglomerates faster than two dimensional Rh_2O_3 because three dimensional Rh_2O_3 has little interaction with support and easily migrates on the support.

Based on this consideration, the Rh reduction behavior in the catalysts with Nd_2O_3 surface-enrichment shown in Fig. 8 is discussed as following. Two Rh reduction peak temperatures at 360 K and 400 K should be also assigned to the reduction of three dimensional Rh_2O_3 and two dimensional Rh_2O_3, respectively. The peak height at 360 K

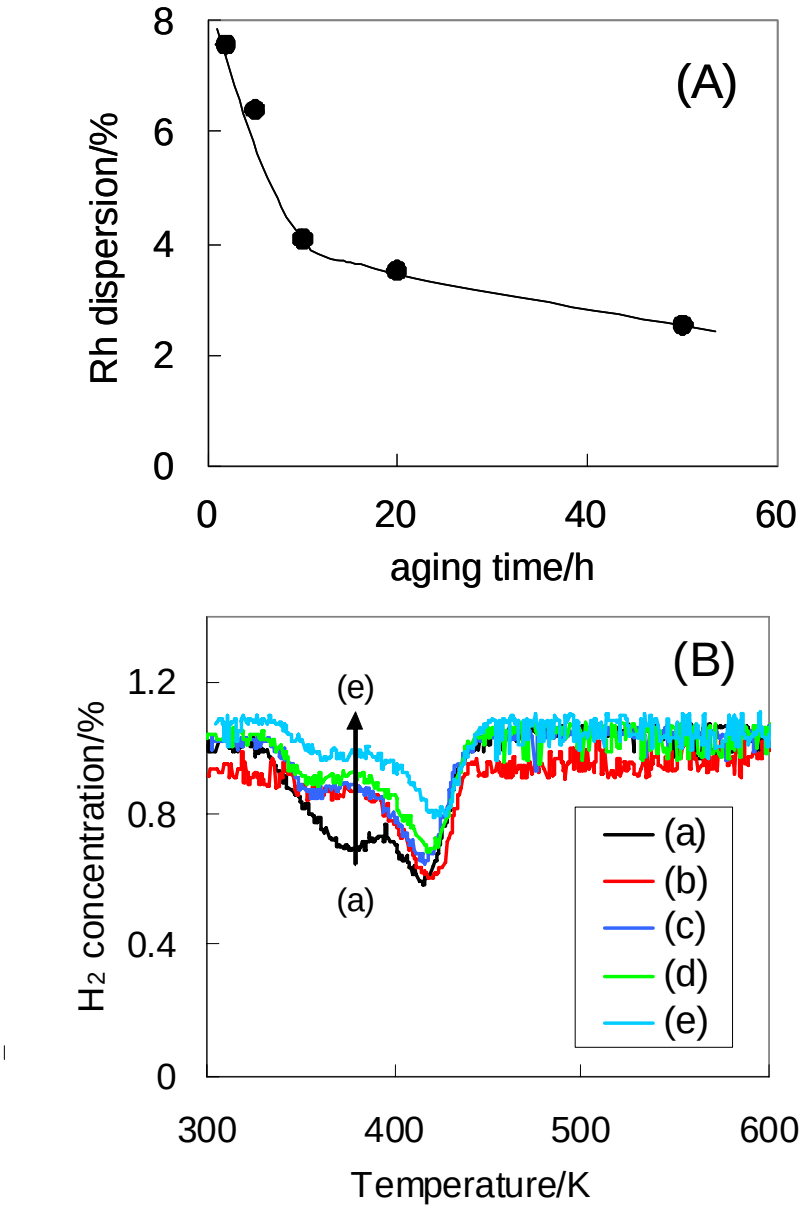

Fig. 9 (A) The change of Rh dispersion in Rh/ZrO_2 with redox aging time at 1273 K. (B) H_2-TPR profiles of Rh/ZrO_2 after redox aging test at 1273 K for (a) 2 h, (b) 5 h, (c) 10 h, (d) 20 h, (e) 50 h.

did not change a lot with the amount of Nd_2O_3-surface enrichment. The peak height at 400 K changed with the amount of Nd_2O_3-surface enrichment and the order was (c) > (b), (d) > (a) > (e), which corresponds to the Rh dispersion order. These results agreed well with the consideration mentioned before. Because three dimensional Rh_2O_3 should have little interaction with support, TPR behavior at 360 K did not change with amount of Nd_2O_3-surface enrichment. On the other hand, TPR behavior at 400 K changed with amount of Nd_2O_3-surface enrichment because two dimensional Rh_2O_3 should interact

with support. The peak height at 400 K and Rh dispersion were highest at 1.11 wt% of Nd_2O_3-surface enrichment. This result suggests two dimensional Rh_2O_3 should interact most effectively at 1.11 wt% of Nd_2O_3-enriched surface layer on the support and this interaction should suppress supported Rh sintering during high temperature aging test.

The second set of experiments was conducted to evaluate the Rh−Nd_2O_3 interaction effect on the H_2-TPR profile. Supported Rh should be in highly dispersed state in fresh catalyst and almost all the supported Rh are considered interacting with support. In this investigation, fresh catalysts of Rh/ZrO_2, Rh/7.89−Nd/La-ZrO_2 and Rh/Nd_2O_3 were used to see only Rh-support interaction without Rh sintering effect. Rh/7.89−Nd/La-ZrO_2 is a 7.89 wt% Nd_2O_3 surface-enrichment sample that corresponds to the fresh state of sample (e) shown in Fig. 8. In Rh/Nd_2O_3, Rh is supported on Nd_2O_3 to evaluate the effect of Nd_2O_3 on Rh reduction behavior more directly. The H_2-TPR profiles of these three catalysts are shown in Fig. 10. The profiles of these catalysts are very different from each other and the Rh reduction peak temperature increased in the order of Rh/Nd_2O_3 > Rh/7.89-Nd/ZrO_2 > Rh/ZrO_2. The shift of Rh reduction peak to higher temperature was reported in TPR characterization of Rh supported catalyst and the cause of that shift is considered the strong Rh-support interaction in oxidizing

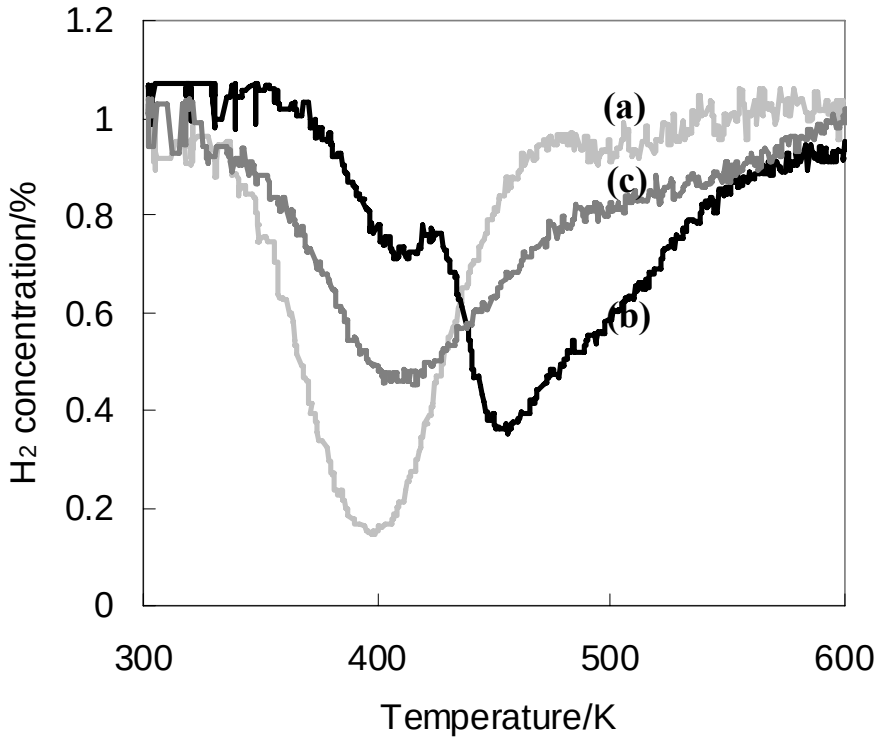

Fig. 10 H_2-TPR profiles of (a) Rh/ZrO_2, (b) Rh/Nd_2O_3 and (c) Rh/Nd/La-ZrO_2 (7.89 wt% of Nd_2O_3 surface enrichment) as prepared sample.

atmosphere [33, 34]. The highest Rh reduction temperature of Rh/Nd_2O_3 should be caused by the interaction between Rh and Nd_2O_3 in the oxidizing atmosphere of pretreatment in the H_2-TPR measurement. The TPR profile of Rh/7.89−Nd/ZrO_2 located between Rh/Nd_2O_3 and Rh/ZrO_2 and the long tail of the Rh reduction from 400 to 500 K should originate from the interaction between the Rh and the Nd_2O_3-enriched surface layer on ZrO_2. These results revealed that Rh reduction peak temperature is affected by the interaction between Rh and Nd_2O_3 and this interaction works also on a ZrO_2 support with Nd_2O_3 surface-enrichment. Based on this fact, the shoulder of the Rh reduction around 440 K observed on a redox-aged sample of Rh/7.89−Nd/La-ZrO_2 (in Fig. 8) should be caused by the very strong interaction between supported Rh and Nd_2O_3 enriched surface layer because this sample has the highest amount of Nd_2O_3-surface enrichment among the investigated samples.

To see the interaction between Rh and Nd_2O_3 from the structural view point, EXAFS analysis was performed on Rh/Nd_2O_3 after thermal treatment in air at 1273 K. The EXAFS analysis results are shown in Fig. 11, with Rh foil and bulk Rh_2O_3 as references.

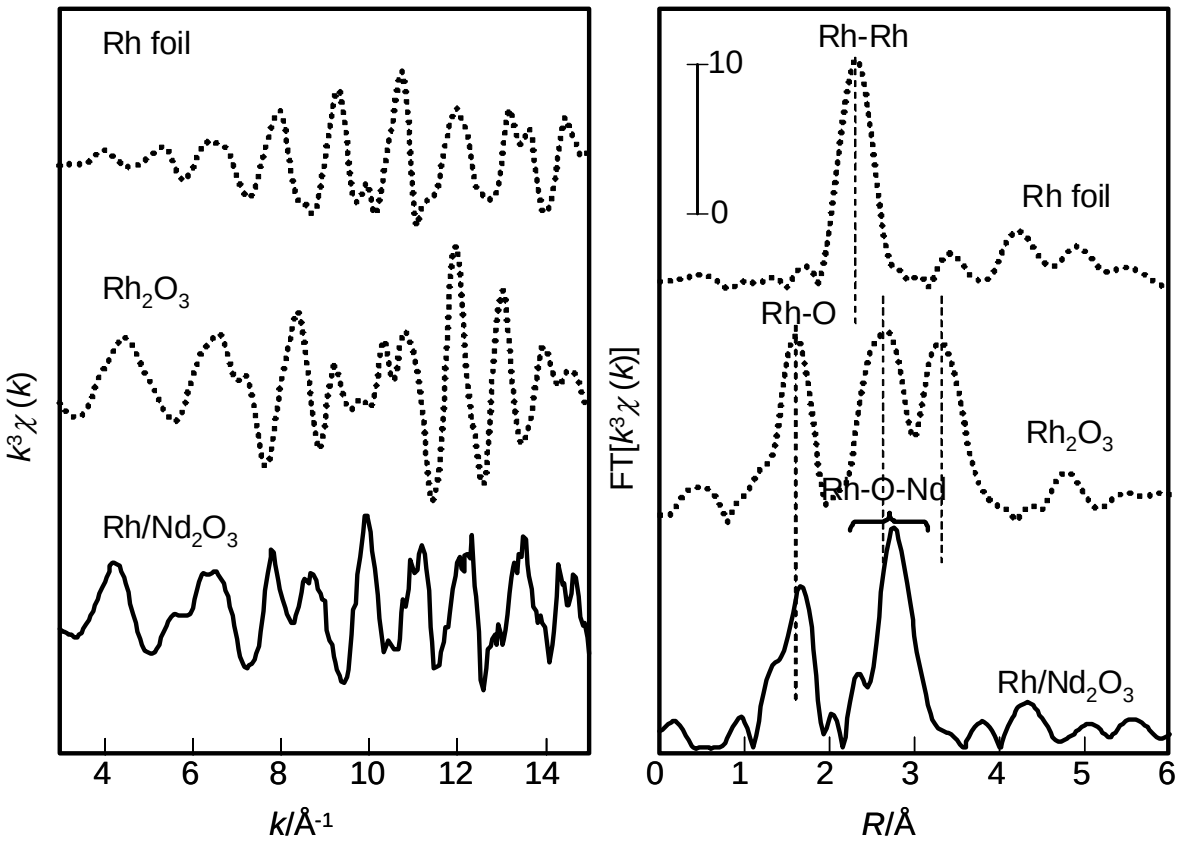

Fig. 11 $k^3\chi$ (k) and corresponding Fourier transforms of Rh K-edge EXAFS measured for (a) Rh/Nd_2O_3, (b) Rh_2O_3 and (c) Rh foil. Rh/Nd_2O_3 was thermally aged at 1273 K in air for 5 h.

The profile determined for Rh/Nd_2O_3 was different from the profile for either metallic Rh foil or bulk Rh_2O_3. The peak observed at 2.8 Å was assigned to Rh−O−Nd by the peak fitting. This result indicates that Rh interacted strongly with Nd_2O_3 with the bond formation of Rh−O−Nd in an oxidizing atmosphere. Taniguchi et al. reported that the formation of $RhNdO_3$ perovskite by the reaction between Rh_2O_3 and Nd_2O_3 in oxygen above 1373 K [30]. Although the bulk phase of $RhNdO_3$ was not observed after the aging test sample in our study, the driving force for the bond formation of Rh−O−Nd should have the same origin as the formation of $RhNdO_3$ compound. This bond formation of Rh−O−Nd in an oxidizing atmosphere should be the main cause of the Rh reduction temperature shift to a higher temperature observed in Fig. 10.

Based on the investigation results with H_2-TPR and EXAFS discussed above, the interaction between supported Rh and the Nd_2O_3 enriched-surface layer should exist on a ZrO_2 support and the origin of this interaction is the bond formation of Rh−O−Nd in an oxidizing atmosphere. This interaction should be effective both in the fresh state and during a redox aging test at 1273 K. As mentioned in Section 3.3, Rh dispersion strongly depended on the Nd_2O_3 surface-enrichment amount while SSA and the crystal structure of the aged catalyst did not change with Nd_2O_3 surface-enrichment amount. In H_2-TPR characterization, two dimensional Rh_2O_3 was suggested to interact with Nd_2O_3 enriched-surface layer and this species should be responsible for Rh dispersion after redox aging test at 1273 K. These results should prove that Rh sintering behavior in high temperature redox aging tests were determined by the interaction between the supported Rh and the Nd_2O_3-enriched surface layer, and the observed improvement of Rh dispersion with adequate Nd_2O_3 surface-enrichment amount should be caused by the anchoring effect of the Rh−O−Nd bond. This anchoring effect with adequate Nd_2O_3 surface-enrichment amount did not degrade the reducibility of the supported Rh, which was proved by the H_2-TPR investigation.

4. Conclusion

A Nd_2O_3-enriched surface layer was prepared on an La-stabilized ZrO_2 support with the aim of investigating its interaction with supported Rh. The H_2-TPR and EXAFS investigation revealed that the interaction between supported Rh and the Nd_2O_3-enriched surface layer should exist on the ZrO_2 support and the origin of the interaction is the Rh−O−Nd bond formation in an oxidizing atmosphere. This interaction suppressed Rh sintering through the anchoring effect of Rh−O−Nd with an adequate Nd_2O_3 surface-enrichment amount. Fig. 12 shows the conceptual scheme of the interaction between supported Rh and the Nd_2O_3-enriched surface layer. The

supported Rh is anchored to the Nd_2O_3-enriched surface layer and this anchoring effect suppressed the sintering of the supported Rh. Adequate control of the interaction should be important to suppress Rh sintering without degrading its reducibility from the view point of developing a highly efficient Rh- supported automotive catalyst.

References

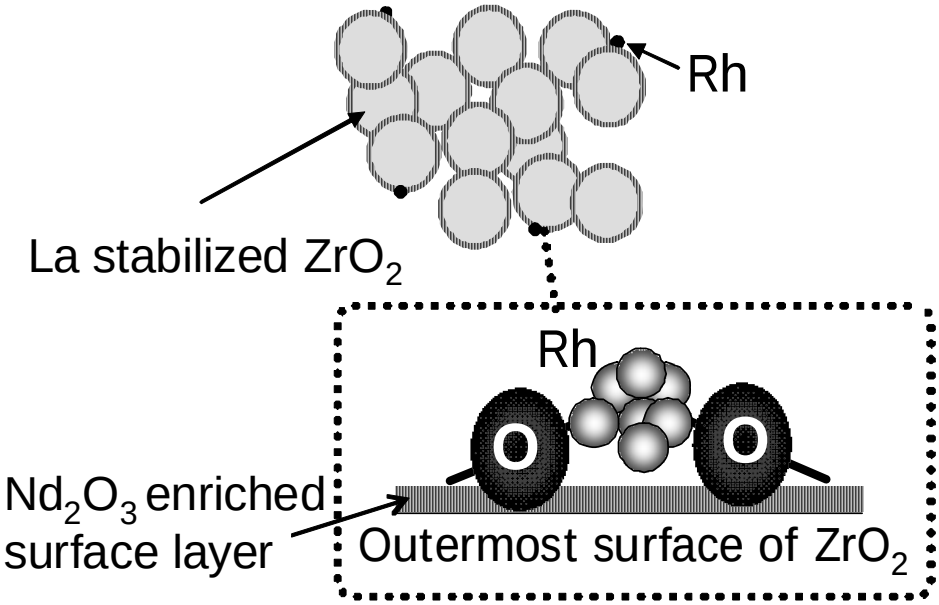

Fig. 12 Conceptual scheme of Rh anchoring effect of Nd_2O_3 enriched surface layer on ZrO_2 support.

[1] Platinum 2010 interim review, Johnson Matthey, (2010) 27.

[2] H. S. Gandhi, G. W. Graham, R. W. McCabe, J. Catal. 216 (2003) 433.

[3] Z. Weng-Sieh, R. Gronsky, A. T. Bell, J. Catal. 170 (1997) 62.

[4] D. D. Beck, T. W. Capehart, C. Wong, D. N. Belton, J. Catal. 144 (1993) 311.

[5] K. Dohmae, Y. Nagai, T. Tanabe, A. Suzuki, Y. Inada, M. Nomura, Surf. Inter. Anal. 40 (13) (2008) 1751.

[6] R. Burch, P. K. Loader, N. A. Cruise, Appl. Catal. A 147 (1996) 375.

[7] H. C. Yao, S. Japar, M. Shelef, J. Catal. 50 (1977) 407.

[8] Z. Hu, F. M. Allen, C. Z. Wan, R. M. Heck, J. J. Steger, R. E. Lakis, C. E. Lyman, J. Catal. 174 (1998) 13.

[9] J. G. Chen, M. L. Colaianni, P. J. Chen, J. T. Yates, Jr.,G. B. Fisher, J. Phys. Chem. 94 (1990) 5059.

[10] R. W. McCabe, R. K. Usmen, K. Ober, H. S. Gandhi, J. Catal. 151 (1995) 385.

[11] S. H. Oh, J. E. Carpenter, J. Catal. 80 (1983) 472.

[12] T. W. Root, L. D. Schmidt, Surf. Sci. 134 (1983) 30.
[13] H. C. Yao, H. K. Stepien, H. S. Gandhi, J. Catal. 61 (1980) 547.
[14] M. Machida, K. Murakami, S. Hinokuma, K. Uemura, K. Ikeue, M. Matsuda, M. Chai, Y. Nakahara, T. Sato, Chem. Mater. 21 (2009) 1796.
[15] K. Ikeue, K. Murakami, S. Hinokuma, K. Uemura, D. Zhang, M. Machida, Bull. Chem. Soc. Jpn. 83 (2010) 291.
[16] S. Suhonen, M. Valden, M. Hietikko, R. Laitinen, A. Savimäki, M. Härkönen, Appl. Catal. A 218 (2001) 151.
[17] J. R. Kim, W. J. Myeong, S. K. Ihm, J. Catal. 263 (2009) 123.
[18] H. He, H. X. Dai, L. H. Ng, K. W.Wong, C. T. Au, J. Catal. 206 (2002) 1.
[19] A. Martínez-Arias, J. Soria, José C. Conesa, J. Catal. 168 (1997) 364.
[20] S**.** Bernal, F. J. Botana, J. J. Calvino, G. A. Cifredo, J. A. Pérez-Omil, J. M. Pintado, Catal. Today 23 (1995) 219.
[21] Y. Nagai, T. Hirabayashi, K. Dohmae, N. Takagi, T. Minami, H. Shinjoh, S. Matsumoto, J. Catal. 242 (2006) 103.
[22] Y. Nagai, K. Dohmae, Y. Ikeda, N. Takagi, T. Tanabe, N. Hara, G. Guilera, S. Pascarelli, M. A. Newton, O. Kuno, H. Jiang, H. Shinjoh, S. Matsumoto, Angew. Chem. Int. Ed. 47 (2008) 9303.
[23] M. Hatanaka, N. Takahashi, T. Tanabe, Y. Nagai, K. Dohmae, A. Suda, H. Shinjoh, J. Catal. 266 (2009) 182.
[24] M. Hatanaka, N. Takahashi, T. Tanabe, Y. Nagai, K. Dohmae, Y. Aoki, T. Yoshida, H. Shinjoh, Appl. Catal. B 99 (2010) 336.
[25] Y. Nagai, K.Dohmae, Y. Ikeda, N. Takagi, N. Hara, T. Tanabe, G. Guilera, S. Pascarelli, M. A.Newton, N. Takahashi, H. Shinjoh, S.. Matsumoto, Catal. Today 175 (2011) 133.
[26] J.A. Anderson, R. A. Daley, S. Y. Christou, A. M. Efstathiou, Appl. Catal. B 64 (2006) 189.
[27] A. G. McKale, B. W. Veal, A. P. Paulikas, S. K. Chan, G. S. Knapp, J. Am. Chem. Soc. 110 (1988) 3763.
[28] P. D. L. Mercera, J. G. van Ommen, E. B. M. Doesburg, A. J. Burggraaf, J. R. H. Roes, Appl. Catal. 78 (1991) 79.
[29] W. D. Kingery H. K. Bowen, D. R Uhlmann, Introduction to Ceramics, second ed., Wiley, New York, 1976, p. 248.
[30] T. Taniguchi, W. Iizuka, Y. Nagata, T. Uchida, H. Samata, J. Alloys Compds. 350 (2003) 24.
[31] C.-P. Hwang, C.-T. Yeh, Q. Zhu, Catal. Today 51 (1999) 93.

[32] H. C. Yao, S. Japar, M. Shelef, J. Catal. 50 (1977) 407.
[33] M. Ferrandon, T. Krause, Appl. Catal. A 311 (2006) 135.
[34] E. Ruckenstein. H. Y. Wang, J. Catal. 190 (2000) 32.

Chapter 7

Summary and general conclusion

Summary of each chapter

Chapter 2: Activation of Pt supported catalyst～operando observation of Pt metallization during catalytic reaction～

Operando X-ray absorption spectroscopic study was performed on Pt/Al_2O_3 catalyst to probe the oxidation state of Pt during C_3H_6 oxidation reaction in oxidizing and reducing atmospheres. Pt metallization was observed prior to the activation of the catalytic reaction during increasing temperature in both oxidizing and reducing atmospheres. These results revealed that metallization of Pt should be necessity for the activation of catalytic C_3H_6 oxidation. Some previous studies claimed that electron deficient Pt on acidic support show high activity for hydrogenation reactions. Other studies claimed that Pt on acidic support are more metallic and show higher activity than that on basic support for C_3H_8 oxidation in oxidizing atmosphere. Our results showed that metallic Pt should be the active site for C_3H_6 oxidation in both oxidizing and reducing atmosphere.

Chapter 3: Controlling factors in catalytic activities of noble metal supported catalysts ～control of self poisoning by reactants ～

In chapter 3, kinetic studies were conducted to investigate controlling factors in $NO\text{-}C_3H_6\text{-}CO\text{-}O_2$ reaction over Pt, Pd or Rh supported catalysts. $C_3H_6\text{-}O_2$ reaction was found as a rate determining reaction for NO reduction on Pt, Pd or Rh supported catalyst. Self-poisoning of C_3H_6 was found to be an important factor in the reaction over Pt or Pd supported catalyst and self-poisoning of oxygen was found to be important in the reaction over Rh supported catalyst. Ba addition to Pt supported catalyst relaxed C_3H_6 poisoning on Pt in $C_3H_6\text{-}O_2$ reaction and increased NO reduction activity. On Rh supported catalyst, Ba addition strengthened oxygen poisoning in $C_3H_6\text{-}O_2$ reaction and decreased NO reduction activity. These results showed that additive to the catalysts can change poisoning behavior of reactants on supported noble metal and increase catalytic activity.

Chapter 4: Design of highly active Pt supported catalyst ～from the view point of Pt-support interaction～

NO reduction by hydrocarbons in reducing atmosphere was investigated to design highly active Pt supported catalyst. Based on the findings in chapter 2, Pt metallization during reaction were investigated from the view point of Pt-support interaction. Four oxides of Al_2O_3, ZrO_2, $CeO_2\text{-}ZrO_2$ or La_2O_3 were used as supports to change the Pt-support interaction that is affected by their acid-base properties. NO reduction by

C_3H_6 or C_3H_8 was performed with oxygen or without oxygen. Metallic state of Pt is required for the catalytic activation, however, too much reduction of Pt causes self-poisoning by HC. As a result, it is clarified that there is an optimum oxidation state of Pt, which can be controlled by an adequate design of support oxide.

Chapter 5: Pt sintering suppression and catalytic activity of Pt supported catalyst

Sintering suppression of supported noble metal is important to achieve high durability of three-way catalyst. Previous study reveled that Pt sintering is suppressed by the anchoring effect of Pt-O-Ce bond on cerium-based oxide in oxidizing atmosphere. In this thesis, MgO was used as support expecting a stronger interaction with Pt than cerium-based oxide. Sintering, re-dispersion behaviors and catalytic activity of Pt supported on MgO were studied to combine high durability and activity. Strong interaction was found between Pt and MgO in oxidizing atmosphere and Pt sintering was suppressed by anchoring effect of the interaction. This anchoring effect suppressed deactivation of the catalytic activity during high temperature aging tests. In fresh catalyst, Pt/MgO showed low activity because too strong interaction between Pt and MgO stabilized Pt oxide. These results revealed that an adequate control of the Pt-support interaction is necessary to combine high activity and durability of catalyst.

For an accurate and easy determination of the dispersion of supported noble metal, a modified method for CO adsorption was proposed, because the conventional CO adsorption at room temperature cannot be applied to cerium-based catalysts. CO pulse adsorption at -78 ˚C was found to suppress CO adsorption on the cerium-based supports. Comparative study with XRD, TEM observation and low energy ion scattering showed that CO adsorption at -78 ˚C gives accurate Pt dispersion on cerium-based oxide.

Chapter 6: Development of highly durable Rh supported catalyst～combining Rh sintering suppression and its metallization～

In order to combine catalytic activity and durability of three-way catalyst, supported metal sintering should be suppressed without formation of stabilized noble metal oxides by control of the metal-support interaction. The control of Rh-support interaction was investigated to combine high activity and durability of supported Rh catalyst. ZrO_2 was used as a support because it has moderate interaction with Rh. Nd_2O_3 has strong interaction with Rh and its enriched surface layer was introduced on ZrO_2. This enriched surface layer enables control of the interaction between Rh and support. An adequate control of the interaction suppressed Rh sintering without formation of stabilized Rh oxide. This technology was applied to the three-way catalyst that was commercialized in 2011 by TOYOTA Motor Corporation. Rh usage in this catalyst is a half of previous commercialized three-way catalyst.

General Conclusion

- Pt metallization is necessity for the activation of Pt supported catalyst in both reducing and oxidizing atmosphere.
- Self poisoning of C_3H_6 or O_2 is important factor in the catalytic reaction over noble metal supported catalysts. Ba addition to the catalyst increased catalytic activity by suppressing C_3H_6 poisoning on Pt supported catalyst.
- Metallization of supported Pt and suppression of HC poisoning on Pt are important for high catalytic activity of NO reduction by hydrocarbons. This result suggests that an adequate support design should be necessary to achieve high catalytic activity.
- Catalyst design combining sintering suppression and metallization of Pt is important for simultaneous achievement of high catalytic activity and durability.
- Nd_2O_3 enriched surface layer was introduced on ZrO_2 support to suppress deactivation of Rh supported catalyst by the control of the interaction between Rh and support. An adequate control of the interaction enabled Rh sintering suppression without formation of stabilized Rh oxide that is important to achieve high catalytic activity.

List of publications

Chapter 2: Activation of Pt supported catalyst～operando observation of Pt metallization during catalytic reaction～

[1] Operando X-ray absorption spectroscopy study of Pt/γ-Al_2O_3 during the total oxidation of C_3H_6. T. Tanabe. Y. Nagai. K. Dohmae, N. Takahashi, N. Takagi, H. Shinjoh, Topics in Catalysis 52 (2009) 1433-1439.

Chapter 3: Controlling factors in catalytic activities of noble metal supported catalysts ～control of self poisoning by reactants ～

[2] Comparative NOx reduction behavior of Pt, Pd, and Rh supported catalysts in simulated exhaust gases as a function of oxygen concentration. H. Shinjoh, T.Tanabe, K. Yokota and M. Sugiura, Topics in Catal. 30/31 (2004) 319.

[3] Effect of Ba addition on catalytic activity of Pt and Rh catalysts loaded on γ-alumina. H. Shinjoh, T.Tanabe, H. Sobukawa and M. Sugiura, Topics in Catal. 16/17 (2001) 95.

Chapter 4: Design of highly active Pt supported catalyst ～from the view point of Pt-support interaction～

[4] Operando X-ray absorption spectroscopy study of supported Pt catalysts during NO reduction by hydrocarbons. T. Tanabe, Y. Nagai, K. Dohmae, N. Takagi, N. Takahashi, S. Matsumoto, H. Shinjoh, Applied Catalysis B: Environmental 105 (2011) 41−49

Chapter 5: Pt sintering suppression and catalytic activity of Pt supported catalyst

[5] Sintering and redispersion behavior of Pt on Pt/MgO. T. Tanabe, Y. Nagai, K. Dohmae, H. Sobukawa, H. Shinjoh, Journal of Catalysis 257 (2008) 117−124.

[6] Low temperature CO pulse adsorption for the determination of Pt particle size in a Pt/cerium-based oxide catalyst. T. Tanabe, Y. Nagai, T. Hirabayashi, N. Takagi, K. Dohmae, N. Takahashi, S. Matsumoto, H. Shinjoh, J. N. Kondo, J. C. Schouten, H. H. Brongersma, Applied Catalysis A: General 370 (2009) 108−113.

Chapter 6: Development of highly durable Rh supported catalyst～combining Rh sintering suppression and its metallization～

[7] The interaction between supported Rh and Nd_2O_3-enriched surface layer on ZrO_2 for Rh sintering suppression. T. Tanabe, A. Morikawa, M. Hatanaka, N. Takahashi, Y. Nagai, A. Sato, O. Kuno, H. Suzuki, H. Shinjoh, Catal. Today 184 (2012) 219-226.